Tampere University

REZA BAYAT

Evaluation of Gear Oils Lubrication Performance in a Rolling/Sliding Contact

Tampere University Dissertations 582

Tampere University Dissertations 582

REZA BAYAT

Evaluation of Gear Oils Lubrication Performance in a Rolling/Sliding Contact

ACADEMIC DISSERTATION
To be presented, with the permission of
the Faculty Council of the Faculty of Engineering and Natural Sciences
of Tampere University,
for public discussion in the Pieni Sali 1 Auditorium
of the Festia Building, Korkeakoulunkatu 8, Tampere,
on 6th of May 2022, at 12 o'clock.

ACADEMIC DISSERTATION
Tampere University, Faculty of Engineering and Natural Sciences
Finland

Responsible supervisor and Custos	Professor Arto Lehtovaara Tampere University Finland	
Pre-examiners	Professor Ulf Olofsson Royal Institute of Technology Sweden	Associate Professor Marcus Björling Luleå University of Technology Sweden
Opponents	Professor Ulf Olofsson Royal Institute of Technology Sweden	Professor Jorge Humberto Oliveira Seabra University of Porto Portugal

The originality of this thesis has been checked using the Turnitin OriginalityCheck service.

Cover design: Roihu Inc.

ISBN 978-952-03-2357-8 (print)
ISBN 978-952-03-2358-5 (pdf)
ISSN 2489-9860 (print)
ISSN 2490-0028 (pdf)
http://urn.fi/URN:ISBN:978-952-03-2358-5

PunaMusta Oy – Yliopistopaino
Joensuu 2022

PREFACE

The work was carried out at Tampere University (formerly the Tampere University of Technology) in the group of Tribology and Machine Elements, which belongs to the laboratory of Materials Science. The work was funded by Tampere University graduate school, and guided by Professor Arto Lehtovaara whose expertise was invaluable in formulating the research. He provided me with the tools that I needed to find direction and complete my dissertation successfully.

I would like to thank Jarmo Laakso, M.Sc., for guiding the roughness measurements, and Olli Orell, M.Sc., Nonna Nurmi, B.Sc., and Dr. Minna Poikelispää for their help in measuring the oil specific heat capacity and thermal conductivity. I would like to especially thank my former colleague Ville Oksanen, M.Sc., for guiding me in the starting phases of the experiments, transferring his valuable experience and his great attitude toward other colleagues. I would also like to express my gratitude to Mr. Rich Baker from TriboTonic for encouraging me and giving me hints in my research, and Dr. Kati Valtonen for her valuable support and empowering attitude. I want to thank once more my supervisor Professor Arto Lehtovaara for providing an opportunity to carry out this work, and his friendly encouragement during all the stages of this research project.

I had fantastic colleagues at Tampere University, and especially at the Tribology and Machine Elements research group. They all provided a great place that truly supports researchers and students to grow. I am so honored that I had the chance to carry out research in such an inspiring atmosphere with top scientists.

All this would not have been possible without the encouragement of my mother and sister. In this path, my father was always with and within me, giving me power and inspiration. Above all, I would like to thank my wife Zahra for her generous life-changing love.

Reza Bayat

October 13, 2021
Tampere, Finland

ABSTRACT

Lubrication in gears is a complex process affected by a wide range of variables. Today's design demands enhanced performance, which causes a more challenging operational environment for machine elements. Failures of machine elements may be minimized via design modification or the use of a superior lubricant. Lubrication may be enhanced by using a higher-quality base oil to reduce friction and temperature, and/or by introducing better additives that protect the surface from failures such as wear and scuffing. There exist standards that provide test methods for measuring the load-carrying capacity of lubricants, but these tests do not provide fundamental information on what occurs at a gear tooth in different locations. While real-world component tests such as the FZG are critical for assessing a lubricant's performance, they do not offer information on the lubrication conditions in various contact locations. In addition, these tests are costly and time-consuming. Alternatively, laboratory tests such as the ball-on-disc test may be utilized for initial screening to provide scientifically evaluated results that can be applied to real components. There are still many engineering problems in the field of tribology which are usually dealt with through estimation methods which do not have a solid theoretical background. Therefore, it is critical to provide a scientific and fundamental understanding of such engineering problems in the field.

On the other hand, as a consequence of environmental concerns, lubricant compositions are changing. Reduced oil reserves, increasing oil prices, and especially environmental regulations have all contributed to an increasing interest in Environmentally Accepted Lubricants (EALs). These oils were first introduced to the market in the 1970s, and manufacturers are continuously enhancing their tribological performance via the formulation of new base oils and additives. By examining the performance of these oils, engineers can gain a better understanding of the risks and advantages linked with their use in machine components.

The main objectives of this thesis are to study the lubrication in a rolling/sliding contact simulating the gear contact along the line of action. The lubrication factors that are targeted include friction, temperature, tribofilm formation, and its influence on scuffing and lubrication regimes. Friction measurements were made using a mini-traction machine that simulated the gear contact by a rolling/sliding ball-on-disc test.

Friction was measured in a wide range of slide-to-roll ratios (SRRs), entrainment speeds, and contact pressures. Then, a methodology was used to generate temperature maps according to the Archard model.

To study the tribofilm evolution in an experimentally simulated gear contact, the Spacer Layer Imaging Method (SLIM) was employed in a ball-on-disc test. The tribofilm was examined in different working conditions, mimicking the locations along the line of action. In another experiment, the SLIM technique was used together with the Electrical Contact Resistance (ECR) technique to investigate the tribofilm evolution and its influence on metal-metal contact. In the scuffing test, the ball is replaced with a barrel specimen capable of generating contact pressures of up to 3 GPa. The contra-rotating technique was used to determine the scuffing capacity. A novel scuffing testing strategy was developed that is a combination of sliding speed steps and load steps. The SLIM method was used to monitor the tribofilm during these scuffing stages.

A comparison was carried out between commercial EALs and mineral oil regarding the EHL friction and contact temperature. The results indicate that EALs decreased friction in the EHL regime by up to 60%, and temperature by up to 20 °C depending on the SRR, entrainment speed, and pressure.

Regarding the development of the tribofilm and its impact on metal-metal contact, it was found that a very thick tribofilm may have a detrimental effect on the EHL film by blocking the inlet. This may result in an increased amount of metal-metal contact. Thus, when there is no risk of excessive wear or scuffing, a thin tribofilm is recommended. Additionally, it was shown that the rate of tribofilm formation in a simulated gear contact is strongly dependent on the pressure along the line of action. Observations indicated that there is a tribofilm threshold pressure at which the growth rate of the tribofilm is maximum. This threshold pressure is linked to the pressure in the asperity level and is very sensitive to the roughness of the surface.

Regarding the scuffing experiment, a new test method was devised that is able to accurately differentiate the scuffing performance of similar industrial lubricants. The test parameters were carefully selected to distinguish between the scuffing properties of the industrial oils with high accuracy. The running-in and test conditions were critical for obtaining repeatability and avoiding excessive wear. Tribofilm images shed light on the evolution of the surface during the scuffing test, emphasizing the contribution of the tribofilm in the micro-scuffing healing process. Among the tested industrial gear oils, EALs showed a higher scuffing capacity compared to mineral gear oils.

CONTENTS

ABBREVIATIONS

α	Pressure-viscosity coefficient
μ	Coefficient of friction
$\dot{\gamma}$	Strain rate
Γ_0	Tribofilm growth pre-factor
$\Gamma_{Growth\ rate}$	Growth rate of tribofilm
ΔG_{act}	Free activation energy of the rate-limiting reaction step
$\Delta\overline{T}_{flash}$	Mean flash temperature rise
$\Delta\overline{T}_{oil}$	Oil film temperature rise above the surfaces
ΔU_{act}	Additive reactivity
ΔV_{act}	Activation volume
η_0	Dynamic viscosity of the lubricant
κ_B	Boltzmann constant
λ	Specific film thickness
ϱ	Density
τ	Shear stress
τ_e	Limiting shear stress
$\Phi_{thermal}$	Thermal correction factor
b	Contact halfwidth
c	Specific heat
E*	Reduced Young's Modulus
F	Force
H_{min}	Minimum oil film thickness
h_c	Central film thickness
$h_{c,\ iso}$	Iso-thermal central film thickness

K	Thermal conductivity
K_{oil}	Oil thermal conductivity
P	Pressure
P_{max}	Maximum Hertzian contact pressure
q''	Rate of heat generation per unit area
R_x	Radius of curvature in the sliding direction
S_a	Average roughness height of area
S_q	Root-mean-square roughness height of area
T	Temperature
U_b	Ball circumferential velocities
U_d	Disc and ball circumferential velocities
U_e	Entrainment speed
U_s	Sliding speed

COF	Coefficient Of Friction
EAL	Environmentally Accepted Lubricant
ECR	Electrical Contact Resistance technique
EHL	Elastohydrodynamic lubrication
EP	Extreme Pressure
HD	Hydrodynamic lubrication
LOA	Line Of Action
MTM	Mini-Traction Machine
PAG	Polyalkylene Glycol
PAO	Polyalphaolefin
SE	Synthetic Ester
SLIM	Spacer Layer Imaging Method
SRR	Slide-to-roll ratio
VI	Viscosity Index
VO	Vegetable Oil

ORIGINAL PUBLICATIONS

Publication I Bayat R, Lehtovaara A. EHL/mixed transition of fully formulated environmentally acceptable gear oils. Tribol Int 2020;146. doi:10.1016/j.triboint.2020.106158.

Publication II Bayat R, Lehtovaara A. Friction and temperature mapping of environmentally acceptable gear oils. Tribol - Finnish J Tribol 2020;37:4–12. doi:10.30678/fjt.96048.

Publication III Bayat R, Lehtovaara A. Scuffing evaluation of fully formulated environmentally acceptable lubricant using barrel-on-disc technique. Tribol Int 2021;160:107002. doi:10.1016/j.triboint.2021.107002.

Publication IV Bayat R, Lehtovaara A. Tribofilm Formation of Simulated Gear Contact Along the Line of Action. Tribol Lett 2021;69:126. doi:10.1007/s11249-021-01499-7.

AUTHORS CONTRIBUTION

By agreement of the authors of the publications:

Authors' roles: Reza Bayat contributed to this work in the following ways: Conceptualization of ideas, Development or design of methodology, Validation of results, Analysis or synthesizing the study data, Performing the experiments or data/evidence collection, Writing and editing the initial draft, Editing of the published work.

Arto Lehtovaara contributed to this work in the following ways: Conceptualization of ideas, Validation of results, Editing the initial draft, Supervision and leadership for the research activity planning and execution, Project administration and coordination for the research activity planning and execution.

Publication I As stated in the authors' roles.

Publication II As stated in the authors' roles.

Publication III As stated in the authors' roles.

Publication IV As stated in the authors' roles.

1 INTRODUCTION

1.1 Tribology

The term tribology was first used in a report from the United Kingdom in 1966. The word was taken from the Greek word tribos that means rubbing, so that "the science of rubbing" would be a literal translation. Tribology has a long history dating all the way back to ancient times. For instance, Egyptian chariots were lubricated with animal tallow (for friction reduction). Throughout the Renaissance, various individuals such as Leonardo da Vinci studied tribological issues [1]. Tribology is often defined as the science and technology of interacting surfaces in relative motion. Tribology can focus on topics such friction, wear, and lubrication. However, these terms are not inclusive enough, as tribology deals with the various phenomena influencing the interacting surfaces. Surface interactions at a tribological interface are very complex, and comprehending them requires knowledge of different fields, including physics, chemistry, applied mathematics, solid mechanics, fluid mechanics, and so on [2].

Tribology is critical to the operation of modern machinery that has sliding and rolling surfaces. Tribological interactions account for 23% of the world's total energy usage. 20% of that is utilized to counteract friction, and 3% is used to remanufacture worn components and spare equipment due to wear and failures caused by wear [3]. The objective of tribology is, unsurprisingly, to minimize and eliminate the losses caused by friction and wear at all levels of technology that involve the rubbing of surfaces. Research in tribology aims at increased machinery efficiency, improved performance, fewer breakdowns, and significant cost savings.

1.2 Lubrication regimes

Lubricants are applied purposefully to reduce friction and wear. Separated by a thick fluid film, two rubbing surfaces have less solid-solid contact and can have very low friction and minimal wear. Lubrication refers to two different mechanisms: solid lubrication and fluid lubrication [2]. In this thesis, fluid lubrication is studied.

Although Sir Isaac Newton hypothesized the fundamental rules of viscous flow in 1668, scientific knowledge of lubricated bearing operations did not arise until the late nineteenth century. The experimental investigations of Beauchamp Tower (1884), the theoretical interpretations of Osborne Reynolds (1886), and related work by N.P. Petroff set the basis for our knowledge of the concept of hydrodynamic lubrication. Since then, hydrodynamic bearing theory and practice have advanced at a rapid pace to satisfy the growing need for reliable bearings in modern machinery. [2]

Hydrodynamic (HD) lubrication is occasionally referred to as fluid-film or thick-film lubrication. HD lubrication usually happens in conformal contacts by a positive pressure build-up in the fluid film due to a converging gap and viscous entrainment. The fluid is dragged in and it is subsequently squeezed between the contact surface, generating a sufficient (hydrodynamic) pressure to sustain the load even without the assistance of an external pump. HD lubrication is frequently considered as the optimum lubrication, since the lubricating films are usually several times thicker (typically 5–500 μm) than the height of the bearing surface imperfections, and no solid contacts occur. HD lubrication is common in components with a relatively large contact area such as journal and thrust bearings in which the pressure range is 1-5 MPa and does not cause considerable elastic deformation. Elastohydrodynamic (EHD) lubrication (EHL) is a type of hydrodynamic (HD) lubrication under which the surfaces experience elastic deformation, and the oil viscosity dependency on pressure plays a significant role. EHL is often associated with non-conformal (Hertzian) contacts. Such non-conformal contacts are found in machine elements such as ball bearings, roller bearings, and gear teeth. The machine components which typically operate under this lubrication regime have a contact pressure ranging between 0.5 and 4 GPa. EHD lubrication generates a thinner film (usually 0.5–5 μm) than HD lubrication, even though the load is still carried fully by the fluid. When the load increases, the speed decreases, or the fluid viscosity decreases, then the coefficient of friction can increase sharply in a regime named “mixed lubrication,” under which the load is partly carried by the asperities and partly by the fluid film. When the load further increases, the speed decreases, or the fluid viscosity decreases, then the coefficient of friction approaches high levels (about 0.1). In this region, it is usual to speak of boundary lubrication. This condition can also occur in a starved contact. Boundary lubrication is the condition in which the solid surfaces are so close together that surface interaction between monomolecular or multimolecular films of lubricants (liquids or gases) and solid asperities dominates the contact. The transition zone between EHL and boundary lubrication regimes is referred to as mixed lubrication. In a mixed lubrication regime, asperity contacts are present, but a portion of the load is still held by a partial hydrodynamic film. [2,4]

The classic Stribeck curve shown in Figure 1 summarizes the lubrication regimes in fluid lubrication without an external pump. The coefficient of friction is shown as a function of the product of absolute viscosity (η) and rotational speed (U) divided by the load per unit of projected bearing area for a hypothetical fluid-lubricated bearing system (P). Lubrication regimes are often identified using a lubricant film parameter (known as specific film thickness) equal to $\lambda=h_{min}/S_q$, where h_{min} is the minimum film thickness and S_q is the composite standard deviation of the surface heights of the two surfaces [2]. The thickness of the film is usually estimated using the well-known Hamrock and Dowson's formula [5] and corrected by considering the thermal correction factor presented by Gupta et al. [6]. It is widely accepted that a λ value below 1 is associated with boundary lubrication, a value between 1 and 3 denotes mixed lubrication, and for a λ bigger than 3 denotes the HD/EHL regime [7]. However, some references report other numbers [2], and several references show the limitations of specific film thickness numbers [8–10].

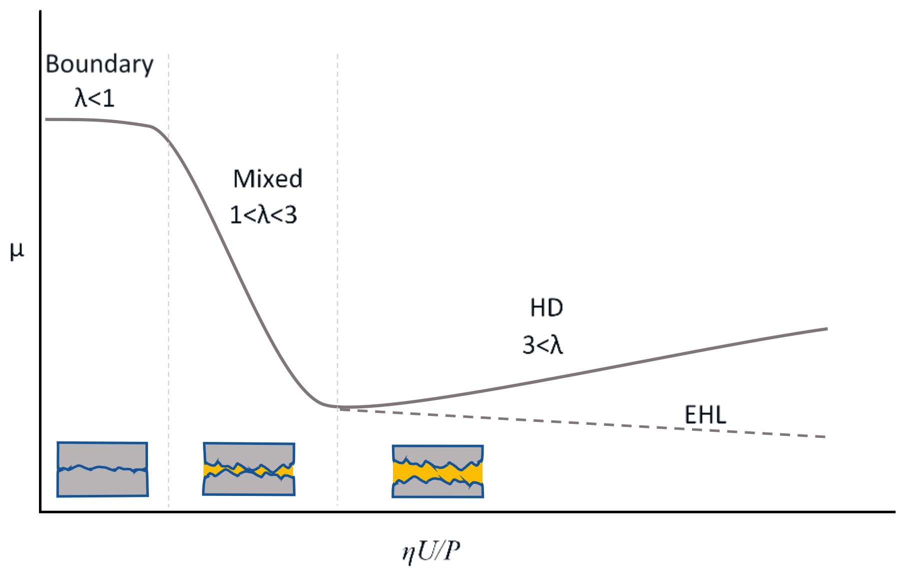

Figure 1. Lubrication regime in a lubricated contact

Abrasive, adhesive, and chemical (corrosive) wear are commonly seen in boundary lubrication. Over the contacting surfaces, boundary additives produce a protective film (often referred to as a Ttribofilm), decreasing the risk of a specific failure or lowering the friction depending on the additive nature. One of the most critical aspects of a lubricant in boundary lubrication is its chemical function or polarity, which dictates the lubricant molecules' capacity to be physisorbed, chemisorbed, or chemically interacted with the surfaces. Improved surfaces reduce the potential for damage caused by frequent asperity interactions [2]. Between 0.1 percent and 30 percent additives are added to oils for some metalworking fluids and greases to form a protective tribofilm for boundary lubrication [2,11].

Additives that are carefully selected can significantly improve an oil's performance. Perhaps for this reason, the majority of additive manufacturers keep the specifics of their goods under wraps. As a result of this concealment, the supplier and user of the lubricant may only be aware that a specific oil has a 'package' of additives, which frequently inhibits the study of lubricant failures. Another consequence is that major companies frequently employ a variety of lubricant brands that are functionally identical or have comparable characteristics and composition. This may be extremely costly for a business, as various lubricants must be kept and updated on a regular basis. Due to the secrecy surrounding additives, their formulation is also partially an artistic effort rather than a strictly scientific or technical approach. Most often a package of additives includes anti-wear and extreme pressure lubricants, oxidation inhibitors, corrosion inhibitors, detergents, dispersants, viscosity improvers, pour point depressants, and foam inhibitors. Additionally, oils may contain other chemicals such as colors and odor improvers. Anti-wear and EP additives are quite efficient at preventing scuffing and other types of failures. [7]

1.3 Environmentally Acceptable Lubricants (EALs)

Environmentally Acceptable Lubricants (EALs) have been used in industry since the early 1970s, and several industries have begun to invest in the development of EALs, for example the development of EAL hydraulic fluids for forestry operations in Germany during the 1980s [12]. Reduced oil reserves, rising oil prices, and concerns about the environmental impact of oil spills have heightened interest in new, less environmentally hazardous lubricants [13].

Different words are used for these lubricants, depending on quality and regulation:

- Environmentally adapted (acceptable/accepted) lubricants (EALs), with a minimum hazard to the environment

- Environmentally friendly lubricants, of perfect quality, which is not usually applicable

- Environmentally compatible lubricants, with no or a low negative effect on the environment

The most logical term is environmentally acceptable/adapted lubricant (EAL). The justification for this is because the presence of oily substances that are not water-miscible results in the staining of soil, fur, or feathers, as well as the development of oil sticks on water in the case of oils with a density of less than one. As a result, it is difficult to believe that an oil has no or little environmental impact, thus it cannot be referred to as "friendly" or "compatible" [12].

Each year, about ten million tons of mineral lubricants and hydraulic fluids lead to environmental pollution [14]. In Europe, different sectors use about five million tons of lubricant, of which 40% ends up polluting the environment [15]. Increased attention is being paid to the friendliness, dependability, compatibility, durability, and efficiency of EALs in order to make them suitable for a variety of applications and industries such as automotive and equipment. According to certain research, EALs may offer even greater lubricity and can be used instead of mineral lubricants in engines, generators, pumps, gears, hydraulic, and metalworking oils [13,16].

1.3.1 EAL environmental properties

To be considered environmentally acceptable, a lubricant requires to pass regulations in the following properties [12,17]:

- Biodegradability

- Renewability

- Toxicity

- Bioaccumulability and biomagnification.

The term "biodegradability" refers to the degradation process carried out by microorganisms [12]. The OECD 301 test is commonly used for determining the biodegradability of lubricants, which need to be readily biodegradable (≥60%) [15]. Generally, synthetic esters have high biodegradability, with the exception of those with a high viscosity, which have low biodegradability [17]. The biodegradability of some base oils can be found in Table 1:

Table 1. Biodegradability of base fluids [13]

Base oil	Biodegradability %
Mineral oils	20–40
Vegetable oils	90-98
Esters	75-100
Polyols	70-100
Trimelliates	0-70

The term "renewability" refers to the quantity of material that may be replenished via reusing, recycling, or natural processes such as regrowth [12]. According to ASTM D-6866, the oil must include at least 25% renewable material to qualify as a biolubricant [15]. To qualify for an EU eco-label, a lubricant's carbon content must include the following proportion of carbon derived from renewable sources [18]:

- ≥ 50 % for hydraulic fluids, tractor transmission oils
- ≥ 45 % for greases, stern tube greases
- ≥ 70 % for chain saw oils, concrete release agents, wire rope lubricants, and other total loss lubricants
- ≥ 50 % for terrestrial and marine two-stroke oils
- ≥ 50 % for industrial and marine gear oils

In recent years, limiting toxicity and decreasing the environmental impact have been prioritized in the formulation of lubricants [19]. The age of the lubricant, the base oil composition, and additive composition may all have an impact on the toxicological characteristics of lubricants, and total toxicities are often quite near to the summation of the toxicities in their compositions [17].

Regarding the European-wide Standardized Minimum Requirements for "Biolubricants", according to CLP Directive 1272/2008/EC, the phrase "dangerous to the environment" shall not appear on the label of a lubricant. To prove this, the fully formulated product is tested according to OECD 201/202/203: EC50/LC50/ IC50>100mgl^{-1} [15].

Bioaccumulation is the process through which lipophilic hazardous chemicals accumulate over time in living organisms [12]. Biomagnification is the process by which an accumulating material increases in quantity as it passes up the food chain. A chemical that is capable of biomagnification must be long-lived, mobile, soluble in fatty tissue, and physiologically active [17].

1.3.2 Base oil types used in EALs

The base fluids with the desired environmental characteristics are selected from low molecular weight polyalphaolefins (PAO), polyalkylene glycols (PAGs), synthetic esters (SEs), and vegetable oils (VOs). However, ester-based lubricants are the most widely used environmentally acceptable lubricants on the market today [15,20], due to their exceptional biodegradability, non-toxicity, and high-quality tailor-made characteristics [21]. The tribological properties of esters are equivalent to those of mineral oils [Publications I-III] and can be easily blended with mineral oils. Another advantage of esters is that they can be formulated with the additive technology established for mineral oils [22].

1.3.3 Synthetic Esters

The most often used EAL on the market is synthetic esters. The ester linkage $R' - O - \overset{\overset{O}{||}}{C} - R - \overset{\overset{O}{||}}{C} - O - R'$ is formed when acids (R-COOH) or their derivatives react with alcohols (R-CH2OH). The organic groups R' and R are derived from alcohol and acid, respectively. In comparison to mineral oils, the ester bond is more stable at elevated temperatures, resulting in improved oxidation resistance. Other qualities that make esters an attractive choice include a greater viscosity index, a lower pour point, a reduced volatility, a higher flash temperature and thermal stability, and a low friction coefficient [15,23,24]. The primary advantage of ester oils is their low toxicity and biodegradability, which makes them the most commonly used oil in environmentally accepted lubricants [17]. However, one issue with esters is that they undergo undesired hydrolysis [25]. Figure 2 illustrates the effect of chain variation on the viscosity, viscosity index, and pour point of esters [24]:

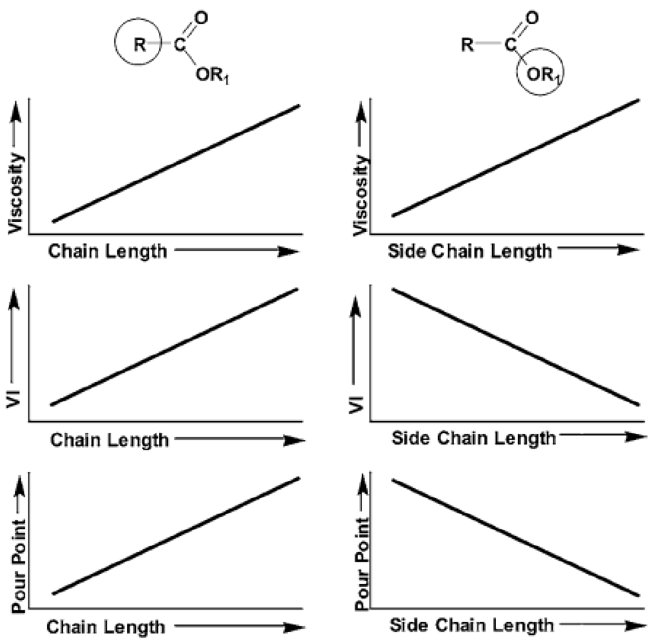

Figure 2. The effect of chain length on the lubrication properties of ester oils [24]

Without additions, the greater polarity of esters results in reduced friction and wear protection; nevertheless, this results in competition for surface absorption between additives and ester molecules. This drawback, along with undesirable hydrolysis, can be reduced by using high-quality saturated esters and additives [22]. Esters may be used alone or in combination with mineral oils or PAOs. In situations where the seal swell is critical, combination with PAOs is very common. Their combination maintains a balance between the shrinking qualities of PAOs and the swelling features of esters [26]. Esters are usually utilized in gear systems in environmentally sensitive places such as the water industry or wind energy, owing to their excellent biodegradability and non-toxicity [22].

Thermal and oxidative stresses may cause lubricant degradation and tribological performance loss. Bartels and Bock cite a recommendation from Flender, a leading manufacturer of industrial gearboxes in Germany, that the temperature range suitable for mineral-based industrial gear oil is between -10 °C and 90 °C with short periods of 100 °C, while the temperature range suitable for ester-based industrial gear oil is between -15 °C and 90 °C with short periods of 100 °C. Additionally, it is stated that 10000 hours is the lifespan of the oil at an average temperature of 80 °C [22].

Numerous investigations have shown that ester-based lubricants have a reduced friction coefficient in the full film and EHL regimes [27–29]. However, José A. Brando et al. have examined the Stribeck curves of many mineral and ester-based lubricants and demonstrated that, although ester lubricants have a lower friction coefficient in the full film regime, they have a bigger friction coefficient in the mixed and boundary lubrication regimes. According to José A. Brando et al., this effect is caused by the different additives employed in the lubricant formulation. Due to toxicity and biodegradability constraints, this assumption may be valid; nevertheless, further research is required to determine if the effect is due to the base oil, the additives, or both [30]. Rieglert and Kassfeldt discovered the same result when they tested hydraulic oil EALs [31]. These oils were shown to have a greater wear rate than mineral oils while having a lower friction coefficient. The increased wear may be a consequence of the insufficient surface coverage of anti-wear and extreme pressure additives, which compete for space on the surface with the polar molecules of the environmentally acceptable oil [31].

In comparison to mineral oils, ester oils have a lower pressure-viscosity coefficient, which results in a thinner film thickness according to EHL theory [32]. Additionally, ester-based lubricants have a greater thermal conductivity and specific heat capacity. Because esters have a high viscosity index, they do not need VI improvers. These parameters are advantageous for film formation, particularly under circumstances of high slip and high stress [21].

1.3.4 Polyglycols

Polyalkylene glycols (PAG) are the byproducts of the reaction of epoxides (e.g., ethylene and propylene oxide) with active hydrogen molecules (usually alcohols or water). By varying the ratio of epoxides to end groups, various molecules can be synthesized. PAGs have been utilized in industrial applications as a lubricant such as gear oil, compressor lubricant, metalworking fluid, and hydraulic fluid. Despite these uses, PAGs are underutilized in industry, regardless of their high viscosity index, low pour point, excellent shear stability, and cleanliness. This poor market share can be attributed to their expensive price or incompatibility with conventional lubricants, but it could also be attributed to the industry's traditional mindset [33].

The VI value of PAGs is around 200, which is often more than the VI of mineral oils [34]. Due to the high polarity of PAG molecules, they have a significant attraction to metallic surfaces. This leads to improved boundary lubrication of the base oil itself, but if there are additives in the oil, the molecules of the base oils compete with the additives, which reduces the performance of polar additives [34]. Polarity can be changed throughout the manufacturing process by selecting an appropriate monomer, which affects their solubility in water and hydrocarbon lubricants. PAGs are water-soluble, which may be considered an advantage [33].

Regarding the environmental properties, the toxicity of PAGs is comparable to that of glycerol for low viscosity products and to that of isopropanol for more viscous PAGs. Due to their very low toxicity, they are an attractive lubricant for use in the food, pharmaceutical, cigarette, and cosmetics sectors [34]. Although PAGs are very low in toxicity, their biodegradability does not meet the criteria required by European environmental legislation to be deemed 'Environmentally Acceptable'. If the lubricant industry is able to develop non-water soluble PAGs with increased biodegradability, they may be used as a substitute for esters in EALs [33,34]. PAGs can be made more biodegradable by reducing their molecular weight (low molecular weight PAGs are more biodegradable), or by employing a co-polymer structure with a high ethylene oxide concentration (with a higher biodegradability than propylene oxide) [33,35].

In summary, the advantages of PAGs are as follows:

- High viscosity index (typically >200)
- Good temperature stability
- High hydrolytic stability
- Low friction coefficient, better boundary lubrication, and good EP performance

The disadvantages are as follows:

- Interference with additive response
- Poor compatibility with mineral and PAO based fluids
- Paint incompatibility
- Seal incompatibility

1.4 Lubrication of gearing

Gears have been used for millennia as critical components of mechanisms and machines [36]. The functioning of a gear is dependent on a number of variables, including meshing conditions, lubricant rheology, and surface topography. The lubrication of gears has two primary functions: lubrication and cooling. In gear teeth, boundary or mixed lubrication occurs most often at low to moderate speeds, on gears that are highly loaded, or on gears that are subjected to strong shock loads. Full film Elasto/Hydrodynamic lubrication is often seen exclusively in high-speed gears with little shock loading [37].

The gear tooth contact is a rolling/sliding non-conformal type in which Hertzian elastic deformation occurs. During gear mesh, the contact point in involute gears follows a straight line, often referred to as the line of action (LOA). In the case of gears, contact conditions vary significantly throughout the line of action due to the constant change in load, surface velocities, and instant contact radius. Figure 3a illustrates the instantaneous contact of spur gear teeth, whereas Figure 3b illustrates the gear contact along the line of action. Constant loading is shown in Figure 3 when the gear contact ratio is 1.45 and the load distribution is uniform in the case of two teeth in contact (half of the single tooth load). Additionally, Figure 3b illustrates the dimensionless distributions of normal force (F_N/F_{Nmax}), Hertzian maximum line pressure (p_0/p_{0max}), surface velocities (u/u_{max}), and combined radius of curvature (ϱ/ϱ_{max}). As shown in Figure 3b, tooth engagement begins on the left and two rapid changes in load and pressure occur when two-tooth engagement becomes single-tooth engagement and vice versa. Pure rolling occurs at the pitch point, i.e., the sliding velocity ($U_s=u_1-u_2$) is zero. The rolling velocity is equal to one, as defined by $U_R=(u_1+u_2)/2$. The sliding and rolling speeds along the line of action have a considerable effect on the lubrication film thickness, and therefore on the gear's performance and life [38]. This will be further discussed in the next sections.

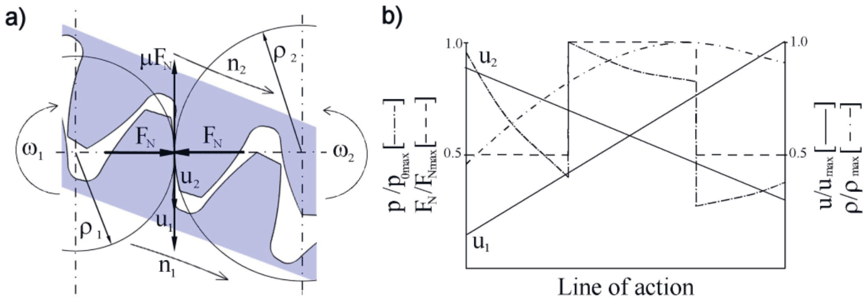

Figure 3. Gear operating condition along the line of action [38]

With actual gears, it is very difficult to examine the instantaneous contact points along the line of action in detail. Usually, spur gear profiles are approximated, using cylinders with the same radius of curvature (ϱ_1/ϱ_2) as that of the gear teeth at the instant of contact, as shown in Figure 3a. This lays the groundwork for the twin-disc test device. A twin-disc machine has steady-state operation and eliminates the majority of the dynamics and manufacturing tolerances that are inherent in actual gears, resulting in precisely regulated contact conditions. This enables the simulation of a variety of critical characteristics and problems associated with gear contact, including scuffing, pitting, power loss, lubricant life, and wear [38]. The same idea is applied to the ball-on-disc test machine; however, the elliptical contact in a twin-disc machine is more similar to what is found in gears. An important study in this regard is the one carried out by Ellen Bergseth et al. [39]; they used laboratory size test rigs to study the factors influencing friction, wear, and the chemically reacted surface layer in gears.

Typical gear failures are divided into two main groups: non-lubrication related and lubrication-related failures. Non-lubrication related failures include both overload and bending fatigue types of failure. Lubrication-related failures are more relevant to the topic of this thesis and are categorized as Hertzian fatigue (pitting), wear, and scuffing. These lubrication-related failures take place at different locations along the tooth flank because the contact conditions change along the line of action, and consequently the lubrication condition is different at each position. For example, pitting is commonly observed near the pitch point where there is high pressure, and scuffing is found at the tip of tooth where high sliding results in a bigger temperature rise [40].

In order to study gear lubrication, many studies have developed measurement tools for real gear contacts [41–43], mathematical models for gear lubrication [44–47], or experimental approaches for the experimental simulation of gear contact [48–

50]. The results of experimental simulations are commonly used as a reference measurement to verify calculated tribological parameters such as friction [51,52]. For the experimental simulation of gear lubrication, a ball-on-disc machine has been used, and it is shown that it can accurately estimate the friction of gear contact [50].

1.4.1 Friction reduction in gears

In a gear transmission, the pressure between the mating teeth can exceed several GPa. Thus, depending on the operating parameters, the frictional losses in a gearbox are strongly influenced by EHL behavior. It has been estimated that 33% of the fuel energy in a vehicle is needed to overcome friction, with the transmission accounting for 7-18% of these losses [53]. Losses in a gear transmission are sometimes classified as load-dependent or load-independent. Load-independent loss is caused by the viscous losses from oil churning, which is mostly influenced by lubricant properties such as viscosity and density, and also the geometrical design of the gears and housing. Load-dependent losses are attributable to the friction in the rolling/sliding contact of the gear teeth, which is a function of several parameters.

There are several ways to reduce the friction in gears and increase their efficiency. These solutions include geometrical changes by increasing the number of teeth and reducing the teeth size, using different materials that provide better interaction with the lubricant [54–56], polishing the surfaces to a lower roughness to achieve less asperity contact [57,58], coating the gear surface [59–62], or using a lubricant with a lower friction coefficient [30,63]. In this study, the focus is on the influence of lubricant on efficiency improvement.

Continuous research efforts have been made to optimize the efficiency and service life of machine components operating in EHL by examining various elements of the lubricated system. The lubricant in a gearbox has been reported to have a considerable influence on gearbox efficiency [64,65]. In full film lubrication, friction losses are influenced by the viscosity, limiting shear stress, pressure-viscosity, and VI, and all of these have an influence on the lubricant film thickness. These lubricant properties are dependent on shear rate, temperature, and pressure; thus, the problem becomes more complicated. In gear tooth contact, the pressure, temperature, shear rate, and slide-to-roll ratio (SRR) all change along the line of action. Studying the behavior of lubricants requires experimental equipment that can simulate the variation of such parameters along the line of action. One of the most widely used tools has been the twin-disc machine, which is employed for investigating the friction and temperature variation along the line of action [66–69]. Additionally, the ball-on-disc test demonstrates the ability of simulating a gear contact. Björling et al. have demonstrated that a ball-on-disc machine can rank lubricants in the same way as a FZG device does [50]. They utilized a method called friction mapping to simulate friction along the line of action. This method was developed by Björling first in 2011 [70], and it was demonstrated that it can be used for estimating the friction at a wide range of SRRs and entrainment speeds. A sample of such friction maps is given in Figure 4, in which a 3D friction map and its projection in a 2D plane are shown.

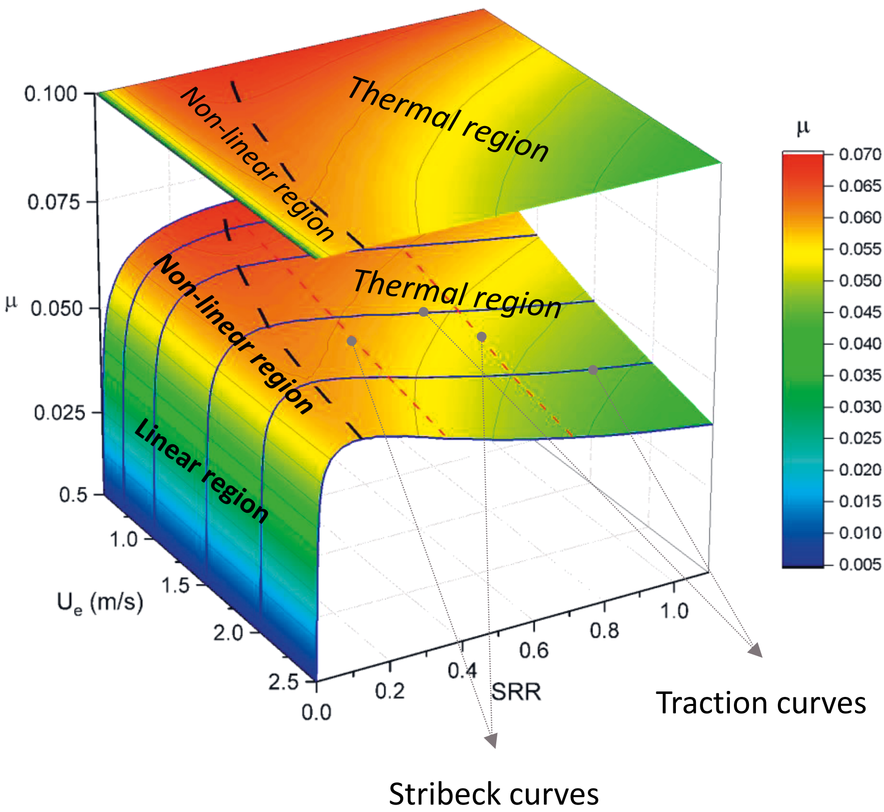

Figure 4. 2D and 3D friction map of an oil

A three-dimensional friction map is produced using the coefficient of friction (COF) values at different SRRs and entrainment speeds. Then, a two-dimensional friction map is created by projecting the three-dimensional map to the plane of U$_e$-SRR while retaining the friction contours and color variations that indicate changes in the COF.

The thermal region and its border are shown in Figure 4. According to [69], the thermal region is the condition under which thermal softening behavior is dominant in the friction, and shear heating has the biggest influence. In Figure 4, the thermal region begins at the point where the COF decreases as the SRR increases. In the thermal region, shear heating has a significant role. There are two more areas before the thermal region: 1) a linear region in which there is Newtonian fluid behavior and the COF increases linearly as the SRR increases, and 2) a non-linear region in which shear-thinning occurs and the maximum friction is primarily governed by non-Newtonian effects. The friction is bound to the limiting shear stress which itself is influenced by the temperature [69,71]. The Stribeck and traction curves are also depicted in Figure 4. Traction curves are shown by dark blue solid lines and correspond to COF curves by increasing the sliding speed while maintaining a constant entrainment speed. The red dashed Stribeck curves are the curves obtained by measuring the COF at various entrainment rates and a constant SRR. The traction and Stribeck curves of a lubricant can be determined simply for a two-dimensional friction map at various SRR and entrainment speeds.

For a spur gear with a constant rotational speed, Figure 3 illustrates how several parameters change along the line of action. The load, and therefore the pressure in the contact, is determined by the transmitted torque, the number of teeth in contact, and the gear tooth geometry. The entrainment speed is determined by the tooth geometry and increases with rotational speed, while the SRR is determined solely by the tooth geometry and is not affected by the rotational speed. In reality, the conditions in a gear contact are quite transient owing to the transmission's load and speed changes and the dynamic behavior of the driveline. By comparing the friction maps of various lubricants, it is possible to determine their energy efficiency under various operating circumstances and along the line of action.

1.5 Scuffing

Scuffing is a type of failure that is characterized by rapid wear and a roughened surface, a sudden rise in temperature and friction, as well as high noise and vibration [72]. Scuffing, in comparison to other tribological failure modes such as moderate wear and fatigue, is difficult to anticipate and analyze due to its catastrophic characteristics. Even a short period of overload may initiate scuffing [73]. As a consequence, selecting an appropriate scuffing test is critical to avoid the misrepresentation of scuffing results.

Scuffing occurs when the elasto-hydrodynamic (EHL) film and protective tribofilm are ruptured [74], and plastic yielding occurs in the sliding surfaces. [75]. The breakdown of the EHL film is linked to frictional heat generation [76–79], lubricant starvation caused by the accumulated wear products [80], high shear stress [81], lubricant degradation [82], and the wettability and roughness of the surface [83]. Tribofilm breakdown is related to high shear stress [81], lubricant degradation [82], and the wettability and roughness of the surface [83]. Tribofilm removal is caused by the desorption of adhered polar molecules of EP additives [84]. However, addressing these factors has not led to a widely accepted theory for scuffing. The flash temperature theory was one of the first scuffing hypotheses, implying that scuffing happens when the contact temperature in the contact center exceeds a threshold value for a specific lubricant/surface combination [85]. Due to the fact that this theory did not account for the effect of EHL film collapse, Dyson proposed a model in which the critical temperature occurs at the contact's inlet [86]. Cheng and Dyson subsequently extended the hypothesis by taking into account the impact of asperity heating [87]. Recent theories place a greater emphasis on the metallic alteration due to the adiabatic shear plastic instability in the near-surface material [88–92]. Ajayi et al. noticed a rapid temperature increase in the contact and argued that this is inconsistent with the critical temperature hypothesis of scuffing initiation. Ajayi et al. also speculated that the dramatic temperature increase is the consequence of scuffing, rather than its cause [89].

Scuffing has been investigated experimentally using a variety of methods, including FZG [93,94], IAE [95], four-ball [96], Ryder [97], Timken [98], and twin-disc [48,73]. Peng et al. examined the shortcomings of these techniques and classified the major factors into two categories: stationary body and conventional increasing-load test sequences [99]. In four-ball and Timken testing, the stationary body experiences accumulated wear prior to scuffing. This wear increases the contact area and decreases the pressure. This geometrical modification may result in an incorrect oil ranking if a low wear capacity oil is tested [99]. One way to avoid this issue is to use rolling-sliding contact, which distributes wear evenly over the surface and avoids excessive wear on a specific location. Thus, in terms of wear, using tests such as Ryder, IAE, and FZG is recommended. However, in these techniques, the increasing-load sequences bring the newly formed asperities into contact at the beginning of each load step. As a result of the interaction with unprotected asperities, the danger of early scuffing is increased. Additionally, one limitation of both traditional rolling-sliding and pure sliding testing is that the sliding speed cannot be increased without increasing the rolling speed. In these tests, the rolling and sliding speed are coupled, so that when the sliding speed increases, the rolling speed increases. As a result, there will be increased lubricant entrainment into the contact and the development of a thick EHL film [99]. To resolve these difficulties, Ingram et al. used a ball-on-disc machine to have a rolling-sliding contact in contra-rotation mode [100]. This method resulted in a low oil entrainment speed and decoupled the sliding and rolling speeds, allowing the scuffing test to be performed using increasing-sliding-speed sequences rather than increasing-load sequences. Peng et al. enhanced the contra-rotating ball-on-disc technique, aiming for increased repeatability and scuffing prediction [99].

1.6 Tribofilm formation in rolling/sliding contacts

A tribofilm is defined as "a thin solid film generated as a consequence of sliding contact, which is adhered on its parent worn surface but has different chemical composition, structure, and tribological behavior" [101]. Tribofilms exist in many tribological contacts where they act as a "third body" playing an important role in friction and wear.

Tribofilms are divided into four categories:

1. Tribofilms generated from the wear of sliding surfaces.
2. Tribofilms which are generated from the preferential wear of soft or lubricious elements existing in composite or multi-phase materials.
3. Tribofilms that are different from the original worn surfaces as a result of sliding contact. This difference is in the chemical composition and/or crystalline structure.
4. Tribofilms generated due to the tribo-chemical reactions between the sliding surfaces and the environment (e.g., lubricant). This is the most common type, since the majority of tribological contacts occur in environments containing chemically reactive substances. [101]

In lubricants, there are different additives that can be divided into rheo-improvers (e.g., viscosity modifiers), maintainers (e.g., dispersants), and tribo-improvers (e.g., anti-wear agents). In lubricated contacts, tribo-improver additives in the lubricating fluid can adsorb on the sliding surface to form a protective tribofilm [101,102]. These tribofilms can play different roles such as reducing wear by anti-wear agents, reducing friction by friction modifiers, or preventing the welding of surfaces at high load/high temperature by extreme pressure additives (EP additives). Studying the reaction of these additives with the surface plays a significant role in the analysis of lubricant performance.

Different analytical tools have been used for studying tribofilm formation on surfaces. These tools include wet chemistry, radiotracer, infrared spectroscopy, XPS, Auger, SIMS, electrical contact resistance, and EELS methods dating from the 1950s up to the 1990s [103]. In the 1990s, attention focused on "in situ" ways of studying tribofilm formation. An in-contact technique was developed and applied by Sheasby in the early 1990s. In this technique, the visual observation of the lubricated contact was made possible through the transparent surface of a glass disc in contact with a steel ball [104]. One of the most versatile in-situ techniques is atomic force microscopy (AFM). This gained popularity in the 1990s remains a common technique for studying a tribofilm. It is used for studying the morphological and physical properties of tribofilms [105–109].

In late 2001, Taylor developed an optical interferometric method to monitor tribofilms without removing the rubbed test specimen from the test rig [110]. Usually termed as the Spacer Layer Imaging Method (SLIM), it has been frequently used for studying tribofilm formation [111–114]. This method is fast and can record the image of a tribofilm on the surface in different stages of the test. There are some limitations, as the SLIM technique cannot distinguish between the tribofilm and air or oil separation; however, usually this does not result in major error as the tribofilm thickness is comparatively higher [115]. This technique has been used in this study for investigating tribofilm formation along the line of action of a simulated gear, and its influence on lubrication regimes and scuffing.

Using the above-mentioned experimental methods such as AFM and SLIM, it has been shown that the overall thickness of the tribofilm is determined by the rate of tribofilm growth and removal. Gosvami et al. demonstrated that the growth rate of tribofilms in a single asperity contact is stress-dependent [109], and consistent with a stress-activated Arrhenius model:

$$\Gamma_{growth\ rate} = \Gamma_0 \exp\left(-\frac{\Delta G_{act}}{\kappa_B T}\right) \quad \mathbf{(1)}$$

where $\Gamma_{growth\ rate}$ is the growth rate of the tribofilm, and Γ_0 a pre-factor, T the absolute temperature, ΔG_{act} the free activation energy of the rate-limiting reaction step, and κ_B the Boltzmann constant. ΔG_{act} is influenced by the stress according to Eq. 2:

$$\Delta G_{act} = \Delta U_{act} - \sigma \Delta V_{act} \tag{2}$$

where ΔV_{act} is the activation volume and σ is the driving stress. Gosvami et al. argued that the driving stress is pressure [109], but Spikes illustrated that it is shear stress [116]. According to this model, the rate of tribofilm growth is proportional to the pressure (or shear stress) at the asperity level (σ), and the additive reactivity (ΔU_{act}).

The aforementioned stress-activated model is commonly accepted for tribofilm growth [116–118]. However, the tribofilm removal process is not well understood, and no accurate equation exists to model it. Jacobs and Carpick used the stress-activated model for the atom loss rate caused by wear [119]. Also, Felts et al. employed it for oxygen removal from graphene [120]. Chen et al. modeled tribofilm removal using a linear wear model [121] in which the tribofilm removal rate is a function of tribofilm height. Azam et al. employed a modified format of the Archard wear model that has a variable wear coefficient [122]. This is considered reasonable since tribofilm hardness decreases with the thickness of the tribofilm [123]. Unfortunately, none of these theories has gained widespread acceptance or been shown to accurately predict the removal of a tribofilm subjected to wear.

1.7 Core of the thesis

Lubrication in gears is a complex phenomenon that is influenced by several factors. Lubrication is a system property, and it is affected by oil properties, oil-surface interaction, and working conditions. All these factors are very important in the gear design process to prevent failures such as scuffing. Today's design trend is toward the higher power density, longer life, and higher energy efficiency of machines. This high performance demand results in a more challenging operational environment for components. The failure probability of machine elements can be reduced by geometrical design, material improvement, or by using a better lubricant. Lubrication may be improved by using a better base oil to reduce the friction and temperature, and/or using additives that protect the surface against failures such as scuffing. There are standards by which a safety factor against the scuffing failure of an oil can be calculated [95–97], but it does not present any detailed information on the fundamental aspects behind the damage occurring in the gear contact. On the other hand, a purely scientific approach is usually far removed from real conditions and cannot easily be used in an industrial approach. Thus, it is very important to develop a method that presents a scientific insight into scuffing and friction, while being applicable for an engineering approach.

On the other hand, lubricant formulations are undergoing changes as a result of environmental and sustainability concerns. Reduced oil reserves, rising oil costs, and environmental concerns have increased interest in environmentally friendly lubricants [13]. Diverse sectors are adjusting their values in order to mitigate environmental harm and prevent the negative consequences of an oil spill. Lubricant leakage is a significant cause of pollution in the environment, accounting for between 40% and 50% of Europe's five million tonnes of spent lubricant [15]. Lubricants that are environmentally acceptable (EALs) and have a high biodegradability (≥60%) [15] are much less ecologically damaging and may be utilized in environmentally sensitive industries such as the maritime sector and wind turbines. These oils have been on the market since the 1970s [12], but are still not widely accepted among designers. These oils are expensive, and the properties are not yet very well-tuned. However, oil manufacturers are continually improving their tribological performance via the development of new base oils and additive packages [12,21,100,124]. Investigating the performance of these oils enables engineers to comprehend the risks and benefits associated with their use in machine components.

To examine a lubricant's performance, it should be tested in a realistic machine under realistic conditions. While real component tests such as FZG gear tests are important for evaluating lubricant performance, they do not provide insight into the lubrication conditions at different contact points. Also, these tests are expensive and time-consuming. Thus, laboratory tests such as the ball-on-disc test may be used for primary screening and achieving scientifically analyzed findings that can be applied to actual components. It is also essential to conduct this preliminary laboratory testing using a fully formulated lubricant, such as industrial EALs whose usage is growing. Using industrial oils will be beneficial as the findings can be linked to the actual component tests. Additionally, it is critical to examine how the base oil and tribofilm contribute to gear lubrication.

1.7.1 Objective and scope

The main objectives of this thesis are to study the lubrication in a simulated gear contact along the line of action. The lubrication factors that were targeted include friction, temperature, tribofilm formation, and its influence on scuffing and lubrication regimes.

The research questions of this thesis are the following:

- How do the friction and contact temperature vary in the EHL regime over a wide range of entrainment speeds and pressures, and how are they different in EALs compared to the mineral oils?

- How does a tribofilm evolve along the line of action in gears, and how is the tribofilm influential in friction and scuffing?

Friction measurements were made using a mini-traction machine that provides a rolling/sliding contact between a ball and a disc. The aim of the friction experimental plan was to simulate the friction of a gear contact along the line of action using the ball-on-disc test technique. After measuring the friction, the friction data were also used in a model that predicted the oil temperature in the contact across a broad range of entrainment speeds, slide-to-roll ratios, and pressures. Both the ball and disc were manufactured from AISI 52100 steel, which has an elastic modulus of 207 GPa and a hardness of 750–770 HV, which is quite close to what is found in gears manufactured from case-hardened steel 20 NiCrMo2-2.

To better understand tribofilm evolution, an experimental method [66] was used that could mimic the gear contact. This technique was able to measure the tribofilm growth at different points along the line of action. The tribofilm was measured using a method called Spacer Layer Imaging (SLIM) that could record the tribofilm image on the contact.

For the scuffing test, the ball was replaced with a so-called barrel specimen that had a smaller contact area. This smaller contact area provided a contact pressure up to 3 GPa, which is sufficient for testing high-performance industrial oils. The scuffing capacity was evaluated by a contra-rotating method. A new testing strategy was defined that consisted of scuffing steps that are a combination of sliding speed steps and load steps. During these scuffing steps, the tribofilm was monitored using the SLIM technique.

1.7.2 Outline and scientific contribution

This thesis is composed of four chapters: 1. Introduction, 2. Methods, 3. Results and Discussion, and 4. Conclusions. The first chapter contains the introduction. This chapter consists of a literature review of the relevant research, the motivation for the research, its objectives and scope, and an outline of the scientific contribution of the work. The second chapter describes the materials and methods used in the experimental work and modeling. The experimental device, developed testing methods, and the numerical models are explained in detail. The third chapter is devoted to presenting and discussing the results. The third chapter is divided into two sections. The first section deals with friction and temperature maps, and the second section discusses tribofilm evolution in the gear contact and during scuffing failure, and also its effect on the lubrication regime. The fourth chapter summarizes and presents the main conclusions of the work.

The scientific contributions of this thesis are as follows:

- Development of a suitable method for estimating oil film temperature maps for a wide range of SRRs, entrainment speeds, and pressures.

- Enhancement of the knowledge of tribofilm influence on friction in an EHL/mixed lubrication regime, its influence on metal-metal contact, and the mechanism by which this phenomenon occurs.

- An increased understanding of tribofilm evolution in a gear contact along the line of action, and during different stages of running-in.

- Development of a novel scuffing test method using a barrel-on-disc specimen setup that is able to accurately evaluate the oil scuffing capacity and reveal the tribofilm evolution during the scuffing test.

2 METHODS

2.1 Mini-traction machine

All the tests were conducted using a mini-traction machine (MTM). As shown in Figure 5, the ball and disc are in rolling/sliding contact. The tilted ball shaft reduces the spin, and the friction force is measured through a load cell placed between the ball shaft and the instrument body. Fully automated control of load, velocity, temperature, and test length enables the completion of a series of tests. The ball and disc are operated separately, allowing for a wide variety of lubricant entrainment speeds and slide-to-roll ratios. Equations 3-5 define the lubricant entrainment speed, sliding speed, and the slide-to-roll ratio (SRR):

$$U_e = \frac{U_d + U_b}{2} \tag{3}$$

$$U_s = U_d - U_b \tag{4}$$

$$SRR = \frac{U_s}{U_e} \tag{5}$$

where U_d and U_b are the disc and ball circumferential velocities, respectively, U_e is the entrainment velocity, and U_s is the sliding velocity.

Two thermometers, one in the lubricant and one on the pot wall, were used to determine the lubricant and pot temperatures. Automatic temperature control was provided by a heater and circulating fluid was supplied by external heater/cooler equipment. Some performance values of the machine are presented below:

- Normal load: 0 to 75 N
- Hertzian maximum contact pressure: 0 to 1.25 GPa (standard specimens) up to 3.1 GPa with alternative specimens

- Ball/disc maximum sliding speed: -4 to 4 m/s
- Temperature Range: -25 to 150 °C
- Test Sample Volume: 35 ml (10 ml with an optional pot filler)

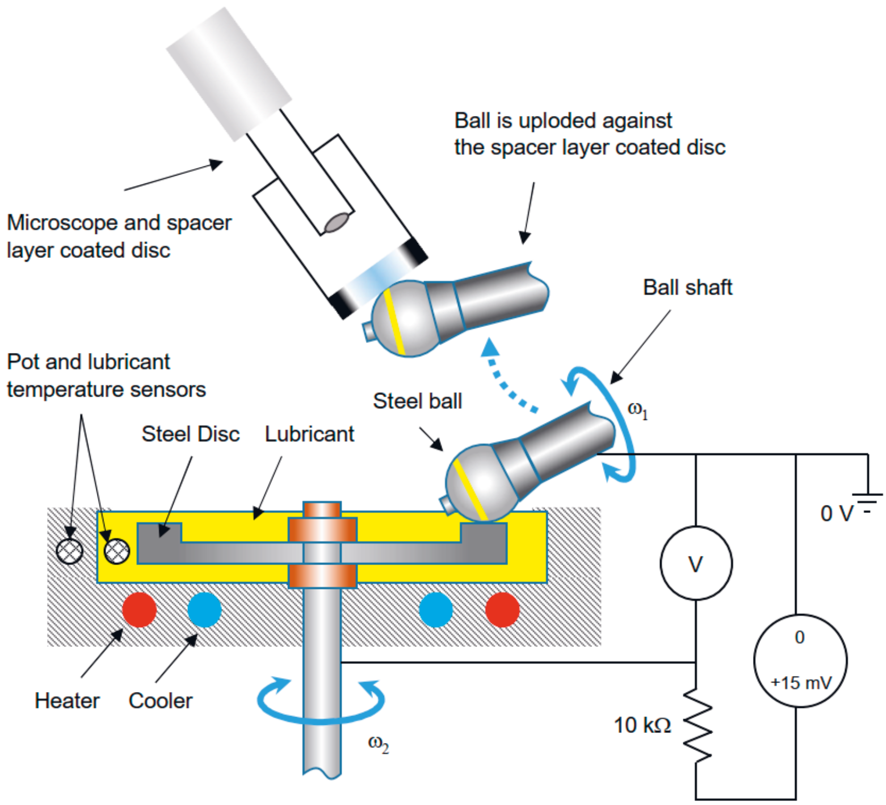

Figure 5. Schematic of MTM [Publication I]

Due to its speed, small size, and safety, the ball-on-disc test is regarded as a critical instrument for the development of novel lubricants. It demonstrates excellent reproducibility and control across a broad variety of parameters, including speed, temperature, and load [11]. There are certain issues when simulating gear contact with a twin-disc machine that apply to ball-on-disc machines as well. These issues can be summarized as follows [66,125]:

- In comparison to contemporary gears, the test specimens have a distinct surface texture and orientation

- Different film formation process that is continuous in ball-on-disc, while a new film is generated in each tooth engagement in the gears

- Lower dynamic effects in MTM compared to gears

Despite these limitations, the ball-on-disc test has been effectively utilized in fundamental lubricant testing research. Björling et al. used the friction maps concept previously generated in Ref. [70] to establish a connection between the friction values obtained using the ball-on-disc test and FZG test equipment [50]. The findings indicated that, when FZG and ball-on-disc devices are used to rank the friction performance of various oils, the results are identical. Thus, it can be concluded that utilizing the ball-on-disc technique is a suitable approach for screening the performance of gear oils prior to doing complete gear testing. This enables the selection of an appropriate lubricant for a given condition.

2.1.1 ECR option

The ECR (Electrical Contact Resistance) is an add-on to the mini-traction machine. The electrical resistance is measured between the disc and the upper specimen (ball or barrel). The schematics of the ECR setup on the MTM and the equivalent circuit are shown in Figure 5. In series with the ball-disc contact, a balancing resistor is connected and an electrical potential of about 15mV is applied across both. A voltage divider is then formed by the contact resistance and balancing resistor. When the ball and disc are completely separated (open circuit), the voltage at the disc equals the supplied voltage (15mV), resulting in a potential of 0V across the balancing resistor. This will represent 100% ECR. When the ball and disc make direct metal-to-metal contact, the disc voltage will be zero volts, since this is a short circuit to ground. As a result, the full voltage drop (15mV) occurs across the balancing resistor. This will account for 0% ECR.

The ECR is a function of:

- Contact area: a smaller contact area results in a larger resistance and therefore a higher ECR value. The contact area is determined by the shape and material properties of the specimens (Young's modulus), as well as the applied load.

- Electrical resistance inherent in the materials in contact

- Inherent electrical resistance of the lubricant

- Interaction between film thickness and asperity. This is closely linked to the contact's lubrication regime.

The Stribeck curve shown in Figure 6 illustrates the various lubrication regimes. When the entrainment speed and/or viscosity are sufficiently high (as in hydrodynamic HD and EHL lubrication regimes), the lubricant film completely separates the contact surfaces. The ECR reading should be equal to (or near to) 100%. As the speed and/or viscosity decrease, the film thickness drops, and the contact enters the mixed lubrication regime, in which the asperities start to contact each other. The ECR value decreases and reaches zero when the asperity contact increases.

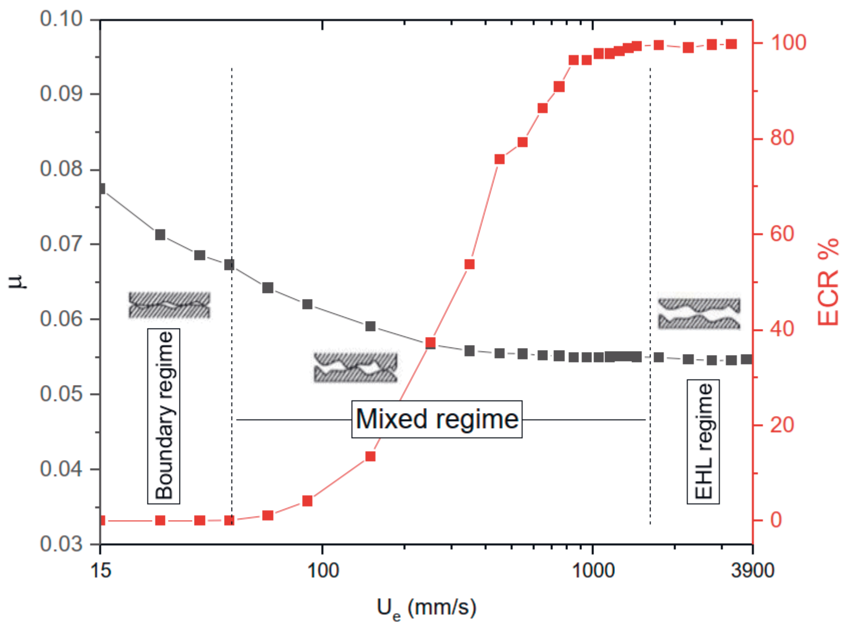

Figure 6. Electrical contact resistance in different lubrication regimes

2.1.2 Tribofilm measurement technique

The spacer layer imaging (SLIM) option uses optical interferometry to determine the thickness of the sub-micron additive layers that develop on the specimens throughout the test. The steel test ball is loaded against a glass disc coated with a chromium and silica film to perform the measurement (Figures 5 and 7). A white light source is directed through the microscope and the glass disc to illuminate the contact. A portion of the light is reflected by the chrome layer on the disc, while the remainder passes through the silica layer and any additive film and is reflected back by the steel ball. The interference picture formed by the recombining light pathways is focused onto the imager of a high-resolution RGB camera. A digital frame grabber captures the camera picture, which can be processed by the control software to determine the contact's film thickness map.

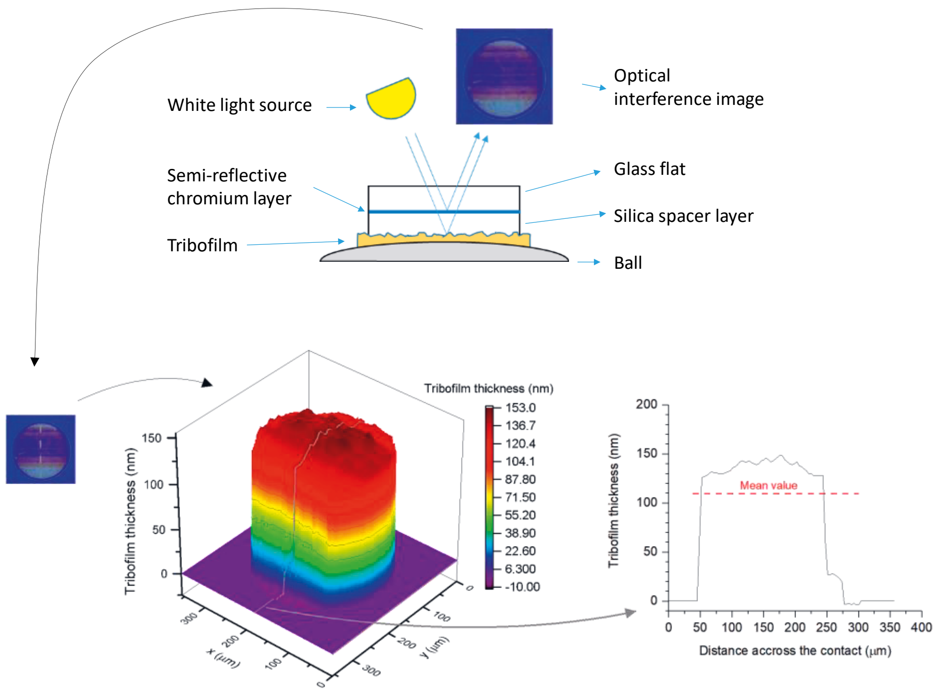

Figure 7. Thickness measurement of a tribofilm using the spacer layer imaging (SLIM) technique

2.2 Test specimen and lubricants

The upper test specimen in Figure 5 can be a ball or a barrel type specimen. The ball and barrel both had a diameter of 19.05 mm, while the barrel featured a 2 mm diameter fillet that made contact with a rotating flat disc. The ball, barrel, and disc specimens were made of AISI 52100 steel with a hardness of 750-770 HV, and elastic modulus of 207 GPa. These parameters are quite close to what is found in a gear manufactured from case-hardened steel 20 NiCrMo2-2. It is important to note that the chemical composition difference between the samples and real gear materials can result in different tribofilm growth rates and surface forces with the lubricant. Thus, the absolute measured parameters of friction and tribofilm growth rate might be different.

The surface roughness is specified in Table 2, where S_a denotes the average roughness height of the area and S_q denotes the root-mean-square roughness height of the area. For each test, a new ball/barrel and disc were utilized, which had been cleaned in an ultrasonic bath for 10 minutes with toluene and isopropanol. A Wyko NT1100 optical profilometer was used for measuring the roughness values. The measured area was at least 0.5×0.5 mm² for the smooth specimens and 4×4 mm² for the rough specimens.

It is worthy of mention that there is a difference between the roughness values of the smooth specimens reported in Table 2, and the values which are reported in Publications I-III. The roughness parameters in the Publications I-III were measured using an Alicona InfiniteFocus G5 optical profilometer, but the values reported in Table 2 were measured using a Wyko NT1100 optical profilometer, which is more accurate. However, this difference does not make any significant difference to the research outcomes, as it did not change the lubrication regimes under which the tests were performed.

Table 2. Ball/Barrel and disc average roughness parameters

Specimen		Sa (nm)	Sq (nm)
Ball & Barrel		8	10
Disc	smooth	8	10
	rough	125	173

Based on each experimental plan, some of the oils listed in Table 3 were chosen for testing. The testing included a total of five different oils. Four of these oils are gear oils with a viscosity grade of 150 VG. Two of these oils comply with the US EPA's "Environmentally Acceptable Lubricants" criteria. Additionally, another mineral engine oil was chosen since it has a comparable kinematic viscosity at 40 °C and is in practice utilized for gear lubrication in ships. Except for oil M1, which is an engine oil, all of the oils conform to DIN 51517 part 3 (CLP) standards. The following table details the properties for the oils:

Table 3. Typical properties of the lubricants used, according to the manufacturer data sheet

	Kin. Vis. @40 °C (mm^2/s)	Kin. Vis. @100 °C (mm^2/s)	ρ @15 °C (kg/m^3)	VI	Comment
EAL 1	148.2	19.1	970	146	Synthetic gear oil, EAL
EAL 2	150	17.8	929.4	135	Synthetic gear oil, EAL
M1	127.6	13.83	908	105	Mineral engine oil
M2	150	14.7	890	97	Mineral gear oil
M3	150	15	897	100	Mineral gear oil

2.3 Friction and temperature mapping

2.3.1 Friction mapping

Björling et al. demonstrated the correlation between the friction of a ball on a disc machine and a gear contact in an FZG machine [50]. The spur gear set was earlier used by Kleemola and Lehtovaara [43], and has a center distance of 91.5 mm, gear ratio of 1, and normal module of 4.5 mm. For this case, the SRR ranges between 0 and 1.1 at various locations along the action line (Fig. 8a), and the entrainment speed indicates the gear set's rotational speed. The entrainment speed of 2.5 m/s corresponds to the rotational speed of 1366 rpm.

According to the method devised by Björling et al. [50], the friction measurement was carried out at different U_es and SRRs. By plotting the coefficient of friction

(COF) of the points, a friction map can be constructed. The COF was determined in this experimental design at the data points shown in Figure 8b.

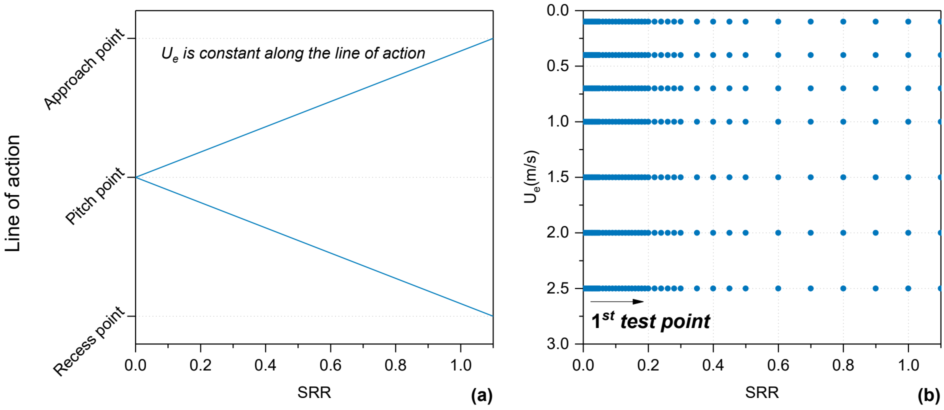

Figure 8. Estimating friction along the gear line of action: (a) Changes in SRR along the line of action [50,66]. (b) Test points for measuring the friction and calculating the temperature [Publication II]

To investigate the effect of pressure, a test was conducted at four distinct maximum Hertzian pressures: 0.65 GPa, 0.95 GPa, 1.10 GPa, and 1.25 GPa. The maximum Hertzian pressure of 1.25 corresponds to a torque of approximately 303 Nm in the aforementioned specific spur gear set.

Notably, for entrainment rates less than 0.5 m/s, the lubrication regime transitions to a mixed regime for the lubricants used. As a result, the friction maps display only data at entrainment speeds greater than 0.5 m/s, excluding the influence of asperity contact.

The technique for deriving the friction maps is shown in Figure 9. In Figure 9a, a three-dimensional friction map is produced using the COF values at the data points. Then, a two-dimensional friction map is created by projecting the three-dimensional map to the plane of U_e-SRR while retaining the friction contours and color variations that indicate COF changes.

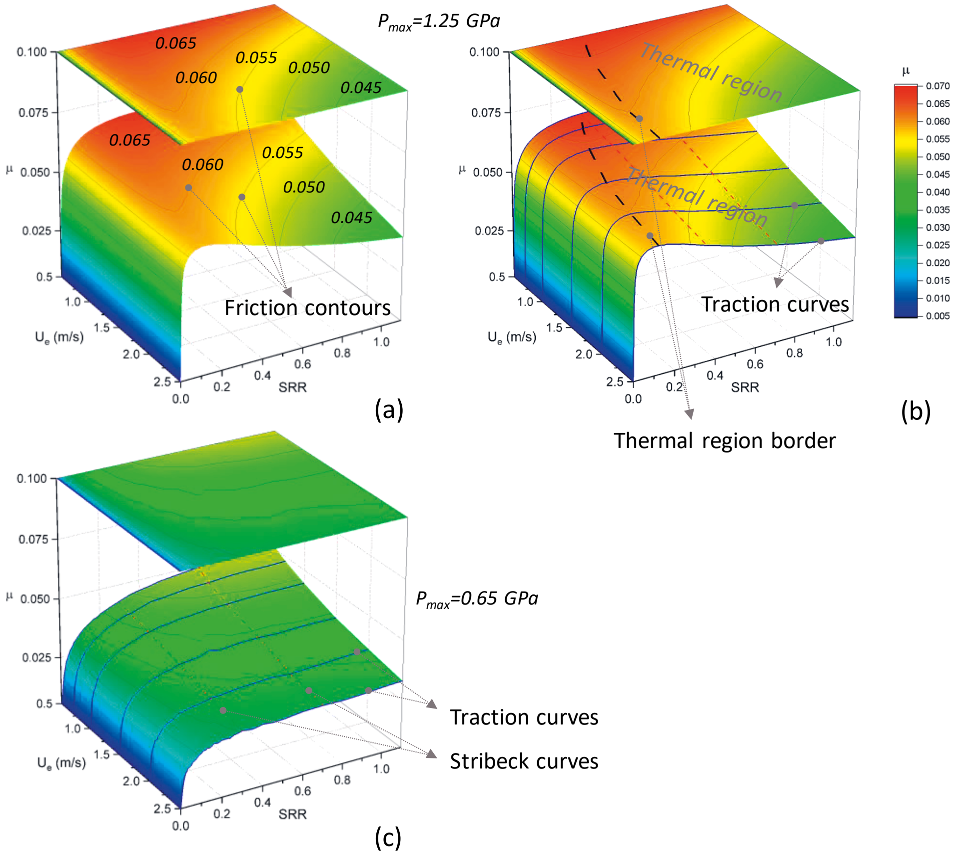

Figure 9. Extracting 2D friction map from 3D friction map of M1: (a) Friction contours on 2D and 3D friction maps of M1 at P_{max}=1.25, (b) Depiction of the thermal region for M1 at P_{max}=1.25, (c) 2D and 3D friction maps of M1 at P_{max}=0.65, and depiction of traction and Stribeck curves [Publication II]

2.3.2 Temperature mapping

The friction maps of the oils were plotted using the technique illustrated in Figure 9, and then temperature maps were generated using the model proposed below. To determine the contact temperature, it is assumed that the rolling/sliding contact has an EHL lubrication regime. Because heat is generated during shearing and dissipated by conduction in the normal direction, there is little heat generated by compressive heating or inlet shear heating caused by Poiseuille flow. Additionally, the Couette flow is considered to be dominant under EHL conditions, and therefore the shear strain rate is given as:

$$\dot{\gamma} = \frac{U_s}{h_c} \tag{6}$$

By examining data points with specific film thickness values greater than 3, the contact may be assumed to be the EHL regime, which ignores the impact of asperity contact on friction and heat generation. The EHL regime was verified by ECR measurement prior to the experiment. With the aforementioned assumptions, the mean oil film temperature in an EHL contact increases above the inlet supply temperature by two temperature rise terms: the transient increase in temperature of the contacting surfaces, denoted by the mean flash temperature rise $\Delta\bar{T}_{flash}$ [85], and the oil film temperature rise above the surfaces, denoted by $\Delta\bar{T}_{oil}$. Each term, according to Ref. [71], can be expressed as Eqs. 7-9:

$$\bar{T} = T_{supply} + \Delta\bar{T}_{flash} + \Delta\bar{T}_{oil} \tag{7}$$

$$\Delta\bar{T}_{flash} = \frac{1}{(2\pi K\rho c)^{0.5}} (\frac{2b}{U_e})^{0.5} q^{"} \tag{8}$$

$$\Delta\bar{T}_{oil} = \frac{h_c}{8K_{oil}} q^{"} \tag{9}$$

where $K, \rho,$ and c are the thermal conductivity, density, and specific heat of the surfaces (AISI 52100 steel), respectively. b is the contact halfwidth and K_{oil} is the oil thermal conductivity. $q^{"}$ is the rate of heat generation per unit area given by Eq. 10 [71]:

$$q^{"} = \frac{\mu F U_s}{\pi b^2} = \bar{\tau}\dot{\gamma}h_c \tag{10}$$

where μ is the coefficient of friction (COF), F the normal applied load, and $\bar{\tau}$ the mean shear stress calculated by $\bar{\tau} = \mu\frac{F}{\pi a^2}$, $\dot{\gamma}$ the strain rate. h_c is the central film thickness calculated from the Hamrock-Dowson formula [5] and corrected by the thermal correction factor proposed by Gupta et al. [6].

Utilizing the speed parameter $U = \frac{\eta_0 U_e}{E^* R_x}$, the material parameter $G = \alpha E^*$, and the load parameter $W = \frac{F}{E^* R_x^2}$, the central film thickness can be calculated from Eqs. 11-13:

$$h_c = h_{c,iso} \cdot \phi_{thermal} \quad \textbf{(11)}$$

$$h_{c,iso} = 2.69 R_x (U^{0.67})(G^{0.53})(W^{-0.068})(1 - 0.61 e^{-0.73k}) \quad \textbf{(12)}$$

$$\phi_{thermal} = \frac{1 - 13.2(p_H/E^*)L^{0.42}}{1 + 0.213(1 + 2.23\mathrm{SRR}^{0.83})L^{0.64}} \quad \textbf{(13)}$$

where L is the thermal loading parameter ($L = -\frac{\partial \eta}{\partial T}\frac{U_e^2}{k_{oil}}$), E^* is the reduced Young's Modulus (Pa), R_x the radius of curvature in the sliding direction (m), η_0 the dynamic viscosity of the lubricant (Pa s), and $k = 1.03$. The pressure-viscosity coefficient α (Pa^{-1}) was calculated using the method presented in Ref. [30].

It is worth noting that the film thickness calculation does not account for shear-thinning, which results in an overestimation of the $\Delta \overline{T}_{oil}$ term. Additionally, the denominator value of 8 is based on the assumption that heat is distributed equally across the film and indicates the highest temperature at the film's median line [71]. Additionally, based on the data in Ref. [126], the thermal conductivity of the oils is calculated by choosing the closest oil type and computing this value for each mean contact pressure. Table 4 summarizes the estimated parameters for the samples:

Table 4. Estimated properties of oils used

	α @40 °C (1/GPa)	**Thermal conductivity (W/mK)**	**Specific heat capacity (J/kgK)**	**Density (kg/m³)**
Ref.	[30]	[127] **for oils, and** [71] **for ball and disc**	[71]	[71] **for ball and disc**
M1	19.95	0.220-0.273	-	Table 3
M2	20.25	0.220-0.273	-	Table 3
EAL1	13.28	0.243-0.295	-	Table 3
EAL2	13.34	0.243-0.295	-	Table 3
Ball and disc AISI 52100 steel	-	21	460	7800

The contact temperature is considered to have a minimal impact on the pressure-viscosity coefficient, thermal conductivity, density, and specific heat capacity of the oils used in this research.

2.4 Tribofilm measurement method in simulated gear contact

Kleemola and Lehtovaara simulated a gear contact along the line of action experimentally using a twin-disc machine [66]. In their test, the spur gear set had a center distance of 91.5 mm, normal module of 4.5 mm, pressure angle of 20 degrees, face width of 20 mm, contact ratio of 1.45, gear ratio of 1, and profile shift of 0.176. With these parameters, it is possible to estimate the pressure and SRR at a contact point along the line of action, as shown in Figure 10.

Four distinct locations along the line of action were chosen to investigate the evolution of the tribofilm using the SLIM technique. These points are labeled 1–4 in Figure 10. Additionally, a point numbered 5* was tested. This point is not in the theoretical line of action and was used to compare the impact of pressure and SRR. By comparing this point to Point 4, we can examine the impact of SRR, and by comparing it to Points 2 and 3, we can examine the effect of pressure. The parameters of the tested locations are listed in Table 5:

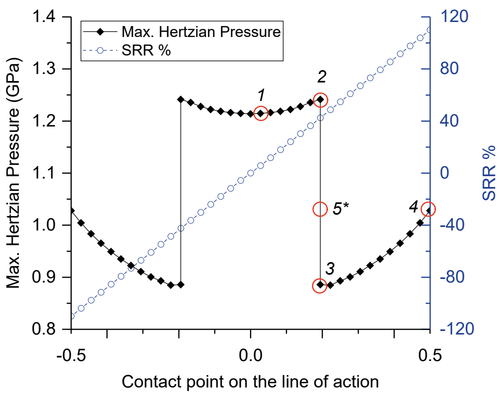

Figure 10. Maximum Hertzian pressure and SRR along the line of action for a specific gear [66]

Table 5. Conditions of the tested points for investigating tribofilm formation along the line of action

	Point 1	Point 2	Point 3	Point 4	Point 5*
SRR %	6.1	42.5	42.5	110	42.5
Entrainment Speed (mm/s)	150	150	150	150	150
Maximum Hertzian pressure (GPa)	1.21	1.24	0.87	1.02	1.02
Temperature °C	100	100	100	100	100

2.5 Method for investigating the influence of the tribofilm on EHL/mixed lubrication transition

In this experiment, the Stribeck curve was tested at different stages of operation under boundary lubrication. Stribeck test represents the coefficient of friction as a function of Hersey number (viscosity*speed/load). Because load and viscosity are constant in this experiment, the Stribeck findings are shown as a coefficient of friction against entrainment speed.

As shown in Figure 11, the Stribeck tests were done three times: once on fresh samples, once after one hour of running, and once after an additional two hours of running. Friction and ECR values were recorded throughout each set of Stribeck tests, and the thickness of the tribofilm was determined using the SLIM method before to and after each test. The evolution of friction, ECR, and tribofilm thickness reveals an oil's capacity to separate contacting surfaces through an EHL film or a tribofilm. The primary objective of this test plan is to assess and compare the EHL/mixed transitions of oils, as well as to investigate the influence of tribofilm thickness on this transition.

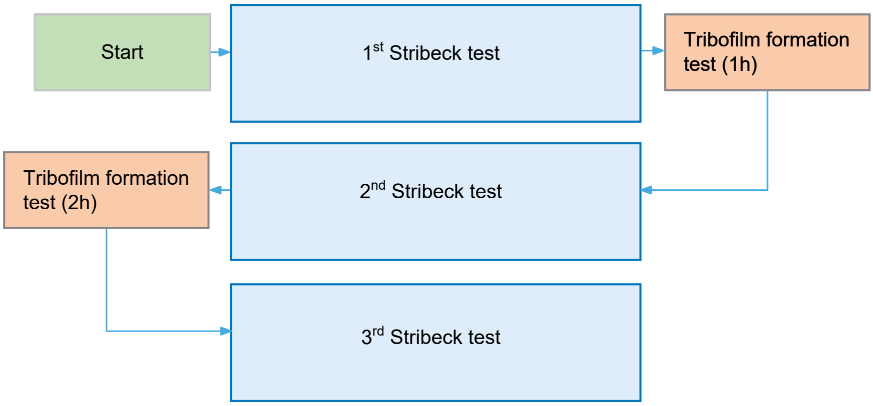

Figure 11. Designed test matrix for investigating the effect of the tribofilm on the lubrication regimes [Publication I]

The test parameters are presented in Table 6:

Table 6. Conditions of Stribeck and tribofilm formation test for investigating the influence of the tribofilm on the lubrication regimes

	Stribeck test	Tribofilm formation test
SRR	0.05	0.50
Entrainment Speed (mm/s)	10-3900	150
Maximum Hertzian pressure (GPa)	1.25	1.11
Temperature °C	40	100
Duration	-	1 h before 2nd Stribeck, and 2 h before 3rd Stribeck

2.6 Scuffing test method

In Section 1.5, the issues of conventional scuffing tests were addressed. These issues include accumulation of wear due to stationary specimens, and severe contact between unworn fresh asperities at the start of each load step. To resolve these issues, in Refs. [99,100], a scuffing test technique for a ball-on-disc test rig was created based on the contra-rotation scuffing test approach. The sliding speed rises in scuffing stages during that contra-rotation scuffing test, but the load and entrainment speed remain constant. This criterion is in direct opposition to the conventional scuffing tests, which use increasing-load stages. This sliding step method [99,100] was intended to overcome the issues with the conventional scuffing tests mentioned earlier. The test technique used in this study is similar to the sliding-step criterion, but modifications were made to account for the high scuffing capacity fully formulated oils.

The first adjustment was to substitute a barrel specimen for the ball specimen. This resulted in high contact pressures of up to 3.06 GPa, which is needed for scuffing testing of industrial oils. The barrel had a diameter of 19.05 mm and a fillet with a diameter of 2 mm that came into contact with the rotating flat disc (Fig. 12).

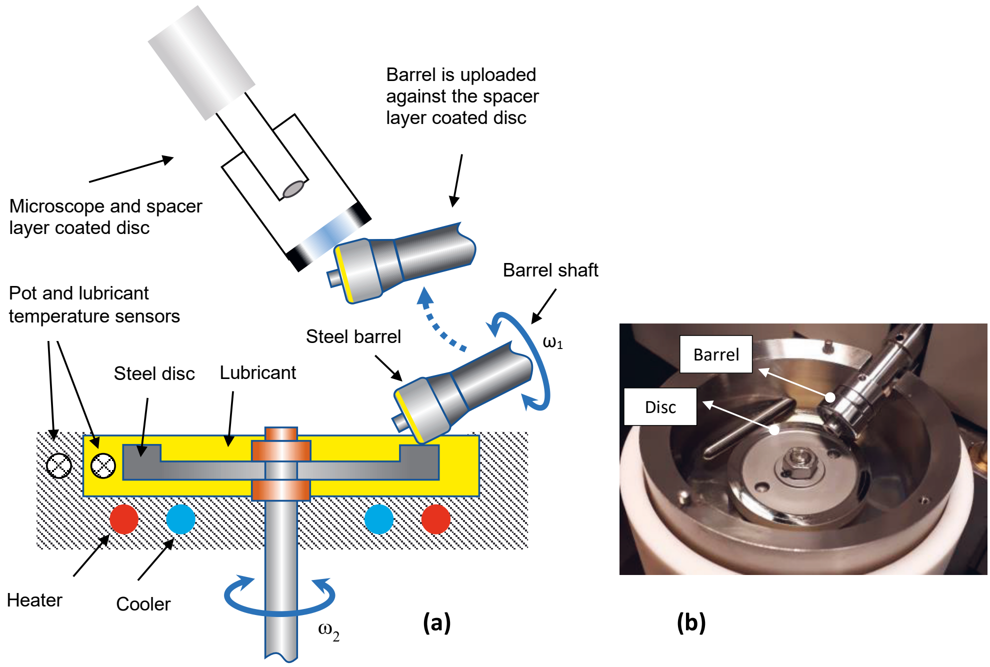

Figure 12. Barrel on disc test: (a) Schematic of MTM with barrel on disc samples (b) Image of the test samples [Publication III]

The next adjustment concerned the running-in stage. It is generally recognized that surface roughness parameters and asperity height distribution play a significant role in the scuffing of machine components [128]. Additionally, running-in modifies not just the roughness and geometry of the surface, but also the material properties of the undersurface [88]. One reason for the wide range of scuffing results is the variation in the microtopography of each of the two surfaces. For the running-in step, Ingram et al. recommended utilizing the actual test load with very low sliding and entrainment rates [100]. Peng et al. found that running-in with the actual test load resulted in significant surface damage and suggested utilizing lower loads to polish the high asperities in the contact area [99]. In this study, a similar low sliding speed, low load running-in with a period of 600 s was used. However, after many tests with this condition, it was revealed that early scuffing occurs, implying unwanted scuffing at low sliding speeds. To avoid this, an additional shorter running-in step with the same load was added to the test plan. These additional run-in periods were carried out with the same pressure as the test but at a reduced sliding speed (red points in Fig. 13 denote running-in).

The third adjustment concerned the load. After fine-tuning the running-in, the initial tests were conducted with a load of 20 N (1.97 GPa) to evaluate the oils' scuffing behavior. The sliding speed was raised in small steps while maintaining a constant 20 N load (Fig. 13 and Table 7). Scuffing appeared for the mineral oils at this load, but not for the EALs, even at sliding velocities of 7000 mm/s. It looked as though the sliding speed-step criterion established in Refs. [99,100] is inefficient for comparing oils with a large variation in scuffing capacity.

In the case of EALs, following the first test with a load of 20 N, the load was raised by 5 N in intermediate steps until it reached 75 N, the machine's maximum load (similar to Fig. 13, but with more intermediate load steps). This procedure was not successful, as no scuffing was seen for EALs. This is because the specimen seemed to have a low maximum pressure owing to progressive wear on the surfaces, as seen in the SLIM images. This demonstrates that raising the load in smaller steps results in wear that postpones the scuffing. The same process was performed at 10-N intervals; however, it was revealed that the wear remained and inhibited scuffing within the machine's operating limits. Three load stages of 20 N (Pmax:1.97 GPa), 50 N (Pmax:2.67 GPa), and eventually 75 N (Pmax:3.06 GPa) demonstrated satisfactory results. Additionally, to avoid excessive wear, the sliding speed was limited to 4000 mm/s for the 20 N and 50 N load steps.

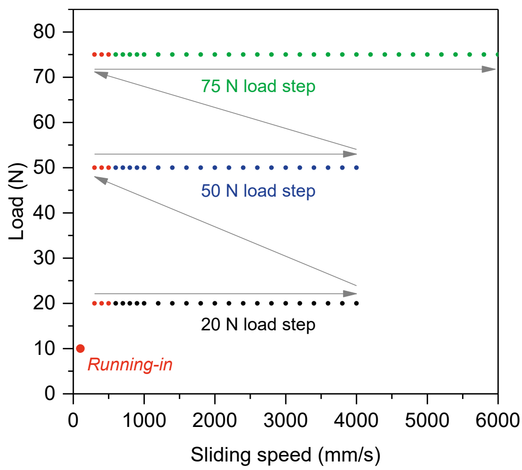

Figure 13. Variation of the load and sliding speed of the developed scuffing test. The duration for each test point is 30 seconds, and there is a rest stage of 30 seconds between each point [Publication III]

The test plan (Fig. 13) begins with the main running-in, followed by an excessive run-in for the load stage of 20 N. Following that, the sliding speed rises from 600 to 4000 mm/s when a force of 20 N is applied (Pmax:1.97 GPa, Pmean:1.31 GPa). If no scuffing is seen, the previously described sliding steps are done with a load of 50 N (Pmax:2.67 GPa, Pmean:1.79 GPa), followed by 75 N (Pmax:3.06 GPa, Pmean:2.05 GPa). Notably, before each load step, an extra running-in period (red points in Fig. 13) with the same load as the load step is considered. This is to avoid contact between unprotected new asperities. In conclusion, this scuffing test technique combines the benefits of the load-step criteria and the sliding speed-step contra-rotation approach. The characteristics are detailed in Figure 13 and Table 7.

Each test point in Figure 13 represents a 30-second test with constant velocity and load. 30 seconds was similarly chosen as the optimal time. Scuffing may be postponed to one or more sliding steps when the duration is between 10 and 20 seconds, as there is insufficient time for temperature increase and adhesion between the surfaces, and when the length is more than 30 seconds, the impact of wear becomes apparent. Following each test point, a 30-second rest step is included to enable the bulk temperature of the specimens to recover to the oil temperature [99]. A SLIM image of the barrel surface is taken during these rest steps.

Table 7. Test parameters

	Running-in	Extra running-in	Test stage	Rest stage
Sliding speed	100 mm/s	300 mm/s-500 mm/s	600 mm/s-4000 mm/s for 20 N and 50 load steps 600 mm/s-6000 mm/s for 70 N	0
Rolling speed	40 mm/s	100 mm/s	100 mm/s	0
Temperature	120 °C	120 °C	120 °C	120 °C
Load	10 N (Pmax: 1.56 GPa)	20 N - Pmax: 1.97 GPa, Pmean: 1.31 GPa 50 N - Pmax: 2.67 GPa, Pmean: 1.79 GPa 75 N - Pmax: 3.06 GPa, Pmean: 2.05 GPa	20 N - Pmax: 1.97 GPa, Pmean: 1.31 GPa 50 N - Pmax: 2.67 GPa, Pmean: 1.79 GPa 75 N - Pmax: 3.06 GPa, Pmean: 2.05 GPa	0
Duration	600 s	30 s per step	30 s per step	30 s

3 RESULTS AND DISCUSSION

3.1 Friction mapping

The friction maps of the oils EAL1, EAL2, M1 and M2 (given in Table 3) were measured using the technique described in Section 2.3. A ball and smooth disc of AISI 52100 steel (Table 2) were in rolling/sliding contact. They both had a hardness of 750-770 HV, and Young's modulus of 207 (GPa). The friction was measured for a wide range of entrainment speeds and SRRs, and the results were plotted as the friction maps. It was observed that there was minimal variation in the COF of two mineral oils. Likewise, this is true for EALs. Thus, just one of the mineral oils (M2) was compared to one EAL (EAL2) regarding the COF.

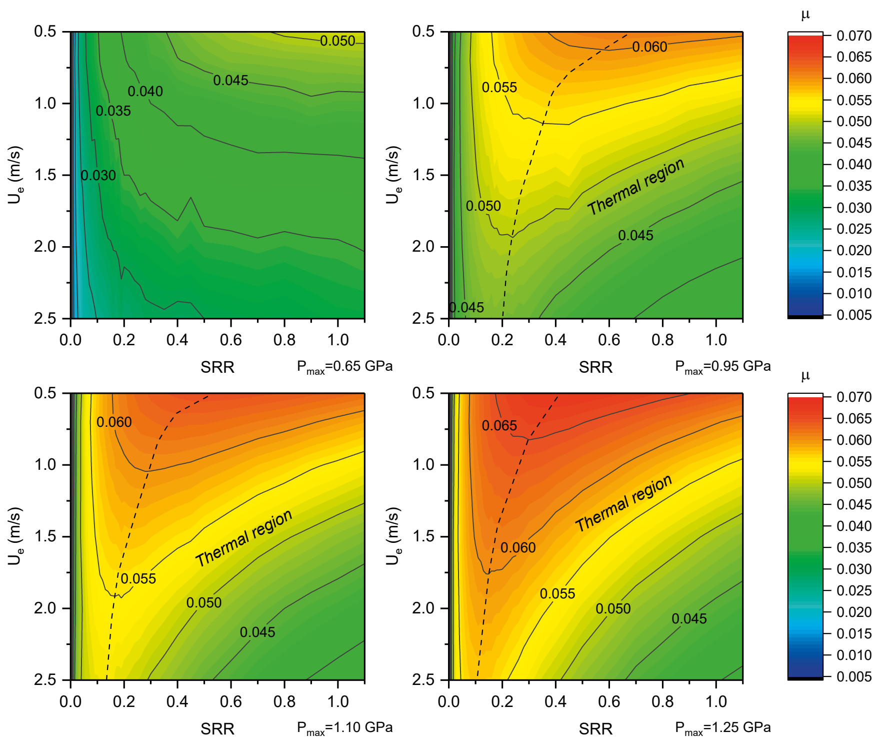

Figure 14. The COF of M2 at different maximum Hertzian contact pressures [Publication II]

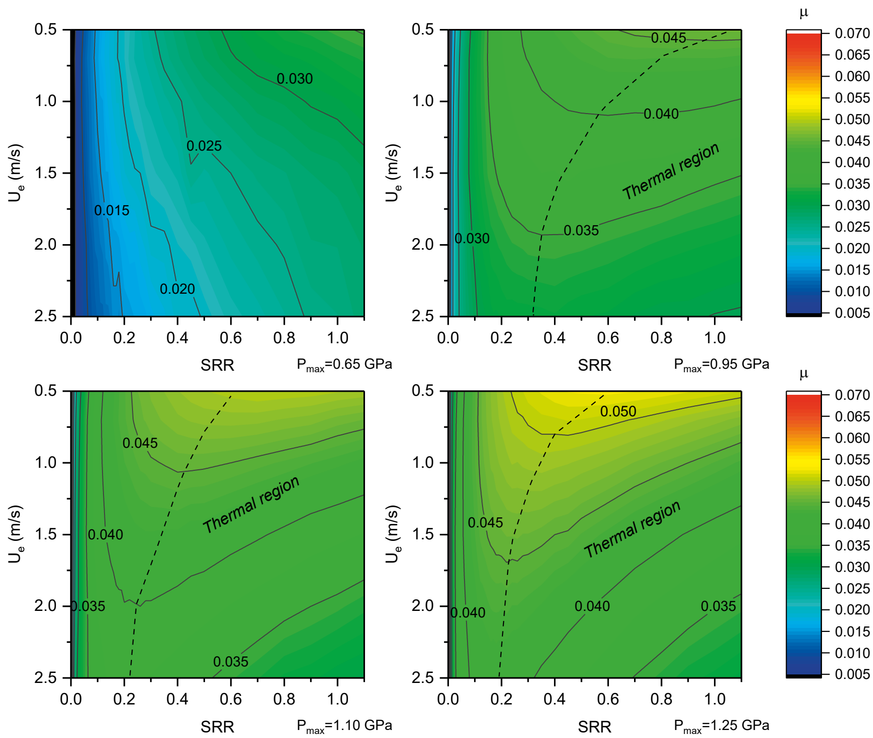

Figure 15. The COF of EAL2 at different maximum Hertzian contact pressures [Publication II]

In all cases (Figs. 14 and 15), increasing the SRR from zero (pure rolling) to higher values caused the friction coefficient to first increase and then peak at the start of the thermal region. For higher SRRs, heat generation is influential, and the temperature increased, resulting in a decrease in viscosity and a decrease in COF. In conclusion, for pressures more than 0.95 GPa, the friction coefficient reaches a maximum near the pitch point (low SRR), while the lowest oil viscosity, and hence the thinnest lubricant film, is observed at the approach or recess points (high SRR).

In Figs. 14 and 15, the increase in entrainment speed results in a decrease in COF when the SRR remains constant. Due to the fact that all friction maps are evaluated under the EHL regime, the increased entrainment speed at a constant SRR results in increased sliding velocity and heat generation, which results in a decrease in oil viscosity and COF.

The COF difference between M2 and EAL2 is seen in Figure 16 at four different pressures:

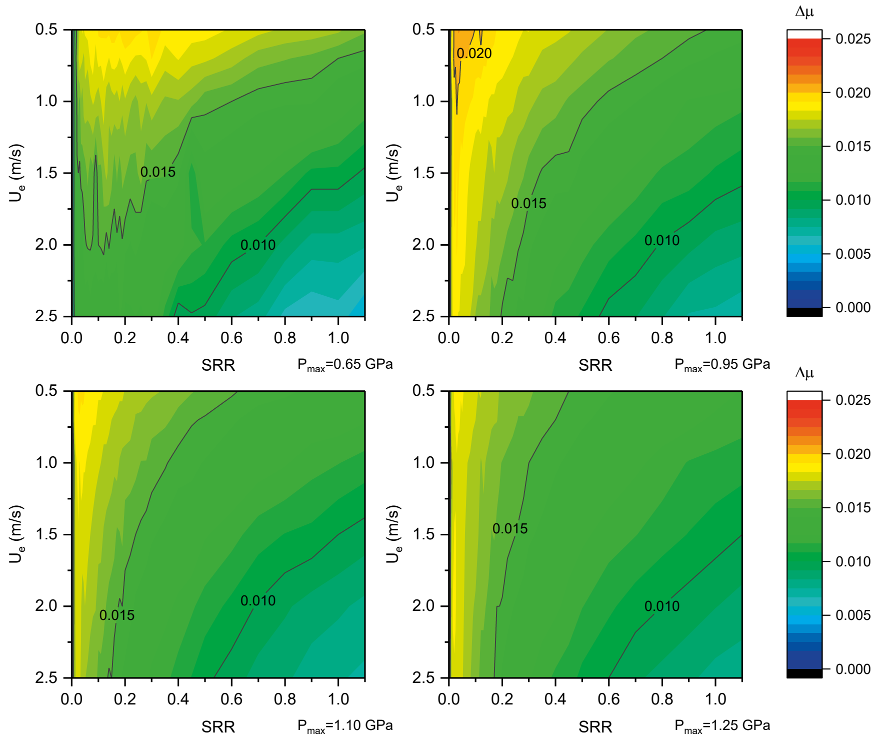

Figure 16. The difference between COF of M2 and EAL2 at different maximum Hertzian contact pressures [Publication II]

The COF is reduced when EALs are used instead of mineral oils, as seen in Figure 16. This decrease is about 0.02 (60% of mineral oil COF) when the SRR and U_e are low, as in the case of roller bearings or gear areas at the pitch point. The COF, on the other hand, decreases by 0.01 (20% of mineral oil COF) at a high SRR and U_e, which corresponds to the conditions near the gear tooth tip.

The results indicate that M2 had a roughly 15 % higher τ_e (limiting shear stress) compared to EAL2. On the other hand, EALs have a lower pressure-viscosity coefficient [Publication II]. Thus, the friction reduction achieved by EALs is mostly due to two rheological parameters: the lower pressure-viscosity coefficient of EALs and their lower limiting shear stress at which shear-thinning occurs.

The friction values might not be directly transferable to the real machine values. The most important limitation lies in the constant pressure assumed in the current methodology, which is in contradiction with the changing radius and pressure in real gears. Also, in real gears, the surface roughness is higher, which leads to operation under the mixed lubrication regime. In the case of high speed gear operation, the friction values can be more relevant. Despite these limitations, this method can be considered as a quick and preliminary test for estimating the oil performance in different gear types. The data elaborated in this experiment are applicable for any gear set in which the SRR and U_e are in the measured range.

3.2 Temperature mapping

Temperature maps are generated from the friction data in the friction maps using the model proposed in Section 2.3.2. The temperature maps of the oils at various pressures are shown in Figs. 17 and 18. When traction curves at constant entrainment speed are considered, the greatest temperatures are seen at high SRRs, which corresponds to gear approach or recess points. When increasing the pressure from 0.65 to 1.25 GPa, the maximum temperature of the mineral oils grows at a rate of 77 °C/GPa, whereas it increases at a rate of 60 °C/GPa for EALs. This reduced rate is mostly owing to the EALs' lower COF and the superior heat conduction of the oil film.

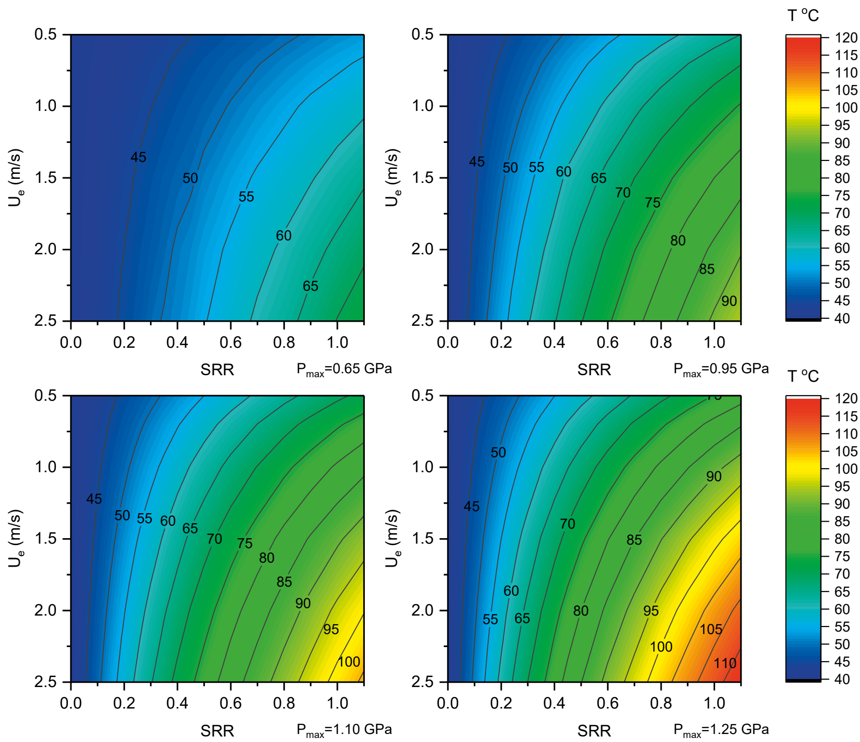

Figure 17. Temperature map of M2 at different maximum Hertzian contact pressures [Publication II]

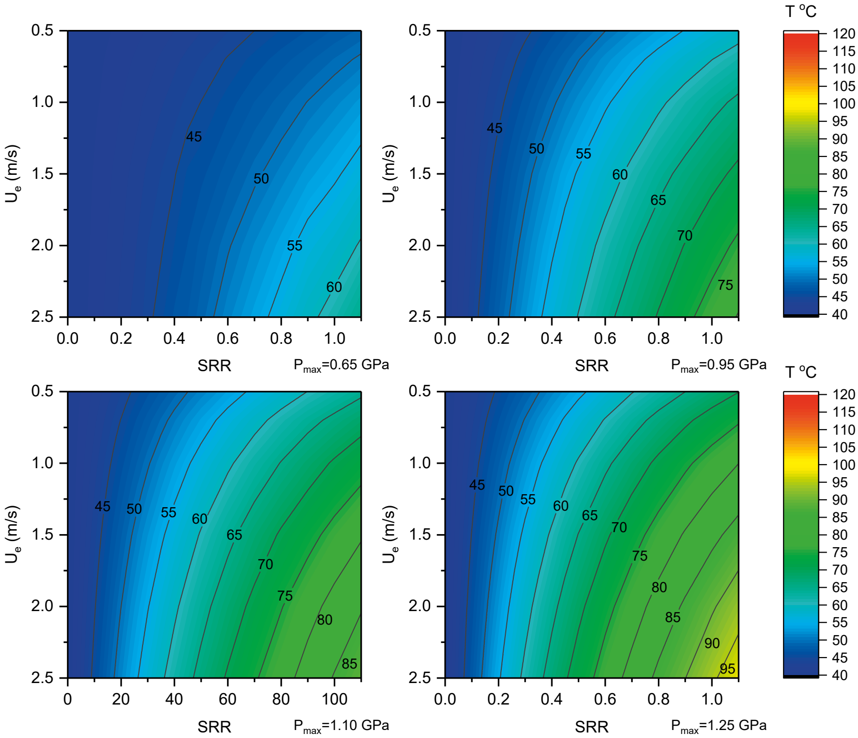

Figure 18. Temperature map of EAL2 at different maximum Hertzian contact pressures [Publication II]

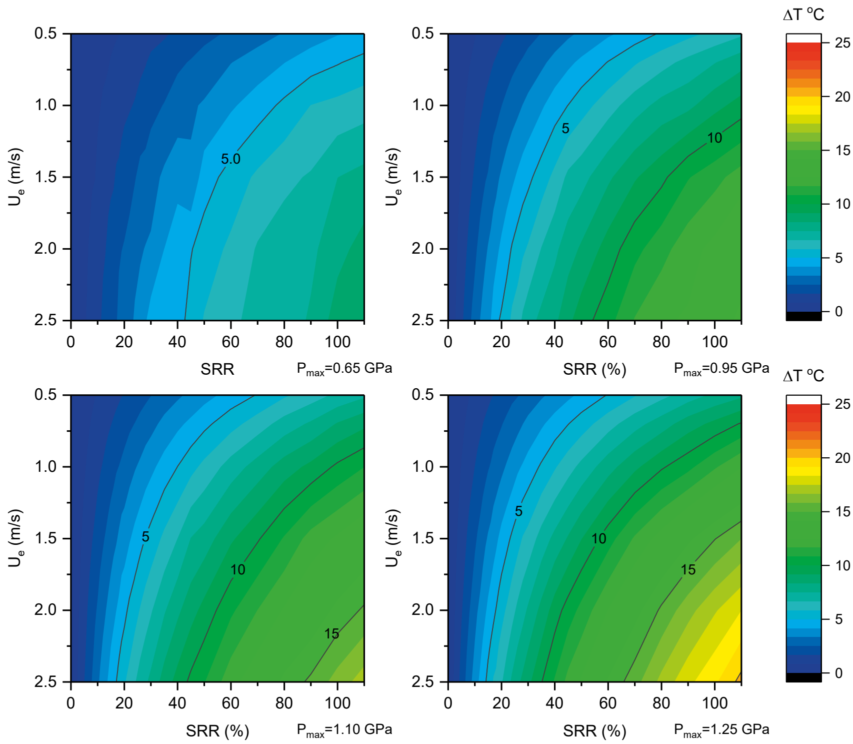

Figure 19. Difference in temperature of M2 and EAL2 at different maximum Hertzian contact pressures [Publication II]

The temperature difference between EAL2 and M2 is shown in Figure 19, and it varies from 5 °C at low SRRs, low U_e, and low pressure to 20 °C at high SRR, high U_e, and high pressure. Equation 8 indicates that EAL2 has a lower temperature due to its lower COF and greater thermal conductivity. The temperature difference between these oils increases when the maximum Hertzian pressure is increased from 0.65 to 1.25 GPa. This demonstrates that EALs are more efficient in terms of heat generation.

3.3 Tribofilm role in lubrication

3.3.1 Influence of the tribofilm on the lubrication regime

In this experiment, a ball and smooth disc of AISI 52100 steel (Table 2) were in rolling/sliding contact. They both had a hardness of 750-770 HV and a Young's Modulus of 207 (GPa). Based on the method explained in Section 2.5, three sets of Stribeck tests were carried out at SRR of 5 %: the 1st Stribeck on the fresh sample, the 2nd Stribeck after a 1-hour rubbing at 100 °C temperature. After the 2nd Stribeck, another additional 2 hours of rubbing at 100 °C was performed, and the 3rd Stribeck was performed (Fig. 11). Friction and ECR values were recorded throughout each set of Stribeck tests, and the thickness of the tribofilm was determined using the SLIM method before and after each test.

According to the Stribeck curves shown in Figure 20, friction was reduced in the EHL regime for all oils. However, in the mixed regime, the responses varied according to the oil. The ECR was raised in all instances as compared to the 1st Stribeck. The ECR may be increased by either flattening high asperity peaks or by forming tribofilms, both of which decrease metal-metal contact [129].

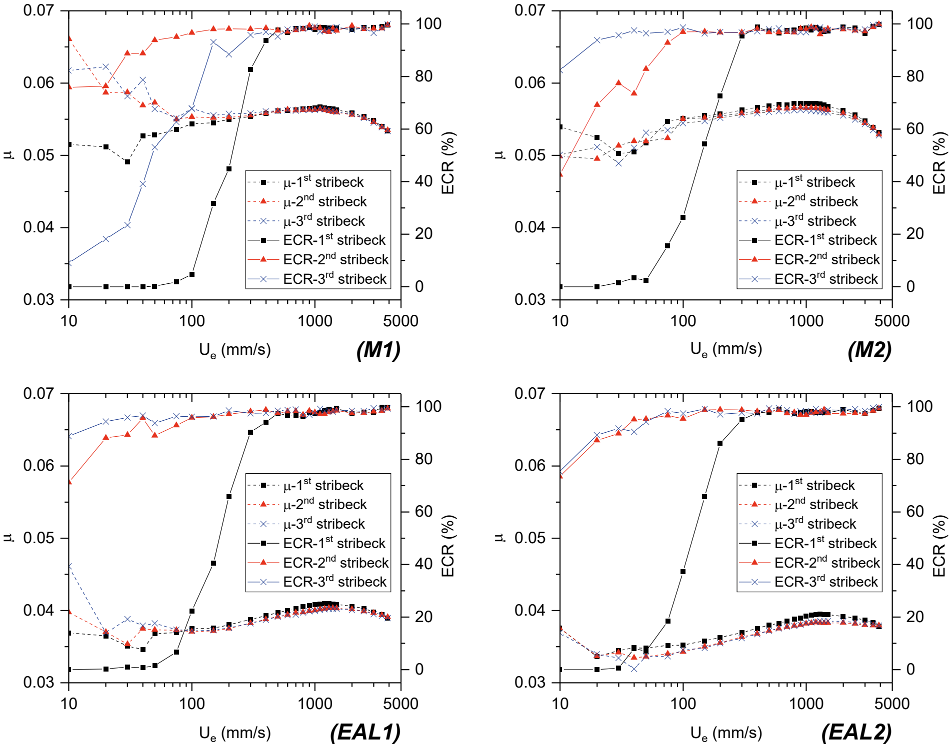

Figure 20. Stribeck curves of the oils. The "1st" is for the fresh samples, the "2nd" after 1 hour of rubbing, and "3rd" after 2 hours of more additional rubbing [Publication I]

On the basis of Figs. 20 and 21, the following observations can be stated about the M1 oil:

a) Friction: With the exception of the first Stribeck, there was increased friction in the mixed and boundary regimes. In the 2nd and 3rd Stribeck curves, the rise in friction started at a higher U_e indicating a weakened EHL film because of the shift of boundary and mixed lubrication to a higher U_e. It is worth noting that the friction was slightly reduced under the EHL regime owing to the flattening of the high peaks.

b) ECR: The ECR was the lowest for the 1st Stribeck. In the 2nd Stribeck, the ECR increased and then decreased for the 3rd Stribeck.

c) Tribofilm: According to Figure 21, the tribofilm thickens at each step, with the thickest occurring before the 3rd Stribeck.

Considering points a) and c), it can be argued that the formation of tribofilms in M1 oil results in increased friction in the mixed and boundary regimes. Dawczyk et al. examined the production of ZDDP tribofilms and found a similar increase in friction, correlating it to increasing roughness [111]. This phenomenon is seen in various tribofilms and is not unique to ZDDP films [130].

From point b), increased ECR in the 2nd Stribeck is consistent with the development of the tribofilm shown in Figure 21 [129]. However, the reduction in ECR in the 3rd Stribeck was unexpected, since the thickest tribofilm can be observed prior to this step (point c)), which would have resulted in the least metal-metal contact. A thick tribofilm may also impact the friction, which is why the increased friction in mixed and boundary lubrication is influenced by increasing tribofilm thickness.

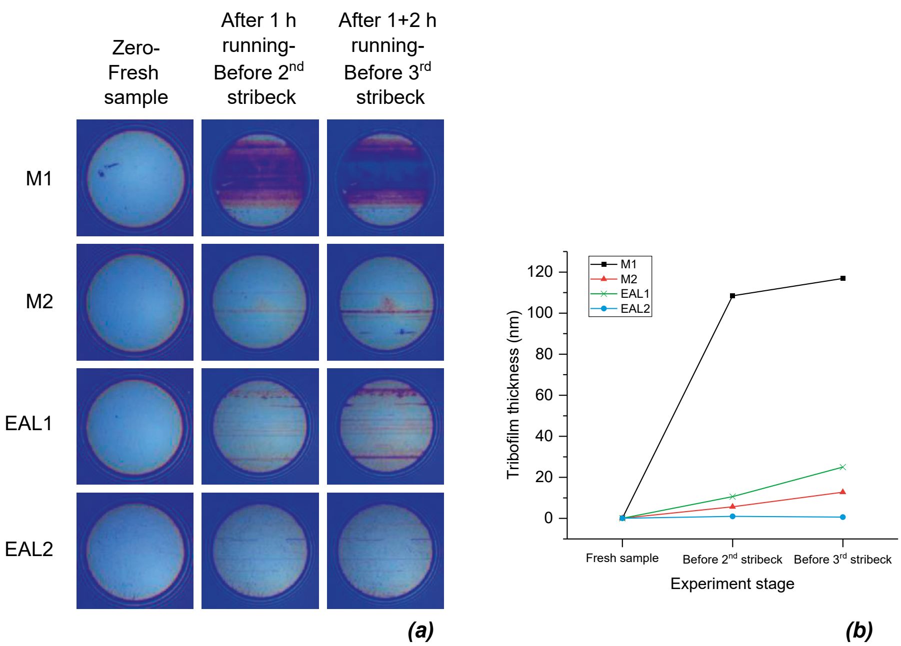

Figure 21. Tribofilm evolution during different stages of the tests: (a) SLIM images, and (b) mean tribofilm thickness [Publication I]

Taylor and Spikes studied the impact of a tribofilm on friction in the mixed regime and suggest that the increased friction in the mixed regime, as well as its extension to a higher U_e, is not only attributable to an increase in roughness. They suggested the following reasons for this shift: [131]:

- Localized oils films around the tribofilm by a lower EHL film due to:
    - Lower pressure-viscosity coefficient
    - Lower viscosity
- Starvation due to
    - Inlet blocking by the tribofilm
    - Lower wettability of tribofilm
- Slip at the boundary of the tribofilm/oil
- Modification of the inlet geometry by the tribofilm

Furthermore, when considering the starvation caused by the buildup of long-chain molecule hydrocarbons in the inlet, the weaker EHL film seems logical. This may explain the drop in ECR in M1's third Stribeck curve. The load is partially sustained by the EHL film and solid-solid contact in mixed and boundary lubrication. When a tribofilm is formed between the surfaces, a portion of the solid contact is covered by the tribofilm, but there is still some degree of asperity contact. By adding the tribofilm share of load carrying capacity, using the equation given in Ref. [132], the load-carrying shares can be written as below:

$$F_T = F_{EHL} + F_C + F_{TF} \tag{14}$$

where F_T is the total load, F_{EHL} is the load carried by the fluid film, F_c is the load carried by the asperities which are not covered by the tribofilm, and F_{TF} is the load carried by the tribofilm. In the case of M1 oil, the oil inhibiting effect of the formed tribofilm results in a poor generation of the EHL film. When the F_{EHL} is reduced, the asperity contacts are raised to compensate for the loss of load from the EHL. Additionally, without the EHL layer, the tribofilm may be penetrated more easily, increasing the probability of metallic contact. The impact of tribofilm development on the metal-metal contact is shown schematically in Figure 22. In Figure 22a, no tribofilm is provided, as is the case with the 1st Stribeck curve. A little expansion of the tribofilm (Fig. 22b) covers a portion of the asperity contacts, increasing the ECR (lower metal-metal contact). For the 3rd Stribeck, the thick tribofilm destroys the

EHL film, resulting in the contact of the asperities separated by the EHL film (Fig. 22c).

The blocking characteristic of the tribofilm produced in the M1 oil may be intensified by the association of the long-chain molecular hydrocarbons present in the oil as impurities. Although Dawczyk et al. argued that roughness is the primary factor affecting the increase in friction [111], it appears that there are other effective parameters that are discussed in the other studies pointing to the inhibiting properties of a patch-like structure in ZDDP tribofilms [130,131,133,134]. This case demonstrates that there is an optimal tribofilm thickness for effective separation of the surfaces; increasing or decreasing the tribofilm thickness results in increased metal-metal contact.

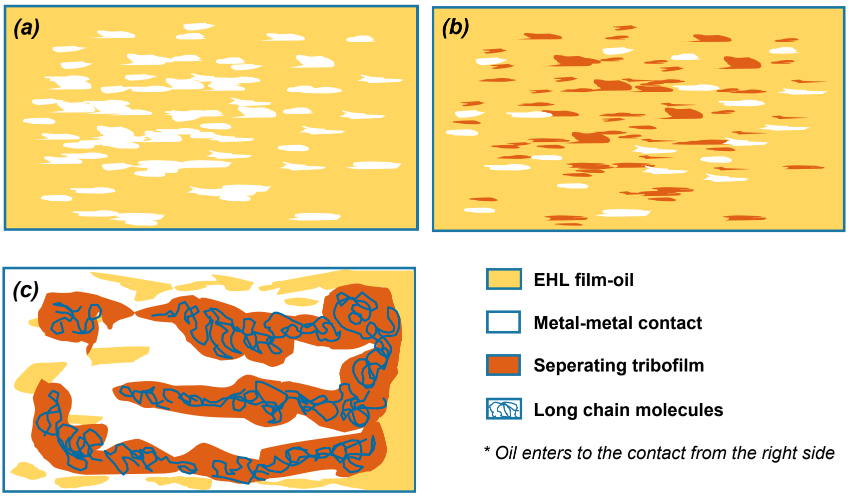

Figure 22. Growth of tribofilm and its effect on solid-solid contact [Publication I]

When compared to the other oils in Figure 20, friction in mixed lubrication was increased for EAL1 as well. This indicates an expansion of the mixed and boundary regimes to higher entrainment speeds, similar to the characteristic seen for M1, albeit with a lower amplitude. This is owing to the development of a tribofilm in EAL1. However, it is not sufficiently big to substantially obstruct the EHL film, and therefore does not result in increased metallic contact (decrease in the ECR). ECR was increased and friction was significantly reduced in the EHL regime for M2 and EAL2. These changes are mostly caused by the flattening of high peaks, the partial covering of the surface by the tribofilm, and perhaps the activation of the friction modifiers. However, none of these two oils exhibits a meaningful change in mixed or boundary friction. Although a trace of tribofilm is evident in the SLIM images of M2, the friction curve does not demonstrate the extension of mixed lubrication to a higher U_e, indicating that the tribofilm in these oils does not cause damage to the EHL film.

3.3.2 Tribofilm evolution along the line of action

The tribofilm formation test was conducted using the technique described in Section 2.4 with two distinct surface roughness (rough and smooth discs in Table 2), one EAL oil (EAL1), and three mineral oils (M1, M2, M3). The aim of the experiment was to determine the tribofilm thickness evolution and the factors that influence the tribofilm presence in a simulated gear contact along the line of action.

Figs. 23 and 24 illustrate the tribofilm evolution of the EAL1 and M3 oils. Four distinct points along the course of action are examined in these pictures (Point 1-4 in Fig 10). Additionally, a point numbered 5* is examined. This point is not in the theoretical line of action and is used to evaluate the effects of pressure and SRR. By comparing this point to Point 4, one can examine the impact of SRR, and by comparing it to Points 2 and 3, the effect of pressure can be examined.

In Figs. 23 and 24, the tribofilm was very thin and difficult to measure owing to wear in the case of Points 1&2. However, the tribofilm thickness was measured at Points 3, 4, and 5*, and the thickness is shown in Figure 25. Points 4 and 5* had the same pressure but a different SRR; nevertheless, in Figure 25, these two points have a nearly identical tribofilm growth rate. Thus, at a constant sliding distance, the SRR has a negligible impact on the tribofilm thickness.

By increasing the maximum Hertzian pressure from 0.87 GPa (Point 3) to 1.02 GPa (Point 5*), the tribofilm thickness grows, as shown in Figs. 23 and 24 . However, by comparing Points 5* and 2, the tribofilm thickness unexpectedly decreases when increasing the pressure (or shear stress). This shows that there is an optimum pressure value at which the tribofilm thickness is at maximum. Gosvami et al. observed the same feature, and suggest that at very high pressures, the wear becomes dominant and prevents tribofilm growth [109]. This excessive wear is clearly visible in Figs. 23 and 24, at Point 2. This pressure can be named **"tribofilm threshold pressure"**. Above this pressure, wear inhibits stable tribofilm growth, but below it, the stress-augmented thermal activation theory can be used to predict the tribofilm thickness.

With oils C and D, wear was significant at all points, and no stable tribofilm could be observed. This indicates a significant level of asperity penetration which immediately removes the tribofilm. Thus, the pressure is too high for these two oils, or, in other words, higher than the tribofilm threshold pressure.

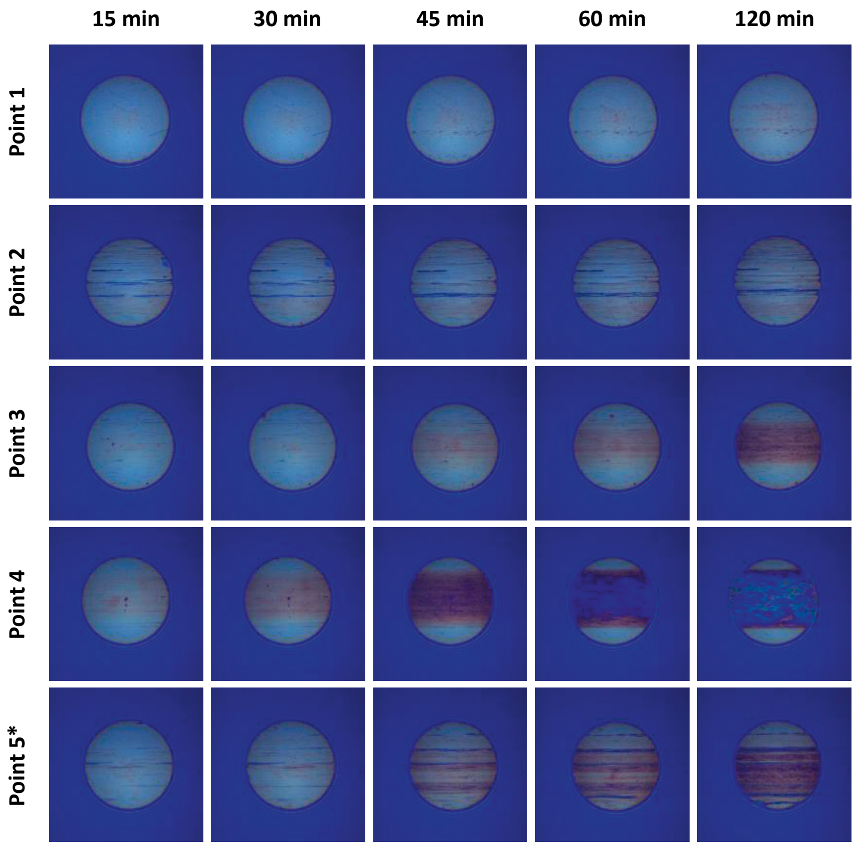

Figure 23. Tribofilm evolution of the EAL1 oil at different points in the line of action [Publication IV]

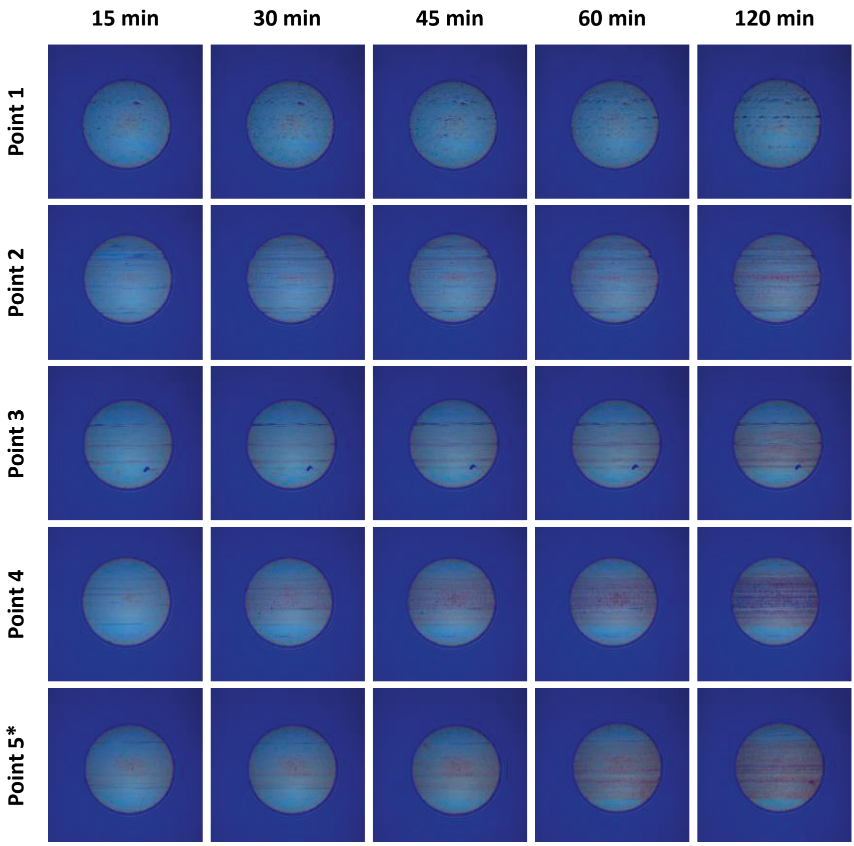

Figure 24. Tribofilm evolution of the M3 oil at different points in the line of action [Publication IV]

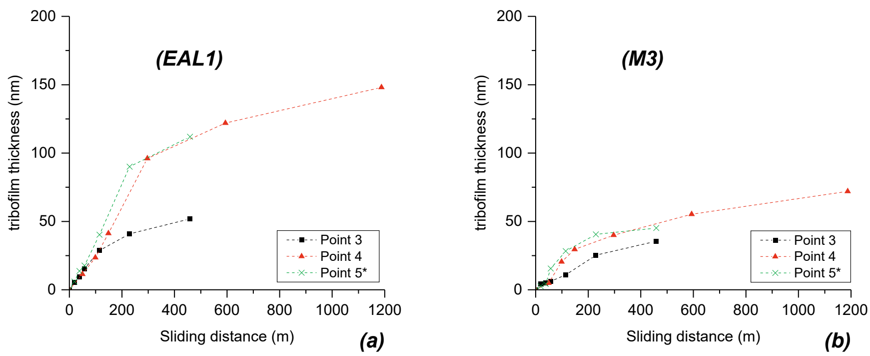

Figure 25. Tribofilm thickness vs sliding distance for oils A and B at different points (rough surface) [Publication IV]

The same experiments were conducted with the smooth disc. During the two-hour period, no significant tribofilm was formed in the case of EAL1. Due to the absence of wear, therefore, the low tribofilm growth rate is attributable to the low shear stress (and low tribofilm growth rate) in the asperity contacts, which was insufficient to drive the mechanochemical reaction of the additive molecules. This highlights the fact that the tribofilm threshold pressure is attributed to the pressure at the asperity level. Thus, for the case of the EAL1 oil, the asperity pressure in the smooth specimen was much less than the threshold pressure.

A different outcome was obtained in the case of the M1 oil. A dense tribofilm was produced on the smooth disc (Fig. 26), whereas no tribofilm had been observed before on the rough disc. In the rough surface test, the wear and tribofilm removal rates were quite high using M1 oil. This implies that for the M1 oil, the asperity pressure was far more than the threshold pressure with the rough disc, while with the smooth disc, the points were less than the threshold pressure but close to it.

In conclusion, the tribofilm threshold pressure is linked to the asperity level pressure. Even though the Hertzian pressure and shear stress remain constant, the pressure at the asperity level may substantially change the tribofilm thickness.

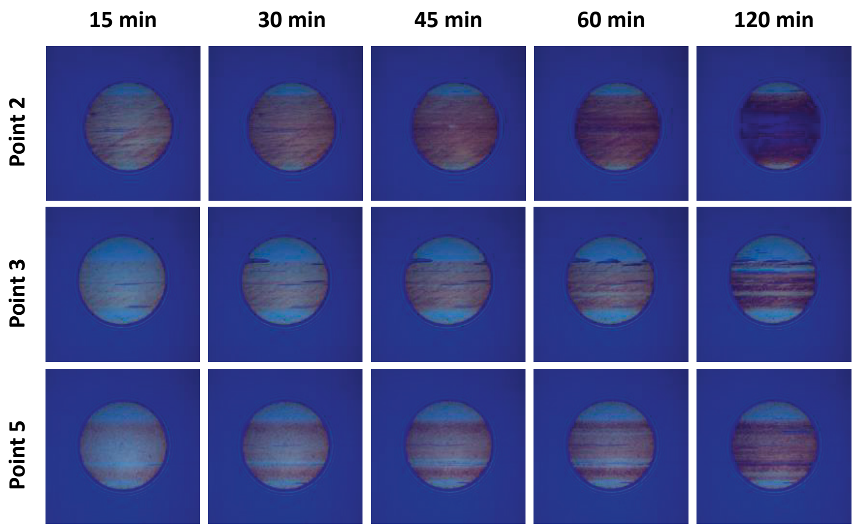

Figure 26. Ball surface after 120 min test with M1 oil using a smooth disc [Publication IV]

If the asperity pressure is less than the threshold pressure, the tribofilm begins to grow and eventually reaches a certain thickness where the growth rate of the tribofilm equals the removal rate of the tribofilm. Thus, the ultimate tribofilm thickness is determined by the rate of tribofilm growth against the rate of tribofilm removal [117]. Eventually, the tribofilm growth rate and removal rate become equal, resulting in the tribofilm height being more or less constant (Fig. 25). On the other hand, the tribofilm removal rate is greater than the tribofilm growth rate when the asperity pressure is higher than the maximum threshold pressure. As a result, no equilibrium is reached, and the specimens will continue to wear.

In conclusion, the thickness of the tribofilm is strongly affected by a specific threshold pressure over which wear prevails. Below this threshold pressure, the rate of tribofilm growth rises with pressure. It is critical to highlight that this pressure is at the asperity level. The tribofilm growth rate versus pressure, and the threshold pressure is schematically illustrated in Figure 27:

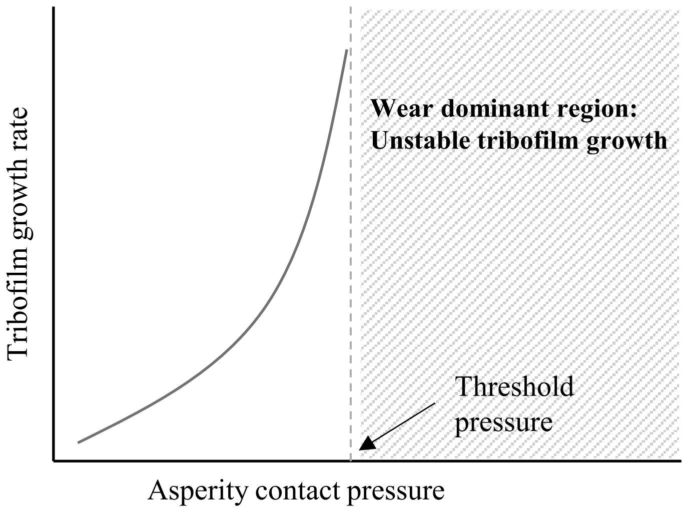

Figure 27. Schematic of the tribofilm growth rate vs asperity contact pressure [Publication IV]

A value for the threshold pressure of EAL1 oil can be roughly estimated using the findings of Khaemba et al. [135]. With the same rough disc specimen and a smooth ball, Khaemba et al. calculated that the average asperity pressure is 3.9 GPa when the applied pressure is equal to 1 GPa. Such values give a "real contact area/nominal contact area" proportion equal to 17%. For the case of the EAL1 oil and the rough disc, the threshold pressure is between 1.02 GPa and 1.24 GPa. Taking the average of 1.13 GPa for such pressure and considering 17% as the proportion of the "real contact area/nominal contact area", the average asperity pressure is 4.4 GPa. This number is a very rough estimation; however, it is comparable to the pressure found by Gosvami et al. [109] for the condition in which wear becomes dominant.

The growth rate of the tribofilm on this simulated gear contact can now be described. The term "rate" refers to the nanometers of tribofilm per meter of sliding distance (Fig. 25). It has been discussed that the SRR had little influence on tribofilm growth, which was confirmed by another study [112]. Thus, the variation in the rate of tribofilm along the line of action is mostly determined by pressure.

When considering a particular location on the line of action, the tribofilm growth rate (nm/m) is proportional to the relative pressure of that point to the tribofilm threshold pressure (Fig. 28). As a result, there are three possible scenarios for a gear set:

1. The pressure on the points in the line of action are all above the threshold pressure.

2. The pressure on the points in the line of action are all below the threshold pressure.

3. The pressure of some points is above, and some points below the threshold pressure.

These three scenarios are illustrated in Figure 28. The points near the threshold pressure have the fastest tribofilm growth rate (nm/m). Above the threshold pressure, wear comes into play and inhibits the formation of a stable tribofilm. A stable tribofilm can be formed below the threshold pressure, but the growth rate is dependent on the distance from the threshold pressure. The optimal situation is when all points are below the tribofilm threshold pressure, since this protects the surface from wear. According to the discussion, the location of the threshold pressure is determined by the asperity pressure and the tribofilm reactivity, and it may be altered by roughness, base oil composition, or additive reactivity.

The loading in gears varies greatly in different applications. The Hertzian pressure levels assumed in this study are representative of a typical value. In cases where the ground gear flanks are new, it is highly probable that the asperity pressure on the gear teeth is above the threshold pressure. However, passing the running-in stage, the asperity peaks can be flattened so that there are fewer harsh asperity contacts, which makes the condition more similar to the current tests. In the case of super-finished gears, surfaces are much smoother, and the roughness levels may be nearer to the tested specimens in this study.

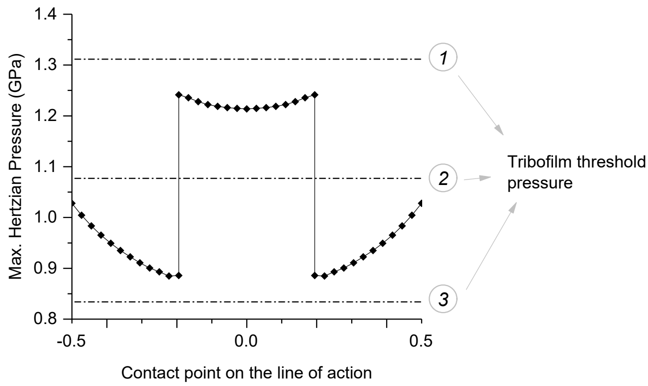

Figure 28. Tribofilm threshold pressure and the pressure distribution along the line of action for a specific gear [Publication IV]

3.3.3 Tribofilm monitoring using the barrel-on-disc scuffing technique

The barrel-on-disc technique was used in this experiment. The specimens were made of AISI 52100 steel, and they were in contra-rotational rolling/sliding contact. They both had a hardness of 750-770 HV, Young's Modulus of 207 (GPa), and surface roughness of the smooth specimens specified in Table 2. Scuffing experiments were conducted in accordance with the experimental procedure described in Section 2.6. After the running-in stage, a Hertzian pressure of 1.97 GPa was applied, and the sliding speed increased in the steps shown in Figure 29. Then the load was increased to the next level, and the sliding speed was increased in the same steps until scuffing appeared for each oil. The friction coefficients of the tested oils are shown in Figure 29. Scuffing was identified by a significant and irreversible rise in the friction coefficient to more than 0.2. This dramatic rise in friction was followed by an increase in test noise and rig vibrations. In Figure 29, a clear difference in the scuffing performance of the oils is evident. The EALs outperformed the mineral oils, with EAL1 being the best and M1 being the worst.

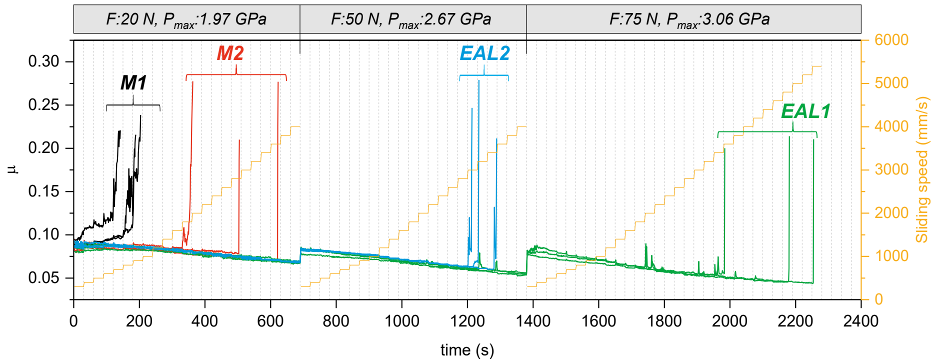

Figure 29. Friction coefficient, sliding speed, and load during the oil scuffing test [Publication III]

The tribofilm is critical for avoiding scuffing failure. The evolution of the tribofilm was recorded using the SLIM method at a load stage of F=20 N and three sliding speeds of 2200 mm/s, 2800 mm/s, and 3400 mm/s. Figure 30 illustrates these tribofilm images (the tribofilm for M1 is not shown, because its scuffing occurred at much lower speeds). It is apparent that the EALs have a thicker tribofilm than M2.

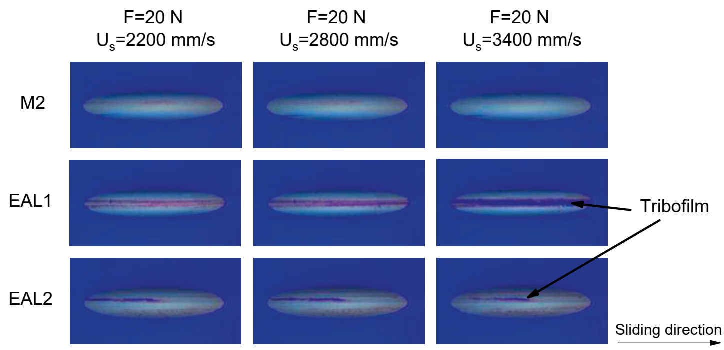

Figure 30. Tribofilm thickness of oils M2, EAL1, and EAL2 at F=20 N and sliding speeds of 2200 mm/s, 2800 mm/s, and 3400 mm/s [Publication III]

As seen in Table 8, M2 contains a considerable amount of sulfuric EP additions. These additions, however, do not compensate for the influence of the low EHL film. With the assumption that M2 includes more reactive additives, it can be concluded that the thinner EHL layer in this oil (Table 9) results in rapid tribofilm removal and prevents the formation of a thick tribofilm. This was also true of M1, which included very reactive additives [Publication I] but did not form a thick tribofilm in this scuffing test owing to its low EHL film thickness. By contrast, in the case of EAL1 and EAL2, the thicker EHL film allows the formation of the tribofilm. As a result, it is concluded that a minimum EHL film thickness is always needed for the formation of tribofilms. The EALs demonstrated better scuffing capacity, which is mostly owing to their higher viscosity index, enabling them to create a thick EHL layer. This EHL film not only improves their capacity to separate the sliding bodies, but also creates the ideal environment for the development of a thick tribofilm.

Table 8. Elemental analysis of additives in oils according to ASTM D5185

	Calcium	Magnesium	Boron	Zinc	Phosphorus	Barium	Sulfur
M1	13822	37	1	399	330	0	4704
M2	0	0	36	0	358	0	8391
EAL1	0	0	1	0	864	0	951
EAL2	1	0	0	1	752	0	2080

Table 9. Estimated dynamic viscosity, pressure-viscosity coefficient, and EHL film thickness of the lubricants at 120 °C

	η @120 °C (mPa.s)	α @120 °C (1/GPa)	hmin @20 N (nm)	hmin @50 N (nm)	hmin @75 N (nm)
M1	7.12	12.58	2.35	2.2	2.14
M2	7.065	12.6	2.34	2.19	2.13
EAL1	10.62	8.94	2.61	2.44	2.37
EAL2	9.868	8.88	2.48	2.32	2.25

The SLIM pictures for the EAL1 oil are shown in Figures 30 and 31. Only the SLIM images that exhibit particular features in this scuffing test are displayed in these graphs. SLIM images are given in Figure 31 before and after increasing the load. As expected, the tribofilm thickness decreased as the load increased. This is more noticeable when shifting from a 50 N to a 75 N load. The removal of the tribofilm results in direct contact between the metallic surfaces; however, this did not result in scuffing in this test due to the extremely low sliding velocity after the load increase. This is why extra running-in steps were added before each load stage (Fig. 13) to provide sufficient time for the tribofilm to regrow. This is a critical point that must be thoroughly examined during scuffing testing using step loads (for example the FZG scuffing test). By increasing the load in the step-load scuffing tests, a new region of the sample with unpolished asperities makes contact, which is not covered by a tribofilm. Additionally, the tribofilm that was previously formed is destroyed. As a result, this may result in early scuffing. The current designed test plan avoids this kind of failure by setting a low sliding speed at the start of the load stages, thus creating a short running-in stage. As a result, it is recommended to conduct a scuffing test with a short running-in period using the same load (as the load step) and a low sliding speed. It is essential to understand this for other situations where overload is an issue in scuffing. In such situations, a low-speed run-in with high loads promotes the formation of a tribofilm over the lubricated contact area. The SLIM images demonstrate that the tribofilm can completely cover the contact surface in less than 60 seconds under high stress conditions.

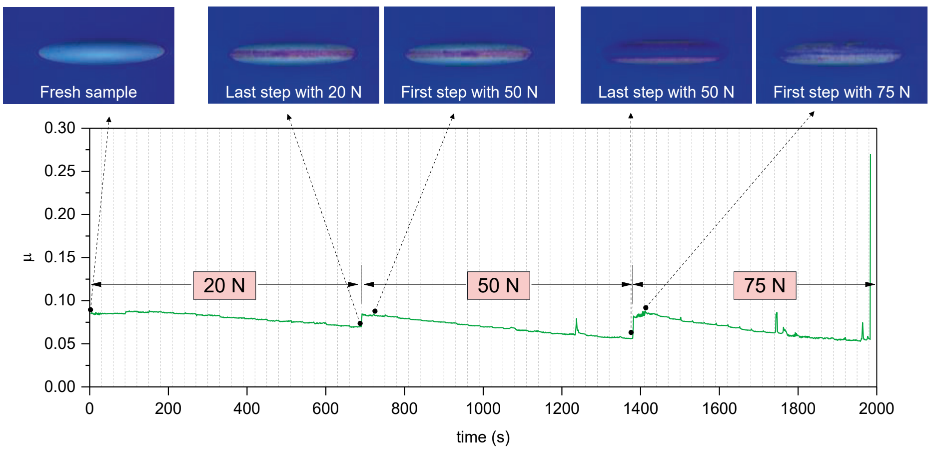

Figure 31. SLIM images for the scuffing test of EAL1, captured before and after changing the load [Publication III]

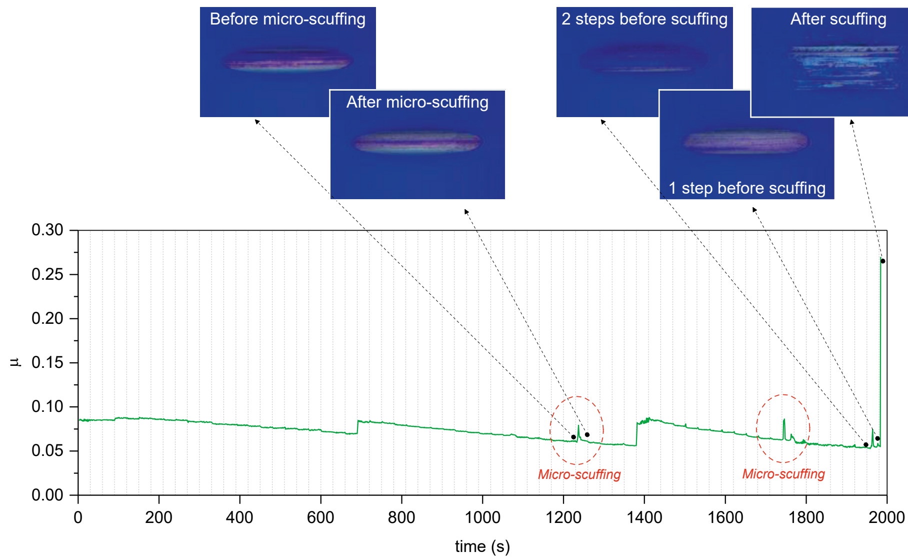

Figure 32. SLIM images for the scuffing test of EAL1, captured before and after a micro-scuffing and the scuffing [Publication III]

SLIM images of EAL1 oil are shown in Figure 32 before and after scuffing, as well as before and after micro-scuffing. The term "micro-scuffing" refers to local scuffing that does not propagate and appears as a sharp increase and rapid decrease in the friction coefficient [75,88,99,128,136–138]. With regard to micro-scuffing, several studies have found a microstructural change and instantaneous plastic flow that is accompanied by a temperature increase [88,89,138]. However, the temperature increase and wear associated with micro-scuffing are insignificant in comparison to those associated with final scuffing [138]. Micro-scuffing occurs when the material's plastic flow does not result in a complete failure, and a "healing" or "quenching" mechanism stops the scuffing from propagating [88,128].

The healing process is linked to rapid dissipation of heat [90] and decreased normal pressure as a result of the enlarged contact area [138]. Figure 32 illustrates the tribofilm removal after micro-scuffing. Additionally, an enlarged contact area was observed after the micro-scuffing shown in Figure 32. In Figure 33, the SLIM images have been magnified to show the contact area of the barrel before and after micro-scuffing. The enlarged contact area in Figure 33 corresponds to a slight modification in the barrel's edge radius and the removal of a very thin layer from the specimen.

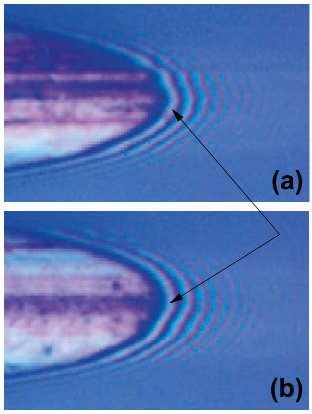

Figure 33. Geometrical change of the barrel after micro-scuffing: (a) Before micro-scuffing, (b) After micro-scuffing [Publication III]

When micro-scuffing occurs, a thin layer of material deforms plastically, generating heat. This is the layer in which thermal softening exceeds work hardening. Subsequently, a fresh layer with different mechanical characteristics comes into contact. If the thermal softening temperature remains high enough to remove that surface, the scuffing propagates [88,89]. At this moment, if the lubricant transfers a significant amount of heat and the tribofilm rapidly recovers, healing will occur. As shown in Figure 29, the healing process and micro-scuffing of EAL1 occurred at the same sliding rates as the scuffing of EAL2. This demonstrates that EAL1 had a greater capacity for scuffing healing. As a result, the increased healing capacity of EAL1 is linked to its tribofilm (Fig. 30) and additivation. Another reason could be its higher EHL film thickness, as shown in Table 9, but the difference between these figures is so small (less than a nanometer) that it cannot be used for any conclusion regarding the influence of the EHL film. While EAL1 and EAL2 are both from the same kind of oil and have the same viscosity class, they exhibit considerably differing scuffing capabilities. This shows that slight modifications to the lubricant composition and additivation may result in the healing of scuffing and an increase in the oil's scuffing capacity. One possible explanation for this is that EAL 1 has a greater phosphorus concentration, which results in a thicker and more reactive tribofilm (Fig. 30) and improved micro-scuffing healing.

Regarding the final scuffing of EAL1 shown in Figure 32, micro-scuffing was detected just before the final friction jump. Prior to the micro-scuffing, the surface was protected by a thick tribofilm, but after the micro-scuffing, the tribofilm thickness was very low, providing opportunities for final scuffing. Although the surface area was slightly enlarged as a result of micro-scuffing, it was not adequate to delay the scuffing. Although the tribofilm-friction graph is presented for EAL1, the relationship between micro-scuffing, scuffing, and tribofilm may be generalized to the other tested oils.

3.4 Ranking the oils

In terms of friction and energy efficiency, the EALs clearly outperformed the mineral oils. The COF in the EHL regime decreased from 60% at a low slide-to-roll ratio (SRR) and low entrainment velocity (U_e) to 20% at a high SRR and high U_e when an EAL was used. EALs reduced friction primarily due to two rheological parameters: their lower pressure-viscosity coefficient and their lower limiting shear stress.

When the oil film temperature was compared, the EALs had a lower oil temperature. The temperature difference between the EALs and the mineral oils varied between 5 °C and 20 °C, depending on the SRRs, U_e, and low pressure. According to the temperature equation, the EALs have a lower temperature because they have less friction and higher thermal conductivity. The impact of pressure on the temperature of the mineral oils was greater. The maximum temperature grew at a rate of 77 °C/GPa for the mineral oils and 60 °C/GPa for the EALs. The temperature rate reduction of EALs was mostly due to the reduced COF and improved heat conductivity of the oil layer in these oils.

Ignoring the thermal and shear thinning effects, mineral oils show a bigger EHL film thickness according to the Hamrock-Dowson formula for central film thickness. The ECR data (Fig. 34), on the other hand, indicate that the tested EALs provide superior surface protection and minimize metal-metal contact. This may be because the EALs generate less frictional heat and have greater thermal conductivity.

Concerning tribofilm formation, EAL1 showed a superior tribofilm formation rate at high pressure and on rough surfaces. One reason for this could be its additive formulation. This was approved by the scuffing tests as well. In the scuffing tests, the higher tribofilm formation capacity of EAL1 increased the micro-scuffing healing capacity of this oil, resulting in a superior scuffing capacity compared to the other oils.

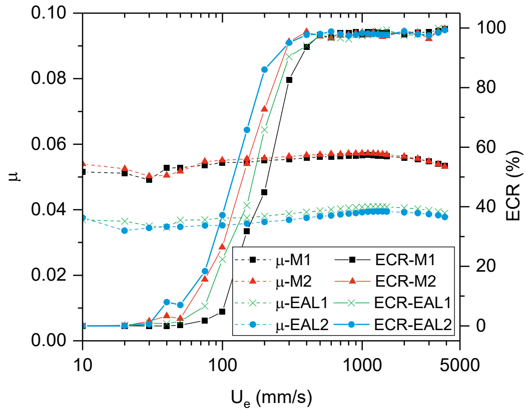

Figure 34. Stribeck curves and corresponding ECR of the oils tested on fresh samples [Publication I]

4 CONCLUDING REMARKS

Today's design of machines requires higher power density, longer life, and higher energy efficiency. This high performance demand results in a more challenging operational environment for components such as gears. Lubrication in gears plays an important role in meeting these requirements. Investigating the lubrication in gears, laboratory machines such as ball-on-disc have been commonly used for different purposes. In this thesis, a ball-on-disc machine was used for simulating the friction, temperature, and tribofilm formation of a simulated gear contact. Novel test methods were devised for investigating the friction and temperature in a wide range of operating conditions, studying the tribofilm formation along the line of action, and the role of tribofilm in the EHL regime and scuffing.

To answer the first research question, the rolling/sliding point contact was provided by a ball-on-disc machine. Friction was measured in a wide range of SRRs, entrainment speeds, and contact pressures. Then, a numerical model was used to generate temperature maps. In conclusion, the results of this study showed that concerning friction, the effective parameters at low sliding speeds (before the maximum friction point) are the pressure-viscosity coefficient and limiting shear stress. However, at high sliding velocities and high pressures, friction is more influenced by shear heating and thermal properties. The thermal region of the EALs started at higher SRRs, and the EALs reduced the friction in the EHL regime from ~60% at a low slide-to-roll ratio (SRR)-low entrainment velocity (U_e), to 20% at a high SRR-high U_e. This approved smaller shear heating that causes smaller influence on their limiting shear stress.

Regarding temperature, the EALs were able to reduce the temperature by 5 °C at low SRRs, low U_e, and low pressure, up to by 20 °C at high SRRs, high U_e, and high pressure. This was mainly the result of their lower friction and higher thermal conductivity. In addition, pressure had a smaller effect on the temperature of the EALs. The maximum temperature of the EALs increased at a rate of ~77 °C/GPa, while this rate was ~60 °C/GPa for the mineral oils.

To answer the second question, the ECR and SLIM techniques were used firstly to investigate the tribofilm evolution and its influence on metal-metal contact. It was observed that a very thick tribofilm can have an adverse effect on the EHL film by inlet blocking. This can result in higher metal-metal contact. Thus, a thin tribofilm is preferable when there is no risk of high wear or scuffing.

After that, the tribofilm imaging was done at a specific pressure and slide-to-roll ratio to mimic the gear condition at different points along the line of action. The findings showed that the tribofilm growth rate in a simulated gear contact is highly dependent on the pressure of a specific point along the line of action. In these experiments, a tribofilm threshold pressure was observed around which the tribofilm growth rate was maximum. This threshold pressure is attributed to the pressure in asperity level, and is highly sensitive to surface roughness. Considering different points in the line of action, those with a pressure above this threshold pressure were not covered by a stable tribofilm, and wear was dominant.

In order to study tribofilm evolution during the stages of the scuffing test, the SLIM technique was employed. However, to achieve a higher contact pressure, the ball specimen was replaced by a barrel specimen that could provide a pressure up to 3.06 GPa. A novel test strategy was developed to carefully distinguish between the scuffing performance of very similar industrial oils. According to the results, setting the running-in and test parameters was crucial for achieving good repeatability and preventing the excessive wear of the samples. It was observed that in micro-scuffing, a temporary friction rise occurred, resulting in the removal of the tribofilm and plastic deformation in several material layers. The tribofilm is very influential in healing of the micro-scuffing by fast formation after small changes in the contact area and accordingly alternation of the normal pressure distribution. A thicker EHL film helps the recovery of the tribofilm during this process. In the scuffing stages, when the load was increasing in a stage, the thickness of tribofilm decreased. This decrease is more evident at high loads, but it could recover when the sliding speed is low. However, at such high loads, if the sliding speed is not low, the increased load brings the fresh unprotected area into contact and results in unwanted scuffing. Thus, it is recommended that during the scuffing tests, the load increase is better accompanied by a low sliding speed to prevent premature scuffing.

Implementing the numerical output parameters on real gears could be a subject for future studies. The oil entrainment in ball-on-disc is continuous while a new film is formed in every tooth engagement in the gears. In addition, there is a lower dynamic effect in ball-on-disc compared to gears, for instance changes in roughness and contact temperature during operation. The tested surfaces may not correspond exactly to the surfaces of real gears in terms of topography, material, and contact size. However, the contact in super-finished gear surfaces may be close to the roughness levels presented in the smooth surfaces in this study.

4.1 Future studies

The study carried out for this thesis has raised several ideas that would be interesting as research topics in future work:

- The shear thinning effect could be considered in the models. Also, the exact oil thermal properties and pressure-viscosity coefficient could be measured to accurately estimate the EHL film thickness and compare it with a measured EHL film thickness.

- The EHL film thickness could be accurately measured using the optical interferometry method, and the results could help the interpretation of tribofilm formation and scuffing results. Measurement of the pressure-viscosity coefficient is also complementary for such a purpose.

- Tests regarding scuffing, and the evolution of a tribofilm along the line of action could be carried out using different materials and surface roughnesses.

- The evolution of surface roughness along the line of action could be investigated. This study would require samples with higher roughness, longer tests, and accurate measurement of the surface roughness.

- Studying the influence of humidity on the lubrication performance of EALs compared to mineral oils.

- Comparing the lubrication performance of different types of EALs such as polyglycols, PAOs, and esters.

- Comparing the results with real gear test methods such as the FZG twin-disc machine. This could first be studied by using the ball and disc specimens with a lambda value similar to that found in FZG test rigs.

REFERENCES

[1] Dowson D. History of tribology. 1st ed. Longman London ; New York; 1979.

[2] Bhushan B. Introduction to Tribology. 2nd ed. The Atrium, Southern Gate, Chichester, West Sussex, PO19 8SQ, UK: John Wiley & Sons, Ltd; 2013. doi:10.1002/9781118403259.

[3] Holmberg K, Erdemir A. Influence of tribology on global energy consumption, costs and emissions. Friction 2017;5:263–84. doi:10.1007/s40544-017-0183-5.

[4] Björling M. Friction in Elastohydrodynamic Lubrication. Luleå University of Technology, 2014.

[5] Hamrock BJ, Dowson D. Isothermal Elastohydrodynamic Lubrication of Point Contacts: Part III—Fully Flooded Results. J Lubr Technol 1977;99:264–75. doi:10.1115/1.3453074.

[6] Gupta PK, Cheng HS, Zhu D, Forster NH, Schrand JB. Viscoelastic effects in MIL-L-7808-type lubricant, part I: Analytical formulation. Tribol Trans 1992;35:269–74. doi:10.1080/10402009208982117.

[7] Stachowiak GW, Batchelor AW. Engineering Tribology. 3rd ed. Burlington: Butterworth-Heinemann; 2013. doi:https://doi.org/10.1016/B978-0-12-397047-3.00007-2.

[8] Hansen J, Björling M, Larsson R. A New Film Parameter for Rough Surface EHL Contacts with Anisotropic and Isotropic Structures. Tribol Lett 2021;69:37. doi:10.1007/s11249-021-01411-3.

[9] Cann P, Ioannides E, Jacobson B, Lubrecht AA. The lambda ratio - a critical re-examination. Wear 1994;175:177–88. doi:10.1016/0043-1648(94)90181-3.

[10] Jacobson B. Thin film lubrication of real surfaces. Tribol Int 2000;33:205–10. doi:10.1016/S0301-679X(00)00032-3.

[11] Mang T, Bobzin K, Bartels T. Industrial Tribology. Weinheim, Germany: Wiley-VCH Verlag GmbH & Co. KGaA; 2010. doi:10.1002/9783527632572.

[12] Norrby T. Environmentally adapted lubricants – where are the opportunities? Ind Lubr Tribol 2003;55:268–74. doi:10.1108/00368790310496400.

[13] Mobarak HM, Niza Mohamad E, Masjuki HH, Kalam MA, Al Mahmud KAH, Habibullah M, et al. The prospects of biolubricants as alternatives in automotive applications. Renew Sustain Energy Rev 2014;33:34–43. doi:10.1016/J.RSER.2014.01.062.

[14] Shi Y, Minami I, Grahn M, Björling M, Larsson R. Boundary and elastohydrodynamic lubrication studies of glycerol aqueous solutions as green lubricants. Tribol Int 2014;69:39–45. doi:10.1016/J.TRIBOINT.2013.08.013.

[15] Luther R. Lubricants in the Environment. In: Mang T, Dresel W, editors. Lubr. Lubr. 3rd ed., Weinheim, Germany: Wiley-VCH Verlag GmbH & Co. KGaA; 2017, p. 153–236. doi:10.1002/9783527610341.ch7.

[16] Bayat R, Lehtovaara A. EHL/mixed transition of fully formulated environmentally acceptable gear oils. Tribol Int 2020:106158. doi:10.1016/j.triboint.2020.106158.

[17] Pettersson A. Environmentally Adapted Lubricants: Properties and Performance. Luleå University of Technology, 2006.

[18] European Commission. 2011/381/EU: Commission Decision of 24 June 2011 on establishing the ecological criteria for the award of the EU Ecolabel to lubricants (notified under document C(2011) 4447) Text with EEA relevance. 2011.

[19] Nagendramma P, Kaul S. Development of ecofriendly/biodegradable lubricants: An overview. Renew Sustain Energy Rev 2012;16:764–74. doi:10.1016/J.RSER.2011.09.002.

[20] Norrby T, Torbacke M, Kopp M. Environmentally adapted lubricants in the Nordic marketplace – recent developments. Ind Lubr Tribol 2002;54:109–16. doi:10.1108/00368790210427461.

[21] Pettersson A. High-performance base fluids for environmentally adapted lubricants. Tribol Int 2007;40:638–45. doi:10.1016/j.triboint.2005.11.016.

[22] Bartels T, Bock W. Gear Lubrication Oils. In: Mang T, Dresel W, editors. Lubr. Lubr. 3rd ed., Weinheim, Germany: Wiley-VCH Verlag GmbH & Co. KGaA; 2017, p. 293–344. doi:10.1002/9783527645565.ch10.

[23] Bhushan B. Principles and Applications to Tribology. 2 nd. New York: John Wiley & Sons, Ltd; 2013. doi:10.1002/9781118403020.

[24] Rizvi SQA. A Comprehensive Review of Lubricant Chemistry, Technology, Selection, and Design. West Conshohocken: ASTM International; 2009. doi:10.1520/MNL59-EB.

[25] Lois J. Gschwender, David C. Kramer, Brent K. Lok, Shashi K. Sharma, Carl E. Snyder, Mark L. Sztenderowicz. Liquid Lubricants and Lubrication. In: Bhushan B, editor. Mod. Tribol. Handb., Boca Raton: CRC Press; 2001, p. 361–73.

[26] Randles SJ. Esters. In: Rudnick LR, Shubkin RL, editors. Synth. Lubr. high-performance Funct. fluids. 2nd ed., Chapman and Hall/CRC; 1999, p. 881.

[27] Ahlroos T, Ronkainen H, Helle A, Parikka R, Virta J, Varjus S. Twin disc micropitting tests. Tribol Int 2009;42:1460–6. doi:10.1016/J.TRIBOINT.2009.05.023.

[28] Brandão JA, Meheux M, Seabra JHO, Ville F, Castro MJD. Traction curves and rheological parameters of fully formulated gear oils. Proc Inst Mech Eng Part J J Eng Tribol 2011;225:577–93. doi:10.1177/1350650111405111.

[29] Fernandes CMCG, Battez AH, González R, Monge R, Viesca JL, García A, et al. Torque loss and wear of FZG gears lubricated with wind turbine gear oils using an ionic liquid as additive. Tribol Int 2015;90:306–14. doi:10.1016/J.TRIBOINT.2015.04.037.

[30] Brandão JA, Meheux M, Ville F, Seabra JHO, Castro J. Comparative overview of five gear oils in mixed and boundary film lubrication. Tribol Int 2012;47:50–61. doi:10.1016/j.triboint.2011.10.007.

[31] Rieglert J, Kassfeldt E. Performance of Environmentally Adapted Hydraulic Fluids at Boundary Lubrication. Tribol Ser 1997;32:467–73. doi:10.1016/S0167-8922(08)70474-7.

[32] Gold PW, Schmidt A, Dicke H, Loos J, Assmann C. Viscosity–pressure–temperature behaviour of mineral and synthetic oils. J Synth Lubr 2001;18:51–79. doi:10.1002/jsl.3000180105.

[33] Lawford. S. Polyalkylene Glycols. In: Rudnick LR, editor. Synth. Miner. Oils, Bio-Based Lubr., CRC Press; 2005. doi:https://doi.org/10.1201/9781420027181.

[34] Dresel W. Synthetic Base Oils. In: Mang T, Dresel W, editors. Lubr. ~~Lubr~~. 3rd ed., Weinheim, Germany: Wiley-VCH Verlag GmbH & Co. KGaA; 2017, p. 83–116. doi:10.1002/9783527645565.ch5.

[35] Brown M, Fotheringham JD, Hoyes TJ, Mortier RM, Orszulik ST, Randles SJ, et al. Synthetic Base Fluids. In: Mortier RM, Fox MF, Orszulik ST, editors. Chem. Technol. Lubr., Dordrecht: Springer Netherlands; 2010, p. 35–74. doi:10.1023/b105569_2.

[36] Kapelevich AL. Direct gear design. 1st ed. Boca Raton: CRC Press; 2013. doi:10.1201/b13920.

[37] Bloch HP. Gear lubrication. Pract. Lubr. Ind. Facil. 2nd ed., Lilburn: The Fairmont Press, Inc.; 2009, p. 277–300.

[38] Kleemola J. Experimental Methods for the Evaluation of Lubrication Conditions in Gear Contacts. Tampere University of Technology, 2010.

[39] Bergseth E, Olofsson U, Lewis R, Lewis S. Effect of Gear Surface and Lubricant Interaction on Mild Wear. Tribol Lett 2012;48:183–200. doi:10.1007/s11249-012-0004-y.

[40] Davis JR (Joseph R. Gear materials, properties, and manufacture. ASM International; 2005.

[41] Kleemola J, Lehtovaara A. Evaluation of lubrication conditions in gear contacts using contact resistance and bulk temperature measurements. Proc Inst Mech Eng Part J J Eng Tribol 2010;224:367–75. doi:10.1243/13506501JET675.

[42] Deng G, Kato M, Maruyama N, Morikawa K, Hitomi N. Initial temperature evaluation for flash temperature index of gear tooth. J Tribol 1995;117:476–81. doi:10.1115/1.2831278.

[43] Kleemola J, Lehtovaara A. Evaluation of lubrication conditions in gear contacts using contact resistance and bulk temperature measurements. Proc Inst Mech Eng Part J J Eng Tribol 2010;224:367–75. doi:10.1243/13506501JET675.

[44] Larsson R. Transient non-Newtonian elastohydrodynamic lubrication analysis of an involute spur gear. Wear 1997;207:67–73. doi:10.1016/S0043-1648(96)07484-4.

[45] Evans HP, Snidle RW, Sharif KJ. Deterministic mixed lubrication modelling using roughness measurements in gear applications. Tribol Int 2009;42:1406–17. doi:10.1016/j.triboint.2009.05.025.

[46] Glodež S, Ren Z, Flašker J. Simulation of surface pitting due to contact loading. Int J Numer Methods Eng 1998;43:33–50. doi:10.1002/(SICI)1097-0207(19980915)43:1<33::AID-NME410>3.0.CO;2-Z.

[47] Chang L, Jeng YR, Huang PY. Modeling and analysis of the meshing losses of involute spur gears in high-speed and high-load conditions. J Tribol 2013;135. doi:10.1115/1.4007809.

[48] Savolainen M, Lehtovaara A. An experimental investigation of scuffing initiation due to axial displacement in a rolling/sliding contact. Tribol Int 2018;119:688–97. doi:10.1016/j.triboint.2017.12.007.

[49] Kleemola J, Lehtovaara A. Development of a high pressure twin disc test device for the simulation of gear contact. Tribologia 2006;25:8–17.

[50] Björling M, Miettinen J, Marklund P, Lehtovaara A, Larsson R. The correlation between gear contact friction and ball on disc friction measurements. Tribol Int 2015;83:114–9.

doi:10.1016/j.triboint.2014.11.007.

[51] Castro J, Seabra J. Coefficient of friction in mixed film lubrication: Gears versus twin-discs. Proc Inst Mech Eng Part J J Eng Tribol 2007;221:399–411. doi:10.1243/13506501JET257.

[52] Diab Y, Ville F, Velex P. Prediction of Power Losses Due to Tooth Friction in Gears. Tribol Trans 2006;49:260–70. doi:10.1080/05698190600614874.

[53] Holmberg K, Andersson P, Erdemir A. Global energy consumption due to friction in passenger cars. Tribol Int 2012;47:221–34. doi:10.1016/J.TRIBOINT.2011.11.022.

[54] Martins R, Seabra J, Magalhães L. Austempered ductile iron (ADI) gears: Power loss, pitting and micropitting. Wear 2008;264:838–49. doi:10.1016/j.wear.2007.05.007.

[55] Martins RC, Cardoso NFR, Bock H, Igartua A, Seabra JHO. Power loss performance of high pressure nitrided steel gears. Tribol Int 2009;42:1807–15. doi:10.1016/j.triboint.2009.03.006.

[56] Magalhàes L, Martins R, Seabra J. Low-loss austempered ductile iron gears: Experimental evaluation comparing materials and lubricants. Tribol Int 2012;46:97–105. doi:10.1016/j.triboint.2011.06.015.

[57] Petry-Johnson TT, Kahraman A, Anderson NE, Chase DR. An experimental investigation of spur gear efficiency. J Mech Des Trans ASME 2008;130:0626011–06260110. doi:10.1115/1.2898876.

[58] Britton RD, Elcoate CD, Alanou MP, Evans HP, Snidle RW. Effect of surface finish on gear tooth friction. J. Tribol., vol. 122, ASME; 2000, p. 354–60. doi:10.1115/1.555367.

[59] Björling M, Habchi W, Bair S, Larsson R, Marklund P. Friction reduction in elastohydrodynamic contacts by thin-layer thermal insulation. Tribol Lett 2014;53:477–86. doi:10.1007/s11249-013-0286-8.

[60] Björling M, Shi Y. DLC and Glycerol: Superlubricity in Rolling/Sliding Elastohydrodynamic Lubrication. Tribol Lett 2019;67:23. doi:10.1007/s11249-019-1135-1.

[61] Martins R, Amaro R, Seabra J. Influence of low friction coatings on the scuffing load capacity and efficiency of gears. Tribol Int 2008;41:234–43. doi:10.1016/j.triboint.2007.05.008.

[62] Amaro RI, Martins RC, Seabra JO, Renevier NM, Teer DG. Molybdenum disulphide/titanium low friction coating for gears application. Tribol Int 2005;38:423–34. doi:10.1016/j.triboint.2004.09.003.

[63] Martins R, Seabra J, Brito A, Seyfert C, Luther R, Igartua A. Friction coefficient in FZG gears lubricated with industrial gear oils: Biodegradable ester vs. mineral oil. Tribol Int 2006;39:512–21. doi:10.1016/J.TRIBOINT.2005.03.021.

[64] Michaelis K, Höhn BR. Influence of lubricants on power loss of cylindrical gears. Tribol Trans 1994;37:161–7. doi:10.1080/10402009408983279.

[65] Yoshizaki M, Naruse C, Nemoto R, Haizuka S. Study on frictional loss of spur gears (Concerning the influence of tooth form, load, tooth surface roughness, and lubricating oil). Tribol Trans 1991;34:138–46. doi:10.1080/10402009108982021.

[66] Kleemola J, Lehtovaara A. Experimental simulation of gear contact along the line of action. Tribol Int 2009;42:1453–9. doi:10.1016/J.TRIBOINT.2009.06.007.

[67] Höhn B-R, Michaelis K, Kreil O. Influence of surface roughness on pressure distribution and film thickness in EHL-contacts. Tribol Int 2006;39:1719–25. doi:10.1016/J.TRIBOINT.2006.01.008.

[68] Wu S, Cheng HS. Empirical determination of effective lubricant rheological parameters. Tribol Trans 1994;37:138–46. doi:10.1080/10402009408983276.

[69] Johnson KL, Tevaarwerk JL. Shear Behaviour of Elastohydrodynamic Oil Films. Proc Ofthe R Soc OfLondon Ser A, Math Phys Sci 1977;356:215–36. doi:10.1098/rspa.1977.0129.

[70] Björling M, Larsson R, Marklund P, Kassfeldt E. Elastohydrodynamic lubrication friction mapping – the influence of lubricant, roughness, speed, and slide-to-roll ratio. Proc Inst Mech Eng Part J J Eng Tribol

2011;225:671–81. doi:10.1177/1350650111403363.

[71] Zhang J, Spikes H. Measurement of EHD Friction at Very High Contact Pressures. Tribol Lett 2020;68:1–12. doi:10.1007/s11249-020-1281-5.

[72] Saeidi F, Shevchik SA, Wasmer K. Automatic detection of scuffing using acoustic emission. Tribol Int 2016;94:112–7. doi:10.1016/j.triboint.2015.08.021.

[73] Savolainen M, Lehtovaara A. An experimental approach for investigating scuffing initiation due to overload cycles with a twin-disc test device. Tribol Int 2017;109:311–8. doi:10.1016/J.TRIBOINT.2017.01.005.

[74] Schipper DJ, De Gee AWJ. Lubrication modes and the IRG transition diagram. Lubr Sci 1995;8:27–35. doi:10.1002/ls.3010080104.

[75] Yagi K, Izumi T, Koyamachi J, Sanda S, Yamaguchi S, Satio K, et al. In Situ Observation of Crystal Grain Orientation During Scuffing Process of Steel Surface Using Synchrotron X-ray Diffraction. Tribol Lett 2020;68:115. doi:10.1007/s11249-020-01357-y.

[76] Christensen H. Failure by collapse of hydrodynamic oil films. Wear 1972;22:359–66. doi:10.1016/0043-1648(72)90394-8.

[77] Höhn BR, Michaelis K. Influence of oil temperature on gear failures. Tribol. Int., vol. 37, Elsevier; 2004, p. 103–9. doi:10.1016/S0301-679X(03)00047-1.

[78] Li S, Kahraman A, Anderson N, Wedeven LD. A model to predict scuffing failures of a ball-on-disk contact. Tribol Int 2013;60:233–45. doi:10.1016/j.triboint.2012.11.007.

[79] Castro J, Seabra J. Influence of mass temperature on gear scuffing. Tribol Int 2018;119:27–37. doi:10.1016/j.triboint.2017.10.032.

[80] Yagi K, Ebisu Y, Sugimura J, Kajita S, Ohmori T, Suzuki A. In situ observation of wear process before and during scuffing in sliding contact. Tribol Lett 2011;43:361–8. doi:10.1007/s11249-011-9817-3.

[81] Spikes H, Jie Z. History, Origins and Prediction of Elastohydrodynamic Friction. Tribol Lett 2014;56:1–25. doi:10.1007/s11249-014-0396-y.

[82] Batchelor AW, Stachowiak GW. Model of scuffing based on the vulnerability of an elastohydrodynamic oil film to chemical degradation catalyzed by the contacting surfaces. Tribol Lett 1995;1:349–65. doi:10.1007/BF00174259.

[83] Wojciechowski L, Kubiak KJ, Mathia TG. Roughness and wettability of surfaces in boundary lubricated scuffing wear. Tribol Int 2016;93:593–601. doi:10.1016/j.triboint.2015.04.013.

[84] Spikes HA, Cameron A. Scuffing as a desorption process—An explanation of the borsoff effect. ASLE Trans 1974;17:92–6. doi:10.1080/05698197408981442.

[85] Blok H. The flash temperature concept. Wear 1963;6:483–94. doi:10.1016/0043-1648(63)90283-7.

[86] Dyson A. The Failure of Elastohydrodynamic Lubrication of Circumferentially Ground Discs. Proc Inst Mech Eng 1976;190:699–711. doi:10.1243/pime_proc_1976_190_074_02.

[87] Cheng HS, Dyson A. Elastohydrodynamic lubrication of circumferentially–ground rough disks. ASLE Trans 1978;21:25–40. doi:10.1080/05698197808982858.

[88] Hershberger J, Ajayi OO, Zhang J, Yoon H, Fenske GR. Evidence of scuffing initiation by adiabatic shear instability. Wear 2005;258:1471–8. doi:10.1016/j.wear.2004.10.010.

[89] Ajayi OO, Hersberger JG, Zhang J, Yoon H, Fenske GR. Microstructural evolution during scuffing of hardened 4340 steel - Implication for scuffing mechanism. Tribol. Int., vol. 38, Elsevier; 2005, p. 277–82. doi:10.1016/j.triboint.2004.08.011.

[90] Ajayi OO, Lorenzo-Martin C, Erck RA, Fenske GR. Scuffing mechanism of near-surface material during lubricated severe sliding contact. Wear 2011;271:1750–3. doi:10.1016/j.wear.2010.12.086.

[91] Ajayi OO, Lorenzo-Martin C, Erck RA, Fenske GR. Analytical predictive modeling of scuffing initiation in metallic materials in sliding contact. Wear 2013;301:57–61. doi:10.1016/j.wear.2012.12.054.

[92] Zhang C, Peng B, Gu L, Wang T, Wang L. A scuffing criterion of steels based on the friction-induced adiabatic shear instability. Tribol Int 2020;148:106340. doi:10.1016/j.triboint.2020.106340.

[93] ISO: ISO 14635 Part 1: Gears-FZG Test Procedures-Part 1: FZG Test Method A/8,3/90 for Scuffing 1736 Load-Carrying Capacity of Oils, 2000 (2000). n.d.

[94] Castro J, Seabra J. Global and local analysis of gear scuffing tests using a mixed film lubrication model. Tribol Int 2008;41:244–55. doi:10.1016/j.triboint.2007.07.005.

[95] Energy Institute (formerly Institute of Petroleum, IP): IP 166: 77(R1992) Determination of Load-Carrying Capacity of Lubricants—IAE Gear Machine Method. n.d.

[96] ASTM D2596: Standard Test Method for Measurement of Extreme-Pressure Properties of Lubricating Grease (Four-Ball Method). n.d.

[97] American Society for Testing and: Materials: ASTM D1947 Test Method for, Load-Carrying Capacity of Petroleum Oil and Synthetic Fluid Gear Lubricants (1993), n.d.

[98] ASTM D2782: Standard Test Method for Measurement of Extreme-Pressure Properties of Lubricating Grease (Timken Method), n.d.

[99] Peng B, Spikes H, Kadiric A. The Development and Application of a Scuffing Test Based on Contra-rotation. Tribol Lett 2019;67:37. doi:10.1007/s11249-019-1149-8.

[100] Ingram M, Hamer C, Spikes HA. A new scuffing test using contra-rotation. Wear 2015;328–329:229–40. doi:10.1016/j.wear.2015.01.080.

[101] Luo Q. Tribofilms in Solid Lubricants. In: Wang QJ, Chung Y-W, editors. Encycl. Tribol., Boston, MA: Springer US; 2013, p. 3760–7. doi:10.1007/978-0-387-92897-5_1252.

[102] Minami I. Molecular Science of Lubricant Additives. Appl Sci 2017;7:445. doi:10.1007/BF00571595.

[103] Spikes H. The History and Mechanisms of ZDDP. Tribol Lett

2004;17:469–89. doi:10.1023/B:TRIL.0000044495.26882.b5.

[104] Sheasby JS, Caughlin TA, Habeeb JJ. Observation of the antiwear activity of zinc dialkyldithiophosphate additives. Wear 1991;150:247–57. doi:10.1016/0043-1648(91)90320-T.

[105] Aktary M, McDermott MT, McAlpine GA. Morphology and nanomechanical properties of ZDDP antiwear films as a function of tribological contact time. Tribol Lett 2002;12:155–62. doi:10.1023/A:1014755123184.

[106] Graham JF, McCague C, Norton PR. Topography and nanomechanical properties of tribochemical films derived from zinc dialkyl and diaryl dithiophosphates. Tribol Lett 1999;6:149–57. doi:10.1023/a:1019124026402.

[107] Warren OL, Graham JF, Norton PR, Houston JE, Michalske TA. Nanomechanical properties of films derived from zinc dialkyldithiophosphate. Tribol Lett 1998;4:189–98. doi:10.1023/A:1019194903262.

[108] Pidduck AJ, Smith GC. Scanning probe microscopy of automotive anti-wear films. Wear 1997;212:254–64. doi:10.1016/S0043-1648(97)00081-1.

[109] Gosvami NN, Bares JA, Mangolini F, Konicek AR, Yablon DG, Carpick RW. Mechanisms of antiwear tribofilm growth revealed in situ by single-asperity sliding contacts. Science (80-) 2015;348:102–6. doi:10.1126/science.1258788.

[110] LJ Taylor. The film-forming and wear-reducing properties of antiwear additives. University of London, 200AD.

[111] Dawczyk J, Morgan N, Russo J, Spikes HA. Film Thickness and Friction of ZDDP Tribofilms. Tribol Lett 2019;67:34. doi:10.1007/s11249-019-1148-9.

[112] Shimizu Y, Spikes HA. The Influence of Slide–Roll Ratio on ZDDP Tribofilm Formation. Tribol Lett 2016;64:1–11. doi:10.1007/s11249-016-0738-z.

[113] Fujita H, Spikes HA. Study of zinc dialkyldithiophosphate antiwear film

formation and removal processes, part II: Kinetic model. Tribol Trans 2005;48:567–75. doi:10.1080/05698190500385187.

[114] Ueda M, Spikes H, Kadiric A. In-situ observations of the effect of the ZDDP tribofilm growth on micropitting. Tribol Int 2019;138:342–52. doi:10.1016/J.TRIBOINT.2019.06.007.

[115] Taylor L, Dratva A, Spikes HA. Friction and Wear Behavior of Zinc Dialkyldithiophosphate Additive. Tribol Trans 2000;43:469–79. doi:10.1080/10402000008982366.

[116] Spikes HA. Stress-augmented thermal activation: Tribology feels the force. Friction 2018;6:1–31. doi:10.1007/s40544-018-0201-2.

[117] Zhang J, Spikes HA. On the Mechanism of ZDDP Antiwear Film Formation. Tribol Lett 2016;63:1–15. doi:10.1007/s11249-016-0706-7.

[118] Brizmer V, Matta C, Nedelcu I, Morales-Espejel GE. The Influence of Tribolayer Formation on Tribological Performance of Rolling/Sliding Contacts. Tribol Lett 2017;65:1–18. doi:10.1007/s11249-017-0839-3.

[119] Jacobs TDB, Carpick RW. Nanoscale wear as a stress-assisted chemical reaction. Nat Nanotechnol 2013;8:108–12. doi:10.1038/nnano.2012.255.

[120] Felts JR, Oyer AJ, Hernández SC, Whitener KE, Robinson JT, Walton SG, et al. Direct mechanochemical cleavage of functional groups from graphene. Nat Commun 2015;6. doi:10.1038/ncomms7467.

[121] Chen Z, Gu C, Tian T. Modeling of Formation and Removal of ZDDP Tribofilm on Rough Surfaces. Tribol Lett 2021;69:13. doi:10.1007/s11249-020-01393-8.

[122] Azam A, Dorgham A, Parsaeian P, Morina A, Neville A, Wilson MCT. The mutual interaction between tribochemistry and lubrication: Interfacial mechanics of tribofilm. Tribol Int 2019. doi:10.1016/j.triboint.2019.01.024.

[123] Demmou K, Bec S, Loubet JL, Martin JM. Temperature effects on mechanical properties of zinc dithiophosphate tribofilms. Tribol Int 2006;39:1558–63. doi:10.1016/j.triboint.2006.01.025.

[124] Jelita Rydel J, Pagkalis K, Kadiric A, Rivera-Dïaz-del-Castillo PEJ. The correlation between ZDDP tribofilm morphology and the microstructure of steel. Tribol Int 2017;113:13–25. doi:10.1016/j.triboint.2016.10.039.

[125] Höhn B-R, Michaelis K, Doleschel A. Frictional behaviour of synthetic gear lubricants. Tribol Ser 2001;39:759–68. doi:10.1016/S0167-8922(01)80156-5.

[126] Larsson R, Larsson PO, Eriksson E, Sjöberg M, Höglund E. Lubricant properties for input to hydrodynamic and elastohydrodynamic lubrication analyses. Proc Inst Mech Eng Part J J Eng Tribol 2000;214:17–27. doi:10.1243/1350650001542981.

[127] Larsson R, Andersson O. Lubricant thermal conductivity and heat capacity under high pressure. Proc Inst Mech Eng Part J J Eng Tribol 2000;214:337–42. doi:10.1243/1350650001543223.

[128] Ludema KC. A review of scuffing and running-in of lubricated surfaces, with asperities and oxides in perspective. Wear 1984;100:315–31. doi:10.1016/0043-1648(84)90019-X.

[129] Yamaguchi ES, Ryason PR, Yeh SW, Hansen TP. Boundary Film Formation by ZnDTPs and Detergents Using ECR. Tribol Trans 1998;41:262–72. doi:10.1080/10402009808983747.

[130] Taylor LJ, Spikes HA. Friction-enhancing properties of zddp antiwear additive: Part i—friction and morphology of zddp reaction films. Tribol Trans 2003;46:303–9. doi:10.1080/10402000308982630.

[131] Taylor LJ, Spikes HA. Friction-enhancing properties of zddp antiwear additive: Part ii—influence of zddp reaction films on ehd lubrication. Tribol Trans 2003;46:310–4. doi:10.1080/10402000308982631.

[132] Jiang X, Hua DY, Cheng HS, Ai X, Lee SC. A Mixed Elastohydrodynamic Lubrication Model With Asperity Contact. J Tribol 1999;121:481. doi:10.1115/1.2834093.

[133] Miklozic KT, Forbus TR, Spikes HA. Performance of Friction Modifiers on ZDDP-Generated Surfaces. Tribol Trans 2007;50:328–35. doi:10.1080/10402000701413505.

[134] Spikes HA. Origins of the friction and wear properties of antiwear additives. Lubr Sci 2006;18:223–30. doi:10.1002/ls.19.

[135] Khaemba DN, Jarnias F, Thiebaut B, Neville A, Morina A. The role of surface roughness and slide-roll ratio on the decomposition of MoDTC in tribological contacts. J Phys D Appl Phys 2017;50. doi:10.1088/1361-6463/aa5905.

[136] Yoon H, Zhang J, Kelley F. Scuffing characteristics of sae 50b38 steel under lubricated conditions. Tribol Trans 2002;45:246–52. doi:10.1080/10402000208982547.

[137] Matsuzaki Y, Yagi K, Sugimura J. In Situ Observation of Heat Generation Behaviour on Steel Surface During Scuffing Process. Tribol Lett 2018;66:142. doi:10.1007/s11249-018-1095-x.

[138] Yagi K, Kajita S, Izumi T, Koyamachi J, Tohyama M, Saito K, et al. Simultaneous Synchrotron X-ray Diffraction, Near-Infrared, and Visible in Situ Observation of Scuffing Process of Steel in Sliding Contact. Tribol Lett 2016;61:1–16. doi:10.1007/s11249-015-0636-9.

PUBLICATIONS

PUBLICATION
I

EHL/mixed transition of fully formulated environmentally acceptable gear oils

R. Bayat, A. Lehtovaara

Tribology International, 146 (2020), 106158
https://doi.org/10.1016/j.triboint.2020.106158

Tribology International 146 (2020) 106158

Contents lists available at ScienceDirect

Tribology International

journal homepage: http://www.elsevier.com/locate/triboint

EHL/mixed transition of fully formulated environmentally acceptable gear oils

Reza Bayat *, Arto Lehtovaara

Tribology and Machine Elements, Materials Science and Environmental Engineering, Faculty of Engineering and Natural Sciences, P.O. Box 589, 33014, Tampere University, Tampere, Finland

ARTICLE INFO

Keywords:
Elastohydrodynamic lubrication
Environmentally acceptable lubricant
Running-in
Tribofilm

ABSTRACT

Understanding the ability of fully formulated industrial oils to protect the contacting surfaces requires techniques revealing the effect of tribofilm growth on the EHL film. This was achieved by employing sliding/rolling smooth contact in a ball-on-disc test for two industrial EAL gear oils and two industrial mineral oils. Friction and electrical contact resistance (ECR) of three stribeck stages at different running-in periods were studied besides measuring the tribofilm thickness evolutions by Spacer Layer Interferometry Method (SLIM). In the end, a wear test was performed and wear scars were measured. Results showed that lower pressure-viscosity coefficient of EALs does not necessarily lead to high metal-metal contact, and their thin tribofilm serves to keep the friction low in mixed and boundary regimes.

1. Introduction

Lubricant formulation is currently changing due to environmental consideration. This change also includes additives formulation and concentration [1–4]. Since the early 1970s, usage of Environmentally Acceptable Lubricants (EALs) in industry increased and different sectors started investing in the development of EALS, e.g. development of EAL hydraulic fluids for forestry operations in Germany in 1980s [4]. Reduction of oil reserves, increasing oil prices and environmental considerations to avoid the negative effect of oil spillage have attracted attention to new and less environmentally harmful lubricants [5].

Having high biodegradability, low toxicity and good thermal and oxidative stability ester oils are the most common EAL used in industrial lubricants [6–9]. The lower friction coefficient of ester-based lubricants in full film and EHL regime is observed in several studies [10–13]. Martins et al. compared two EAL oils with a mineral oil in terms of power loss, oil temperature rise and wear prevention in FZG test rig using type C gears. The results show that the tested ester oils give lower friction, temperature and wear [14].

José A. Brandão et al. studied the stribeck curves of some mineral and ester-based lubricants and illustrate that while the friction coefficient of ester lubricants is lower at full film regime, it is higher under mixed and boundary lubrication [11]. The same result is found by Rieglert and Kassfeldt testing the environmentally acceptable hydraulic fluids [15]. José A. Brandão et al. suggest that poorer boundary performance is due to the undesirable additives used in the lubricant formulation. EALs should have limitations for toxicity and biodegradability, so it is not possible to use some additives [11]. This assumption can be true; however, it requires further investigation to find out whether it is a result of the base oil, the additives, or both.

Compared to a mineral oil with a certain viscosity, ester oils have lower pressure-viscosity coefficient which, according to EHL theory, leads to lower film thickness [16]. However, ester-based lubricants show higher thermal conductivity and heat capacity. The film thickness in the EHL contact is very small, so the heat capacity would not be very effective in the performance. Yet, the thermal conductivity can play an important role in the friction [17] and film thickness by faster heat transfer to the contacting bodies.

In addition, the higher viscosity index of esters excludes the usage of VI improvers. The ester linkage is stronger than the C–C bond in mineral oils resulting in better viscosity-temperature behavior and oxidation stability [18]. Also, the high polarity of ester molecules makes them sticky to the surface which improves the boundary lubrication [6] though it can compete with the additives and negatively influence their function. These parameters are also beneficial in film formation especially under high slip and high load conditions [3].

In the worm and hypoid gears, the lubricant usually fails to prevent the asperity contacts, so the lubrication is performed under the mixed

* Corresponding author.
E-mail address: reza.bayat@tuni.fi (R. Bayat).

https://doi.org/10.1016/j.triboint.2020.106158
Received 5 October 2019; Received in revised form 16 December 2019; Accepted 2 January 2020
Available online 7 January 2020
0301-679X/

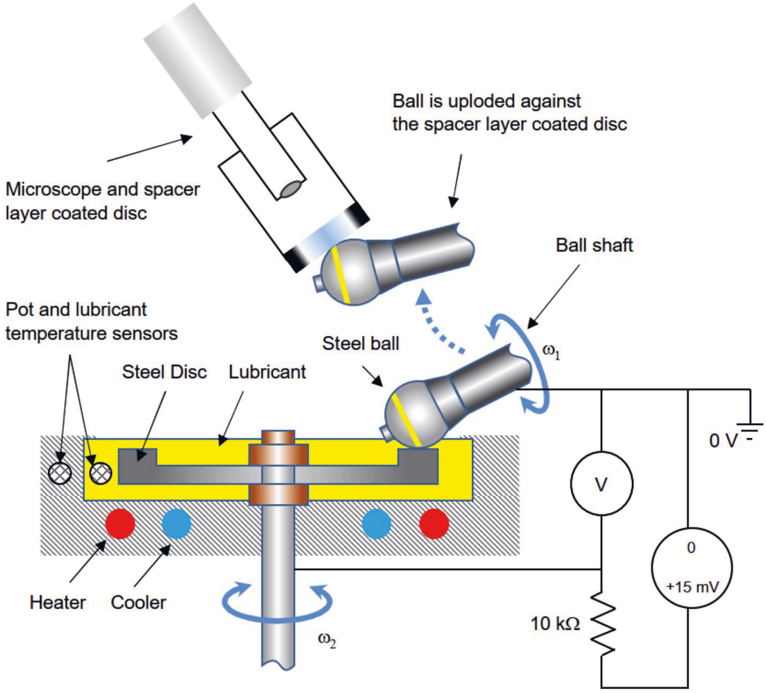

Fig. 1. Schematic of MTM.

lubrication. The same condition happens for the cylindrical and bevel gears operating at low speed and high loads [19]. Concerning wear, pitting, and scuffing, the EHL film formation ability hinders the transition from EHL to mixed lubrication and consequently less asperity contact and lower abrasive and adhesive wear. AW and EP additives play an important role in wear, scuffing and pitting, but they are functioning in the boundary and near boundary lubrication [20].

Being fast, compact, and safe, ball-on-disc test is considered to be an important tool for the development of new lubricants. It provides good repeatability and control over a wide range of parameters like speed, temperature, load [21]. There are some problems with the simulation of gear contact with a twin-disc machine which are also present in ball-on-disc machine. These problems can be listed as below [22,23]:

- The different surface topography and orientation between test specimens compared to the modern gears
- Different film formation process which is continues in ball-on-disc, while a new film is formed in every tooth engagement in the gears
- Lower dynamic effects in MTM compared to gears

Despite the mentioned limitations, ball-on-disc test is successfully used in fundamental researches on lubricant testing. Björling et al. used friction maps developed earlier in Ref. [24] to make a correlation between the friction measured by ball-on-disc test and FZG test rig [25]. The results showed that ball-on-disc device is able to well simulate the working condition of FZG gears. It is observed that using FZG and ball-on-disc devices leads to the same results in ranking the friction performance of different oils. So, it can be said that using ball-on disc method is a reasonable way to understand the performance of gear oils before testing with full gear test equipment. This will help to select a proper lubricant for a known condition.

With the development of new traction machines, the experimental studies on the lubrication regime [11,26] and EHL film formation of the oils [27] became very popular. Optical interferometry has been vastly used to measure the film EHL film thickness under different lubrication conditions [28–30]. In this method, the requirement for a transparent disc is the main disadvantage causing differences with the contacting metallic surfaces that are common in machine elements [31]. The electrical contact resistance (ECR) technique, though unsuccessful to measure the film thickness [32], has been used for qualitative analysis of contact in real components. In gear teeth contacts, the running-in leads to changes in the lubrication regime, surface roughness alteration and tribofilm formation between two metallic surfaces. These changes are influential in the performance of lubricant regarding efficiency [33], or failure [34]. The ECR technique is successfully used to evaluate the tribofilm formation [35–38], the mapping of lubrication regime and the influence of running-in on the lubrication regimes [26], influence of the texture on the transition between lubrication regimes [39] and checking the contact lubrication conditions along the line of action of a simulated gear pair [22,40].

Rizvi discusses the effect of the chemical structure of different base oils including esters and shows the correlations between tribological characteristics and the structures. Depending on the type of alcohol and fatty acid used in the production of the ester, the final properties can be optimized for a special application. Influential parameters on EHL film formation ability like density, viscosity index, pressure-viscosity coefficient, heat conductivity and capacity, polarity are enhanced by manipulating the chemical composition and molecular structure of esters. The final EHL performance of the lubricant is the superposition of all these parameters [41].

In order to examine the performance of a lubricant, it should be tested by a practical machine under real conditions. These tests are costly and time-intense. Therefore, it is critically important to have laboratory tests with scientifically analyzed results which are applicable to the real components. Using a fully formulated lubricant in these prior laboratory tests is necessary to correlate the results to the real

Table 1
Ball and disc average roughness parameters.

Specimen	Ra (nm)	Rz (nm)
Ball	39	284
Disc	25	191

component tests. There are scientific papers using fully formulated lubricants to investigate the wear and pitting of engine oils [42], friction [11,14] and tribofilm generation of gear oils [43]. However, there is a literature gap in the interaction of EHL and tribofilm formation for the fully formulated lubricants. Also, the mechanism by which EALs can compete with mineral oils is not examined clearly. This paper focuses on the EHL-to-mixed transition in three stages of running-in, the effect of tribofilm thickness on the EHL film and mild wear protection of the industrial EALs formulated for the gears. These objectives are achieved by studying stribeck curves in a rolling/sliding contact of a ball-on-disc machine, together with ECR technique and Space Layer Imaging (SLIM) technique. The experimental strategy used in this paper provides a scientific experimental means to evaluate the fully formulated lubricants. Investigating the tribological performance of the EALs would help to understand the advantage and disadvantages of the available oils in the market.

2. Experiment detail

2.1. Experimental rig

All the ball-on-disc tests were performed using a mini-traction machine (MTM) developed by PCS instruments. As it can be seen in Fig. 1, a ball and a disc are in rolling/sliding contact. The tilted ball shaft minimizes the spin, and a load cell attached between the ball shaft and the instrument body measures the friction force. A series of tests can be performed by fully automated control overload, velocity, temperature and the test duration. The ball and disc are driven independently in order to achieve a wide range of lubricant entrainment speed and slide to roll ratio. Lubricant entrainment speed, sliding speed and slide-to-roll ratio (SRR) are expressed by the Eqs. (1)–(3):

$$U_e = \frac{U_d + U_b}{2} \tag{1}$$

$$U_s = U_d - U_b \tag{2}$$

$$SRR = \frac{U_s}{U_e} \tag{3}$$

where U_d and U_b are respectively the disc and ball circumferential velocities in the contact point, U_e is the entrainment velocity and U_s is the sliding velocity.

Lubricant and pot temperatures are measured by two thermometers placed respectively in the lubricant, and the pot wall. These temperatures are automatically adjusted by a heater, and a circulating fluid provided by an external heater/cooler equipment.

The electrical contact resistance between the ball and disc can be measured by coupling an electrical bridge between them. As it is shown in Fig. 1, a balance resistor of 10 kΩ is mounted in series with the ball and disc, and an electrical potential of 15 mV is applied. If the contacting bodies are fully separated, the ECR corresponding to the electrical resistance of the contact is 100%, and if they are in contact, the ECR is 0. The amounts between 0 and 100% indicate the partial separation by EHL film or tribofilm.

The tribofilm formed on the ball surface can be observed using a technique called Spacer Layer Imaging (SLIM). In this technique, the ball is loaded against a spacer layer of transparent silicon dioxide coated with a thin, semireflective layer of chromium. When white light is shone into the contact, a colored interference image of the contact is formed and recorded by the camera. The evolution of this interferometry images gives the tribofilm thickness changes during each step [44]. The tribofilm thickness was calculated according to the technique shown in Appendix A used in Ref. [45].

2.2. Test specimen

The ball (19.05 mm diameter) and disc specimens were both AISI 52100 steel with hardness 750–770 VPN polished to the surface roughness indicated in Table 1, where R_a is average roughness of profile, and R_z is mean peak to valley height of roughness profile. Fresh ball and test were used for testing each oil, and they were cleaned by immersion in toluene and isopropanol in an ultrasonic bath for 10 min.

2.3. Tested lubricants

In order to get an overview of the environmental acceptable lubricants, two different EALs with the same viscosity class from different companies were selected. Both oils meet the US EPA requirements for "Environmentally Acceptable Lubricants". Additionally, two mineral oils were selected: one gear oil with the same viscosity class, and an engine oil with the similar 40 °C kinematic viscosity that is practically used in ships for gear lubrication. All the oils except M1 that is an engine oil, comply with the DIN 51517 part 3 (CLP) standard. The oils specifications can be found in Table 2:

2.4. Experimental procedure

Four types of test were performed for each oil: stribeck test, traction test, tribofilm formation test, and high-sliding wear test.

Stribeck test represents the variation of coefficient of friction as a function of stribeck parameter (viscosity*speed/load). In this experiment, load and viscosity are constant, so the stribeck results are presented as a coefficient of friction versus entrainment speed while keeping SRR constant. Traction curve shows the variation of friction coefficient by increasing sliding speed while having a constant entrainment speed. As the sliding speed is equal to SRR multiplied by entrainment speed, so the curve is usually shown as friction versus SRR. The traction curve can give an explanation about the shear properties of the lubricant [46], and gives an estimation of the frictional behavior of the oils along the line of action of a gear pair [25].

As it is illustrated in Fig. 2, the set of stribeck and traction tests were repeated three times: the first set on the fresh samples, the second set after 1 h of rolling/sliding running, and the third set after an additional 2 h of running. During each set of stribeck and traction test, friction and ECR were recorded, and tribofilm thickness was checked by SLIM technique before and after each test. The evolution of friction, ECR, and tribofilm thickness indicates the ability of each oil to separate the contacting surfaces by either EHL film or boundary tribofilm. The main idea of this test plan is to evaluate and compare the EHL/mixed transition of oils and study the effect of tribofilm thickness on this transition.

The parameters for each of the tests are presented in Table 3:

After finishing three sets of stribeck and traction tests, a wear test inspired by Ref. [47] was performed. The advantage of this wear test is minimization of the contact geometry changes, and providing a slide-roll ratio greater than two that leads to high sliding speed and low entrainment speed. The surface roughness of worn and new discs was checked by an Alicona InfiniteFocus G5 optical profilometry system from Optimax.

3. Results and discussion

3.1. Evaluation of the fresh samples

Fig. 3 (a) and (b) respectively show the stribeck and traction curves of the lubricants performed on the fresh samples. As it is performed on

Table 2
Measured lubricants properties.

	Kin. Vis. @40 °C (mm^2/s)	Kin. Vis. @100 °C (mm^2/s)	ρ @15 °C (kg/m^3)	VI	Comment
Method	ASTM D445	ASTM D445	EN ISO 12185	ASTM D 2270	
M1	127.60	13.83	908	105	Mineral engine oil
M2	142.50	14.24	888	97	Mineral gear oil
EAL1	147.50	18.84	972	145	Synthetic oil, EAL
EAL2	150.57	18.44	929	137	Synthetic oil, EAL

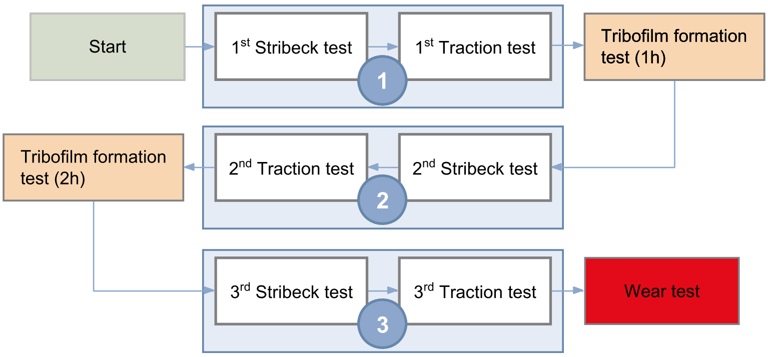

Fig. 2. Designed test matrix for the mini-traction machine.

Table 3
Conditions of each test.

	Traction test	Stribeck test	Tribofilm formation test	Wear test
SRR	0–1.9	0.05	0.50	100
Entrainment Speed (mm/s)	700	10–3900	150	70
Maximum Hertzian pressure (GPa)	1.25	1.25	1.11	1.25
Temperature °C	40	40	100	40
Duration	–	–	1 h before 2nd stribeck, and 2 h before 3rd stribeck	2 h

the new samples, and the tribofilm thickness after the test was negligible, it can be supposed that the friction and ECR are not yet affected by the tribofilm.

Fig. 3 (a) shows stribeck curves performed at 5% SRR. Decreasing the entrainment speed from 3900 mm/s, at first the friction increases. Then at an entrainment speed between 1200 and 1600 mm/s (depending on the oil), it reaches the maximum, and then it decreases till a minimum appears at an entrainment speed around 50 mm/s, and then it rises. This curve is different from an ideal stribeck curve in which the transition from (elasto)hydrodynamic to mixed lubrication goes with a sharp increase of friction coefficient till it reaches the maximum at the transition to the boundary lubrication regime. Lafountain et al. observed the same trend as presented in Fig. 3 (a), and described that it is due to the heating effect. The ideal stribeck is considered to be isothermal, while a non-isothermal stribeck curve can be affected by the shear heating. By calculating the viscosity changes due to temperature rise in the contact, the isothermal model can be corrected. The thermal correction results in a matched theoretical and experimental stribeck curve [48].

The thermal effects can vary the stribeck curve to the extent that the friction coefficient does not represent the EHL/mixed transition. Hansen et al. illustrate that the friction coefficient does not signify the initial asperity contacts, and consequently the transition to the mixed lubrication [26]. From ECR changes presented in Fig. 3 (a), it can be seen that the transition to the mixed lubrication takes place at an entrainment

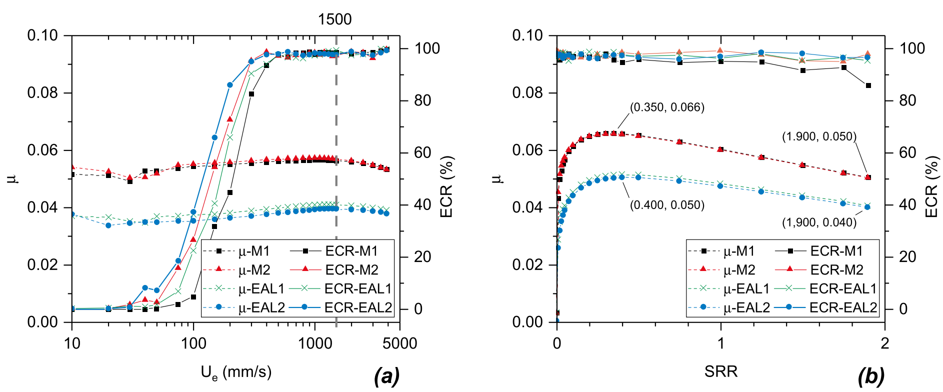

Fig. 3. Fresh samples friction and ECR: (a) Stribeck curves and corresponding ECR. (b) Traction curves and corresponding ECR.

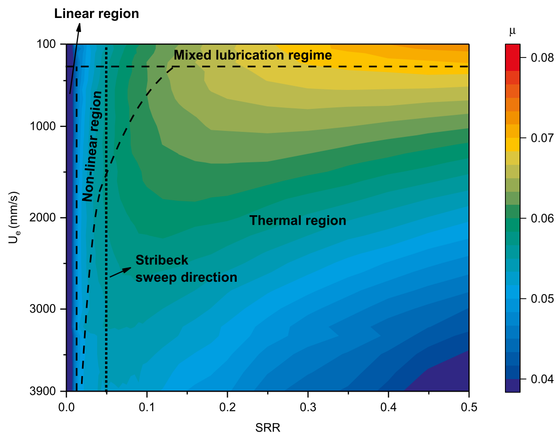

Fig. 4. 3D map of friction for the oil M2.

Table 4
Estimated pressure-viscosity coefficient and dynamic viscosity of the lubricants.

	α @40 °C (1/GPa)	η @40 °C (mPa s)	LP = $\alpha^{0.53} \times \eta^{0.67}$ @40 °C
M1	19.95	113.50	116.37
M2	20.25	124.00	124.46
EAL1	13.28	140.50	108.24
EAL2	13.34	137.10	106.73

speed around 500 mm/s for all the oils, and a minimum in the friction is not visible, whereas interestingly the friction coefficient is decreasing in the mixed lubrication regime. However, for the case of transition to the boundary lubrication, the friction stays constant or increases that signifies the onset of severe asperity contacts.

Johnson and Tevaarwerk proposes three friction regions in the traction curves of a lubricant: 1) a linear region in which the fluid behavior is Newtonian, 2) a non-linear (isothermal) region in which the shear-thinning happens and the maximum friction is bound to the limiting shear stress, and 3) a thermal region in which thermal softening behavior is dominant in the friction [46]. Björling discussed friction mapping in Ref. [49], and based on works in Refs. [46,50] extends the friction regions into a 3D friction map. Fig. 4 illustrates a similar friction map for the oil M2 as an example. The border between non-linear and thermal region is set at the point in which the friction drops with either increase or decrease of entrainment speed. With increasing the entrainment speed in a constant SRR, depending on the SRR, the lubricant experiences different transitions. In low SRR, by increasing the U_e, the lubrication is first affected by the shear-thinning in the non-linear region, then by the limiting shear stress, and at the end by the thermal region. However, for the high SRR or near zero SRR, the stribeck curve will remain respectively in the thermal region or linear region [50]. If a specific lubrication condition is considered near to the border of the non-linear and thermal region, by keeping the SRR and increasing the entrainment speed, it will fall into the thermal region and consequently lower friction coefficient. This is what happens in the friction of tested oils when the speed increases from 1200 to 3900 mm/s.

In Fig. 3 (a), the friction coefficient is decreasing by reducing the entrainment speed even in the mixed lubrication regime of all the oils. Therefore, with the smooth contacts specified in Table 1, the effect of asperity contact on the friction coefficient is considerably less than the effect of fluid shear stress drop.

In Fig. 3 (a), the ECR changes show the EHL/mixed and mixed/boundary transition of the oils. Although it is difficult to exactly find the EHL/mixed transition point, it is clear that the ECR of EAL2 is the highest. The better protection provided by EAL2 is approved by the 3D image of wear scar in section 3.3, Fig. 9. Finding an explanation for the higher ECR of EAL2 calls for comparing effective parameters on EHL film thickness. Jackson and Rowe defined a parameter named *Lubricant Parameter (LP)* which is the product of pressure-viscosity coefficient (α) and dynamic viscosity (η) at a specific temperature [51]. This parameter is used as an indication of EHL film formation ability of the oils in line contact and is employed in Ref. [43]. Coseausu et al. used Hamrock and Dowson's formula [52] and redefined the lubricant parameter as $LP = \alpha^{0.53}\eta^{0.67}$ for elliptical contacts [53]. In order to find the LP parameter for the oils, pressure-viscosity coefficient and dynamic viscosity were estimated using a method presented in Ref. [11]. This method is based on an experimental equation developed in Ref. [16], and it is used for modeling the traction curves of gear oils [12] and approximating the EHL film thickness [43,54]. Calculated values of pressure-viscosity coefficient (α) and dynamic viscosity (η) and LP are given in Table 4.

In order to approve the estimated values of the pressure-viscosity coefficient, the specific EHL film thickness was calculated using Hamrock and Dowson's formula [52]. The specific film thickness is plotted in Fig. B.12 in Appendix B. It is clear that the transition to mixed lubrication happens at the lambda ratio equal to 3, and the transition to boundary lubrication is visible at the lambda ratio equal to 1. It is noticeable to say that the calculated EHL film thickness does not consider the thermal effect and inlet shear heating, so that is why the Lambda value (and consequently EHL film thickness) of EAL2 is lower than the others.

From Table 4, EAL2 has the lowest LP value which is not consistent with its higher ECR and EHL film thickness. The temperature rise within the EHL film was not considered in LP value, so the higher ECR of EAL2 can be attributed to the lower generated heat by friction, the higher thermal conductivity, higher heat capacity, higher viscosity index of ester-based oils compared to mineral oils. The oil entrapped in the contact is so small, so heat capacity should not be significant compared to the thermal conductivity. In addition, the higher polarity of ester-based oils can be another parameter enhancing EHL film thickness. EAL1 with a similar oil type as EAL2 shows lower ECR than EAL2 and M2. This indicates that the chemical composition and molecular design play an important role. Although the LP value did not signify the EHL film of EAL2 and EAL1, it well confirmed the lower ECR of M1 oil in comparison with M2.

The traction curves in Fig. 3 (b) clearly show lower friction of EALs compared to the mineral oils. Björling et al. show that the friction performance of oils can be ranked by their traction curves, and it gives the same result as FZG device [25]. Based on this, the power loss by using EAL1 and EAL2 is lower than the mineral ones.

Brandão et al. show that the lubricants can be classified according to the similarity of their EHL traction curves [12]. This interesting feature is visible in the present tested lubricants, and the lubricants can be classified into two groups: M1, M2 with high friction, and EAL1, EAL2 with low friction. In each group, the friction, VI and pressure-viscosity coefficient are almost similar, while the kinematic viscosity and lubricant parameters (LP) are different. This indicates that friction in the EHL regime is more dependent on the pressure-viscosity coefficient than the dynamic, kinematic viscosity or the lubricant parameter.

In the traction curves (Fig. 3 (b)), except for the case of M1 oil, the ECR of the other oils is not sensitive to the SRR and remains around 100% providing EHL lubrication. So, just for the oil M1 the viscosity drop with SRR is significant and causes EHL/mixed lubrication transition. Hansen et al. observe that the ECR is sensitive to SRR for the fresh rough samples (Ra of ball = 208 nm and disc = 7 nm), but it becomes insensitive to SRR (in the range of 0–0.5) after running-in period [26]. Therefore, the insensitivity of ECR to SRR in Fig. 3 (b) is due to the smooth surface of the samples compared to the EHL film thickness at 700 mm/s entrainment speed.

The data points of traction test were acquired by increasing from

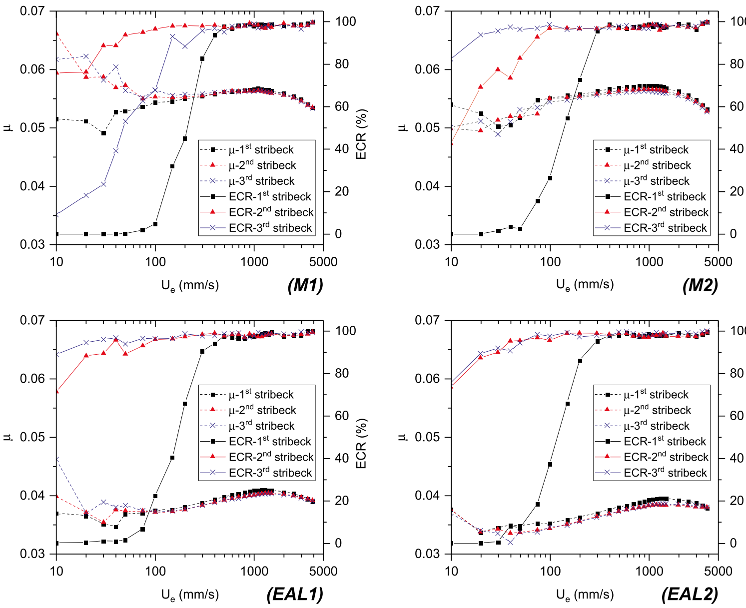

Fig. 5. Stribeck curves of the oils. The "1st" is for the fresh samples, the "2nd" after 1 h rubbing, and "3rd" after 2 h more additional rubbing.

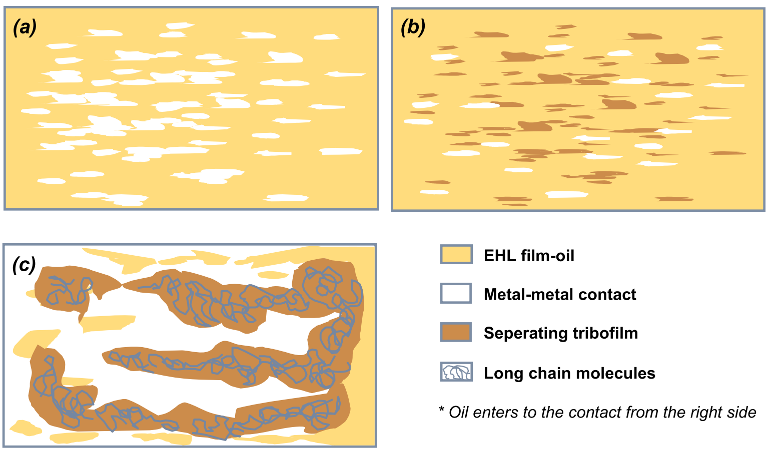

Fig. 6. Growth of tribofilm and its effect on the solid-solid contact.

SRR = 0, and each data point is the average of data for 20 s. By increasing the SRR, if the asperity contact is very small, it can be polished during 20 s. So, a very short running-in happens during each data point measurement. However, if the oil film thickness is small enough, the asperity contacts are more severe and the change of the lubrication regime can be detected by ECR technique. This is the case of M1 in Fig. 3 (b) that the transition to mixed lubrication is evident in the high SRRs.

Kumar and Khonsar show that the lower thermal conductivity leads to appearance of limiting shear stress at lower SRR [17]. From Fig. 3 (b), it is noticeable that the limiting shear stress of the EALs happens at higher SRRs compared to the case of mineral oils. Also, the drop of their traction is less (0.016 for EALs vs 0.010 for mineral oils). Based on the literature [6], it is also expected that EALs, mostly consisted of ester molecules, show better shear stability. Based on what was discussed on the stribeck curve variations and the lubrication regions, it can be said that the latest the limiting shear stress is reached, the less the oil is affected by the temperature rise. The mean oil film temperature rise is equal to Ref. [55]:

$$\Delta \overline{T}_{oil} = \frac{h}{(8K_{oil})} \overline{\tau} U_s \tag{4}$$

where K_{oil} is the oil thermal conductivity, h is the film thickness, and the generated heat is equal to mean shear stress ($\overline{\tau}$) multiplied by the sliding speed (U_s). From traction curves of the oils in Fig. 3 (b), for the case of EAL2, it has the lowest friction coefficient, so it generates the lowest amount of heat. Based on the Eq. (4), the EALs provide less temperature rise by providing firstly lower friction, and secondly higher thermal conductivity. This lower temperature rise results in less viscosity drop in

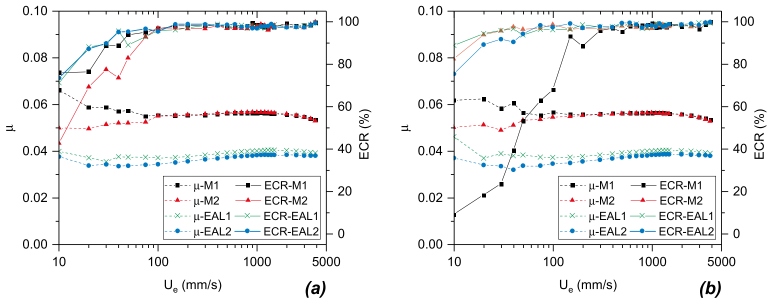

Fig. 7. Comparison of friction and ECR of the oils: (a) after 1 h, and (b) after 2 h of rubbing.

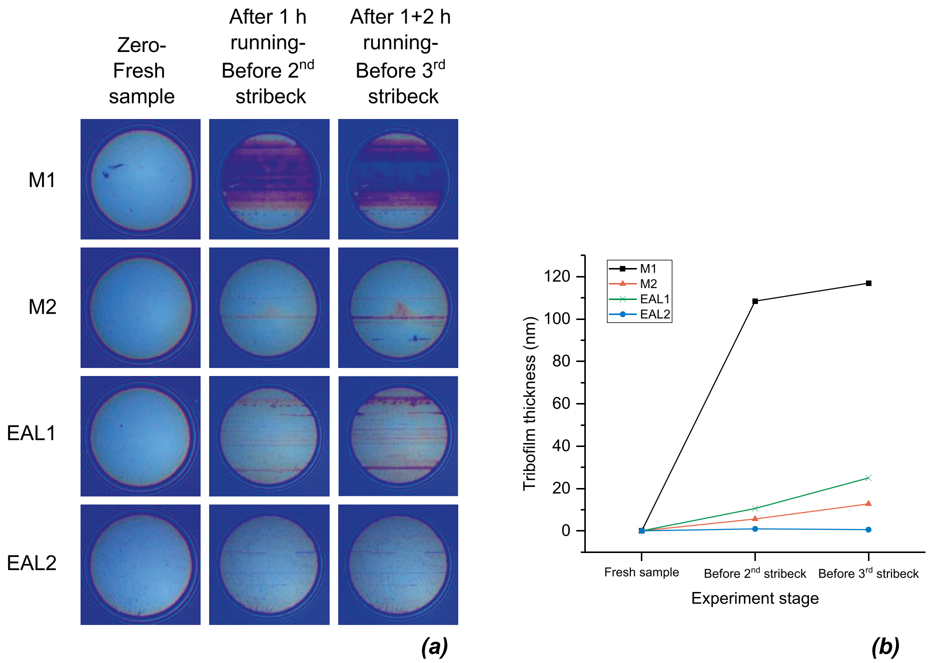

Fig. 8. Tribofilm evolution during different stages of the tests: (a) SLIM images, and (b) mean tribofilm thickness.

high loads and high shear contacts. High viscosity index of ester-based oils makes them free from viscosity index improver leading to better shear stability and film formation ability [56]. In conclusion, higher thermal conductivity, higher viscosity index and lower heat generation help them to keep their viscosity less affected by the heat generation in the contact.

3.2. Running-in effect

After the 1st stribeck and traction tests, a 1-h rubbing at high temperature (100 °C) was carried out to accelerate the tribofilm formation and increase asperity contacts. Then the 2nd stribeck and traction tests were performed. After that, another additional 2 h of rubbing at high temperature was performed, followed by the 3rd stribeck and traction tests (Fig. 2). For the case of traction curves, a small amount of decrease in friction was observed and the ECR of all oils was around 100% showing an EHL lubrication.

Regarding the stribeck curves shown in Fig. 5, the friction in the EHL region decreased for all the oils. However, in the mixed region, the reactions were different from one oil to another. In all the cases, the ECR was increased compared to the 1st stribeck. The ECR can increase by flattening of high asperity summits, or by the formation of tribofilm that both reduce metal-metal contact [38]. As the ECR variations were different from one oil to another, it is good to first discuss each case.

For the case of M1, the following points can be remarked based on Figs. 5 and 8:

a) Friction: In the mixed and boundary regime, friction was increased. Also, in the 2nd and 3rd stribeck curves, the friction rise is started in higher U_e which indicates weakened EHL film due to the shift of boundary lubrication to higher U_e. It is noticeable to say that in the EHL regime, the friction is a bit decreased due to the flattening of the high summits.
b) ECR: The ECR has the lowest amount for the 1st stribeck. In the 2nd stribeck, the ECR is increased and then decreased in the 3rd stribeck.

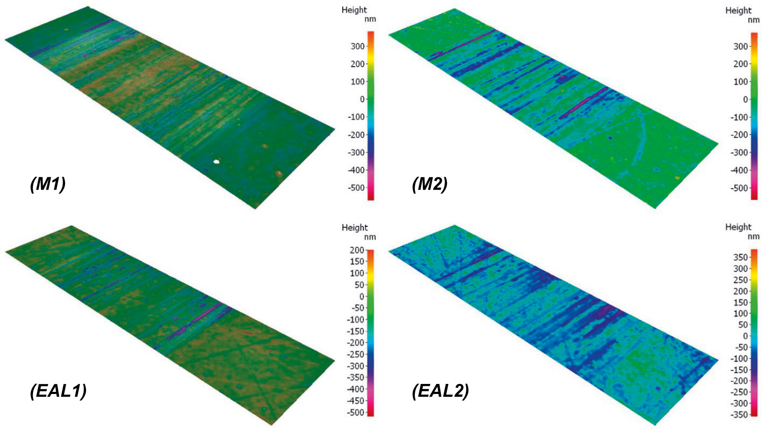

Fig. 9. 3D images of the disc wear scar.

c) Tribofilm: From Fig. 8, the Tribofilm is growing in every stage, and the thickest is found before the 3rd stribeck.

Considering the point a) and c), it can be said that the growth of tribofilm in oil M1 leads to higher friction in mixed and boundary regime. It seems that the available AW additives in this oil enhanced the protection against wear by scarifying the effect of FM additives. Dawczyk et al. investigated the tribofilm formation of ZDDP and observed the same friction rise, and correlated it to the increased roughness [57]. This behavior can be seen in the other tribofilms, and it is not just the characteristics of ZDDP films [58].

From point b) the increased ECR in the 2nd stribeck seems logical as signifies the formation of the tribofilm [38] in Fig. 8. However, the decrease of ECR in the 3rd stribeck was not expected, because the thickest tribofilm is found before this stage (point c)), and it had to lead to the lowest metal-metal contact. A thick tribofilm can also change the friction, so the higher friction in mixed and boundary lubrication is affected by growing tribofilm.

Taylor and Spikes observed the effect of tribofilm formation on the friction in the mixed regime, and argue that the increased friction in the mixed regime and its extension to higher U_e is not just due to an increase in the roughness. They proposed the following possible mechanisms by which this change happens [59]:

- Starvation due to
  - o Lower wettability of tribofilm
  - o Inlet blocking by the tribofilm
- Localized oils films around the tribofilm by lower EHL film due to:
  - o Lower viscosity
  - o Lower pressure-viscosity coefficient
- Modification of the inlet geometry by the tribofilm
- Slip at the boundary of tribofilm/oil

In addition, if we consider the starvation due to the accumulation of the long-chain molecule hydrocarbons in the inlet, the weakened EHL film seems reasonable. Now, the ECR decrease in the 3rd stribeck curve of M1 can be explained. In the mixed and boundary lubrication, the load is partly supported by the EHL film and solid-solid contact. If a tribofilm is formed between the surfaces, part of the solid contact is supported by the tribofilm, but still, there is a degree of asperity contacts. By adding the tribofilm load carrying capacity to the equation presented in Ref. [60], the load carrying shares can be formulated as below:

$$F_T = F_{EHL} + F_C + F_{TF} \tag{5}$$

where F_T is the total load, F_{EHL} is the load carried by the fluid film, F_c is the load carried by the asperities which are not covered by the tribofilm, and F_{TF} is the load carried by the tribofilm. For the case of M1 oil, the inhibiting effect of grown tribofilm weakens the primary EHL film, so the separating EHL film is not generated very well. When the F_{EHL} is decreased, the asperity contacts are increased to compensate for the EHL load share. Furthermore, when there is no EHL film, the tribofilm can be penetrated easier and the probability of metallic contact will increase. Fig. 6 shows a schematic of the effect of tribofilm growth on the metal-metal contact. In Fig. 6 (a), there is no tribofilm available which is the case of 1st stribeck curve. By a small growth of the tribofilm (Fig. 6 (b)), part of asperity contacts are covered, so the ECR is increased (lower metal-metal contact). For the 3rd stribeck, the thick tribofilm damages the EHL film, so consequently the asperities that were separated by the EHL film come to the contact (Fig. 6 (c)).

The blocking character of tribofilm formed in oil M1 can be amplified by its combination with the long-chain molecule hydrocarbons found as impurities in the oil. Though Dawczyk et al. show that the roughness is the most important parameter influencing the friction increase [57], it seems that other parameters are also important, as there are several pieces of research indicating the inhibiting effect of patch like structure in ZDDP tribofilms [58,59,61,62]. From this case, it can be concluded that there is an optimum tribofilm thickness being able to separate the surfaces properly, higher or lower thickness leads to higher metal-metal contact.

Discussing the other oils in Fig. 5, friction in mixed lubrication was increased for EAL1 showing an extension of mixed and boundary regimes to higher entrainment speed, same as the feature observed for the case of M1, though it is with smaller amplitude. This is due to the tribofilm growth in EAL1; however, it is not too large to significantly block the EHL film, so it did not result in high metallic contact (decrease in the ECR). For the case of M2 and EAL2, ECR was raised and the friction was slightly decreased in the EHL regime. These changes are mainly due to high summits flattening, and partial surface coverage by the tribofilm, and maybe activation of the friction modifiers. Nevertheless, no meaningful change of mixed and boundary friction is visible in any one of these two oils. Although some small amount of tribofilm is visible in the SLIM images of M2, the friction curve does not show the extension of mixed lubrication to higher U_e, so the tribofilm in these oils are not damaging the EHL film.

3.3. Ranking the oils regarding surface protection

As was mentioned in section 3.2, the ECR is a result of the separation

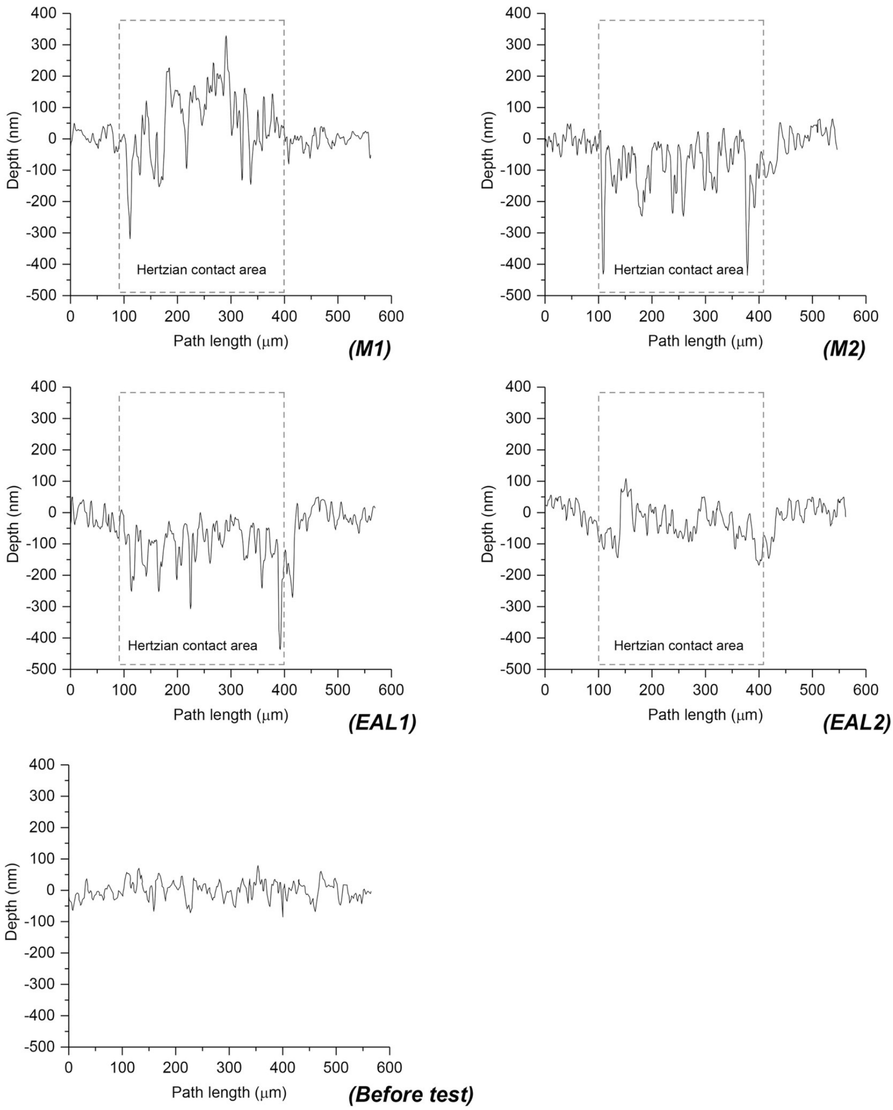

Fig. 10. Roughness profile of the disc across the wear scar before and after finishing all the test stages.

Table 5
Roughness parameters of the disc after the wear test.

	Ra (nm)	Rz (nm)
M1	64	415
M2	62	482
EAL1	49	393
EAL2	30	198

between ball and disc by EHL or tribofilm. For a specific oil, if the ECR of a stribeck curve is increased after a running-in, it means that high asperity summits are flattened resulting in a stronger EHL film, or the tribofilm thickness is grown [38]. For the case of 1st stribeck test, the ECR and EHL film of oils was discussed in section 3.1. Regarding the 2nd and 3rd stribeck, it is necessary to check Figs. 3 (b), 5, 7 and 8 together in order to separate the effect of tribofilm thickness and EHL on the ECR.

In the 2nd and 3rd stribeck test, performed after a 1 h and 2 h of running-in, the tribofilm thickness in M1 and EAL1 is noticeably high (Fig. 8). So for these two oils, the increase of ECR in 2nd and 3rd stribeck (Fig. 5) is originated from the tribofilm growth. For the EAL2, the tribofilm is negligible in all stribeck stages (Fig. 8), so the high ECR of EAL2 in all the stribeck tests is mainly attributed to its high ability to form and maintain EHL film. For this oil, the ECR changes in Fig. 5 are mostly from the high summits flattening. For the oil M2, the tribofilm thickness is not as thin as EAL2, and not as thick as M1 and EAL1, so the tribofilm and asperity flattening both are effective in ECR changes of this oil.

Comparing EAL2 and M2 in Fig. 7(a) using Eq. (5), F_{EHL} of M2 is lower to the extent that it is not able to be compensated by the tribofilm, so its F_C is bigger and consequently, it has lower ECR. Compared to EAL2, EAL1 had lower ECR in 1st stribeck (Fig. 3(a)), but its tribofilm is able to compensate for the difference of F_{EHL} that it had with EAL1. For the 3rd stribeck, all the oils except the M1 have almost similar ECR but the share of loads that are carried by each term of Eq. (5) is different for them.

After the 3rd stribeck curves, a high sliding wear test was performed to accelerate the wear. The 3D images of the worn surface of discs are shown in Fig. 9, and the surface roughness profiles before and after the tests can be observed in Fig. 10. The EAL2 has a very smooth disc surface with few scratches similar to the new sample. The surface height is not grown showing that there is negligible tribofilm on its surface which is in agreement with the slim images of Fig. 8. So it approves that for the oils EAL2, the surfaces are protected mostly by the EHL film. In Fig. 9, M2 has more scratches compared to the EAL2, and from Table 5, its higher roughness clarifies that the surface lubricated with M2 has more damages than the surfaces lubricated with EAL2. For the case of M1, the thick tribofilm does not allow to see a clear image of the damages to the surface, nevertheless, deep scratches comparable to those of M2 are visible. These scratches and a thin tribofilm are present also in the case of EAL1 making it comparable to the case of M2.

4. Conclusion

The objective of this work was to examine the EHL film formation ability of fully formulated EALs compared to mineral ones. Besides, the interaction between EHL film and tribofilm was investigated. A ball and disc test equipment provided sliding/rolling contact between two smooth surfaces loaded with 1.25 GPa maximum Hertzian pressure. Friction and ECR variations in the Stribeck and traction curves were analyzed together with an in-situ measurement of tribofilm thickness. Two industrial EALs formulated for gears and two fully formulated mineral oils were evaluated regarding their EHL/mixed transition. The overall conclusions are as follow:

- The excessive growth of tribofilm damages the EHL film and additionally can result in higher metal-metal contact. So, a thin tribofilm is an advantage for the components working is the EHL regime.
- The damage of EHL film by a thick tribofilm is not just due to the roughened surface. It is mostly related to the inlet blocking by the tribofilm.
- Comparing two tested EALs, the one with lower LP value showed less metal-metal contact. This indicates the importance of chemical composition and molecular design of base oil and additive in EHL film formation.
- Compared to the tested mineral oils, EALs showed better or similar EHL film formation ability though having lower LP value. The lower LP value of EALs can be compensated by:
    - o Less generated heat
    - o Their higher VI makes them free from VI improver
    - o Their better thermal conductivity
    - o Higher polarity
- In the EHL regime, friction is more dependent on the pressure-viscosity coefficient than the dynamic, kinematic viscosity or the lubricant parameter. Regarding this point, the lower pressure-viscosity coefficient of EALs is an advantage that causes lower friction.
- Friction does not signify the transition between EHL to mixed lubrication regime.
- ECR technique together with the friction and SLIM technique provide a good understanding of the interaction of tribofilm and EHL film.

A fully formulated industrial oil is composed of several chemical compositions for the base oil and additive. Studying EHL formation ability of these oils calls for considering the interaction of different compositions. Physical properties like viscosity and pressure-viscosity coefficient, though useful for rough approximations, are not enough to estimate the EHL/mixed transition especially when the tribofilm is formed between the surfaces. The results and approach in this study provides an insight into the interaction of tribofilm with EHL film and approves that industrial EALs can be substituted for mineral oils, especially for the components working in the EHL regime.

Author contribution section

Reza Bayat: Conceptualization, Methodology, Software, Validation, Formal analysis, Investigation, Resources, Data Curation, Writing - Original Draft, Writing - Review & Editing, Visualization.

Arto Lehtovaara: Conceptualization, Writing - Review & Editing, Supervision, Project administration.

Declaration of competing interest

The authors declare no potential conflicts of interest with respect to the research, authorship and/or publication of this article, and we have fully respected the research ethics principles.

Acknowledgments

We gratefully acknowledge the financial support from Tampere University graduate school. The authors would like to thank Mr. Jarmo Laakso from Tampere University for carrying out the roughness measurements, and Fluidlab Oy for measuring the viscosity and density of the oils.

Appendix A. Tribofilm thickness measurement

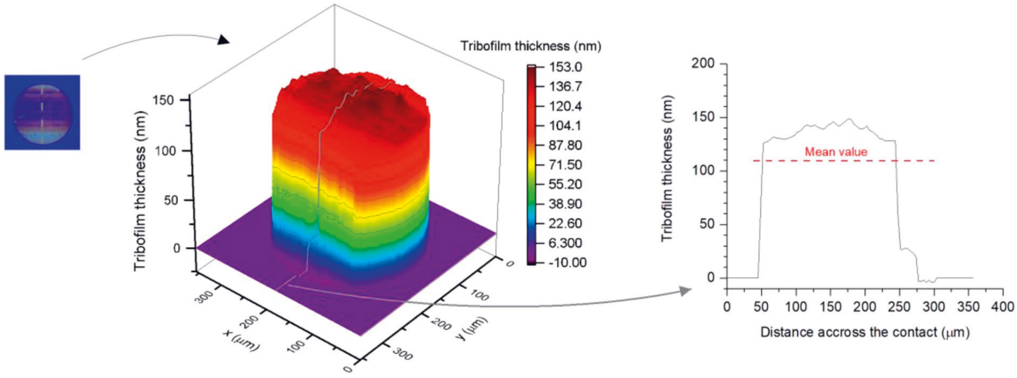

Fig. A.11. Thickness measurement of the tribofilm for oil M1 before the 2nd stribeck.

Appendix B. Specific film thickness

The specific film thickness is calculated using Eqs. (B.6-B.8):

$$\Lambda = \frac{h_{min}}{\sigma_{rms}} \tag{B.6}$$

$$h_{min} = 3.63 R_x \left(\frac{U_e \eta_0}{E^* R_x}\right)^{0.68} (\alpha E^*)^{0.49} \left(\frac{F}{E^* R_x^2}\right)^{-0.073} \left(1 - e^{-0.68k}\right) \tag{B.7}$$

$$\sigma_{rms} = \sqrt{R_{q1}^2 + R_{q2}^2} \tag{B.8}$$

where R_x is the radius of curvature in the x-direction (m), U_e is the entrainment speed (m/s), η_0 is the dynamic viscosity of the lubricant (Pa.s), E^* is the reduced Young's Modulus (Pa), α is the pressure-viscosity coefficient (Pa^{-1}), F is the applied load (N), k = 1. R_{q1} and R_{q2} are the Root-Mean-Square roughness of disc and ball respectively amounting 34.08 (nm) and 50.95 (nm).

The specific film thickness is shown in Fig. B.12:

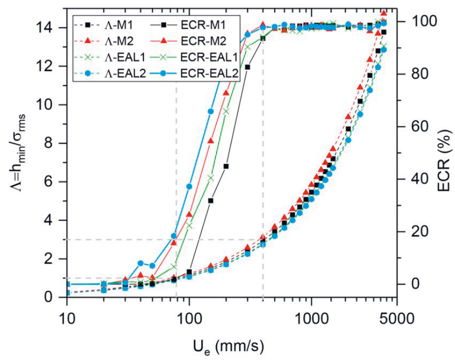

Fig. B.12. Specific film thickness and ECR vs entrainment speed for the 1st stribeck test.

References

[1] Ingram M, Hamer C, Spikes HA. A new scuffing test using contra-rotation. Wear 2015;328–329:229–40. https://doi.org/10.1016/j.wear.2015.01.080.

[2] Jelita Rydel J, Pagkalis K, Kadiric A, Rivera-Dïaz-del-Castillo PEJ. The correlation between ZDDP tribofilm morphology and the microstructure of steel. Tribol Int 2017;113:13–25. https://doi.org/10.1016/j.triboint.2016.10.039.

[3] Pettersson A. High-performance base fluids for environmentally adapted lubricants. Tribol Int 2007;40:638–45. https://doi.org/10.1016/j.triboint.2005.11.016.

[4] Norrby T. Environmentally adapted lubricants – where are the opportunities? Ind Lubric Tribol 2003;55:268–74. https://doi.org/10.1108/00368790310496400.

[5] Mobarak HM, Niza Mohamad E, Masjuki HH, Kalam MA, Al Mahmud KAH, Habibullah M, et al. The prospects of biolubricants as alternatives in automotive applications. Renew Sustain Energy Rev 2014;33:34–43. https://doi.org/10.1016/J.RSER.2014.01.062.

[6] Randles SJ. Esters. In: Rudnick LR, Shubkin RL, editors. Synth. Lubr. high-performance Funct. fluids. second ed. Chapman and Hall/CRC; 1999. p. 881.

[7] Luther R. Lubricants in the environment. In: Mang T, Dresel W, editors. Lubr. Lubr. third ed. Weinheim, Germany: Wiley-VCH Verlag GmbH & Co. KGaA; 2017. p. 153–236. https://doi.org/10.1002/9783527610341.ch7.

[8] Pettersson A. Environmentally adapted lubricants: properties and performance. Luleå University of Technology; 2006.
[9] Bartels T, Bock W. Gear lubrication oils. In: Mang T, Dresel W, editors. Lubr. Lubr. third ed. Weinheim, Germany: Wiley-VCH Verlag GmbH & Co. KGaA; 2017. p. 293–344. https://doi.org/10.1002/9783527645565.ch10.
[10] Fernandes CMCG, Battez AH, González R, Monge R, Viesca JL, García A, et al. Torque loss and wear of FZG gears lubricated with wind turbine gear oils using an ionic liquid as additive. Tribol Int 2015;90:306–14. https://doi.org/10.1016/J.TRIBOINT.2015.04.037.
[11] Brandão JA, Meheux M, Ville F, Seabra JHO, Castro J. Comparative overview of five gear oils in mixed and boundary film lubrication. Tribol Int 2012;47:50–61. https://doi.org/10.1016/j.triboint.2011.10.007.
[12] Brandão JA, Meheux M, Seabra JHO, Ville F, Castro MJD. Traction curves and rheological parameters of fully formulated gear oils. Proc Inst Mech Eng Part J J Eng Tribol 2011;225:577–93. https://doi.org/10.1177/1350650111405111.
[13] Ahlroos T, Ronkainen H, Helle A, Parikka R, Virta J, Varjus S. Twin disc micropitting tests. Tribol Int 2009;42:1460–6. https://doi.org/10.1016/J.TRIBOINT.2009.05.023.
[14] Martins R, Seabra J, Brito A, Seyfert C, Luther R, Igartua A. Friction coefficient in FZG gears lubricated with industrial gear oils: biodegradable ester vs. mineral oil. Tribol Int 2006;39:512–21. https://doi.org/10.1016/J.TRIBOINT.2005.03.021.
[15] Rieglert J, Kassfeldt E. Performance of environmentally adapted hydraulic fluids at boundary lubrication. Tribol Ser 1997;32:467–73. https://doi.org/10.1016/S0167-8922(08)70474-7.
[16] Gold PW, Schmidt A, Dicke H, Loos J, Assmann C. Viscosity–pressure–temperature behaviour of mineral and synthetic oils. J Synth Lubric 2001;18:51–79. https://doi.org/10.1002/jsl.3000180105.
[17] Kumar P, Khonsari MM. Traction in EHL line contacts using free-volume pressure-viscosity relationship with thermal and shear-thinning effects. J Tribol 2008;131. https://doi.org/10.1115/1.3002331. 011503-1-011503–8.
[18] Stachowiak GW, Batchelor AW. Engineering tribology. third ed. Burlington: Butterworth-Heinemann; 2013. https://doi.org/10.1016/B978-0-12-397047-3.00007-2.
[19] O'Connor BM. Gear lubricants. In: Wang QJ, Chung Y-W, editors. Encycl. Tribol. Boston, MA: Springer US; 2013. p. 1488–93. https://doi.org/10.1007/978-0-387-92897-5_940.
[20] Minami I. Molecular science of lubricant additives. Appl Sci 2017;7:445. https://doi.org/10.1007/BF00571595.
[21] Mang T, Bobzin K, Bartels T. Industrial tribology. Weinheim, Germany: Wiley-VCH Verlag GmbH & Co. KGaA; 2010. https://doi.org/10.1002/9783527632572.
[22] Kleemola J, Lehtovaara A. Experimental simulation of gear contact along the line of action. Tribol Int 2009;42:1453–9. https://doi.org/10.1016/J.TRIBOINT.2009.06.007.
[23] Höhn B-R, Michaelis K, Doleschel A. Frictional behaviour of synthetic gear lubricants. Tribol Ser 2001;39:759–68. https://doi.org/10.1016/S0167-8922(01)80156-5.
[24] Björling M, Larsson R, Marklund P, Kassfeldt E. Elastohydrodynamic lubrication friction mapping – the influence of lubricant, roughness, speed, and slide-to-roll ratio. Proc Inst Mech Eng Part J J Eng Tribol 2011;225:671–81. https://doi.org/10.1177/1350650111403363.
[25] Björling M, Miettinen J, Marklund P, Lehtovaara A, Larsson R. The correlation between gear contact friction and ball on disc friction measurements. Tribol Int 2015;83:114–9. https://doi.org/10.1016/j.triboint.2014.11.007.
[26] Hansen J, Björling M, Larsson R. Mapping of the lubrication regimes in rough surface EHL contacts. Tribol Int 2019;131:637–51. https://doi.org/10.1016/J.TRIBOINT.2018.11.015.
[27] Spikes HA. Sixty years of EHL. Lubric Sci 2006;18:265–91. https://doi.org/10.1002/ls.23.
[28] Johnston GJ, Wayte R, Spikes HA. The measurement and study of very thin lubricant films in concentrated contacts. Tribol Trans 1991;34:187–94. https://doi.org/10.1080/10402009108982026.
[29] Choo JW, Olver AV, Spikes HA. The influence of transverse roughness in thin film, mixed elastohydrodynamic lubrication. Tribol Int 2007;40:220–32. https://doi.org/10.1016/J.TRIBOINT.2005.10.009.
[30] Cambiella A, Benito JM, Pazos C, Coca J, Ratoi M, Spikes HA. The effect of emulsifier concentration on the lubricating properties of oil-in-water emulsions. Tribol Lett 2006;22:53–65. https://doi.org/10.1007/s11249-006-9072-1.
[31] Glovnea R, Furtuna M, Nagata Y, Sugimura J. Electrical methods for the evaluation of lubrication in elastohydrodynamic contacts. Tribol Online 2012;7:46–53. https://doi.org/10.2474/trol.7.46.
[32] Albahrani SMB, Philippon D, Vergne P, Bluet JM. A review of in situ methodologies for studying elastohydrodynamic lubrication. Proc Inst Mech Eng Part J J Eng Tribol 2016;230:86–110. https://doi.org/10.1177/1350650115590428.
[33] Sjöberg S, Sosa M, Andersson M, Olofsson U. Analysis of efficiency of spur ground gears and the influence of running-in. Tribol Int 2016;93:172–81. https://doi.org/10.1016/J.TRIBOINT.2015.08.045.
[34] Mallipeddi D, Norell M, Sosa M, Nyborg L. Influence of running-in on surface characteristics of efficiency tested ground gears. Tribol Int 2017;115:45–58. https://doi.org/10.1016/J.TRIBOINT.2017.05.018.
[35] Viesca JL, Battez AH, González R, Reddyhoff T, Pérez AT, Spikes HA. Assessing boundary film formation of lubricant additivised with 1-hexyl-3-methylimidazolium tetrafluoroborate using ECR as qualitative indicator. Wear 2010;269:112–7. https://doi.org/10.1016/J.WEAR.2010.03.014.
[36] Adebogun A, Hudson R, Breakspear A, Warrens C, Gholinia A, Matthews A, et al. Industrial gear oils: tribological performance and subsurface changes. Tribol Lett 2018;66:65. https://doi.org/10.1007/s11249-018-1013-2.
[37] Tonck A, Martin JM, Kapsa P, Georges JM. Boundary lubrication with anti-wear additives: study of interface film formation by electrical contact resistance. Tribol Int 1979;12:209–13. https://doi.org/10.1016/0301-679X(79)90190-7.
[38] Yamaguchi ES, Ryason PR, Yeh SW, Hansen TP. Boundary film formation by ZnDTPs and detergents using ECR. Tribol Trans 1998;41:262–72. https://doi.org/10.1080/10402009808983747.
[39] Boidi G, Tertuliano IS, Profito FJ, de Rossi W, Machado IF. Effect of laser surface texturing on friction behaviour in elastohydrodynamically lubricated point contacts under different sliding-rolling conditions. Tribol Int 2019. https://doi.org/10.1016/J.TRIBOINT.2019.02.021.
[40] Kleemola J, Lehtovaara A. Evaluation of lubrication conditions in gear contacts using contact resistance and bulk temperature measurements. Proc Inst Mech Eng Part J J Eng Tribol 2010;224:367–75. https://doi.org/10.1243/13506501JET675.
[41] Rizvi SQA. A comprehensive review of lubricant chemistry, technology, selection, and design. West Conshohocken: ASTM International; 2009. https://doi.org/10.1520/MNL59-EB.
[42] Vrcek A, Hultqvist T, Baubet Y, Björling M, Marklund P, Larsson R. Micro-pitting and wear assessment of engine oils operating under boundary lubrication conditions. Tribol Int 2019;129:338–46. https://doi.org/10.1016/j.triboint.2018.08.032.
[43] Hammami M, Rodrigues N, Fernandes C, Martins R, Seabra J, Abbes MS, et al. Axle gear oils: friction, wear and tribofilm generation under boundary lubrication regime. Tribol Int 2017;114:88–108. https://doi.org/10.1016/J.TRIBOINT.2017.04.018.
[44] Fujita H, Spikes HA. Study of zinc dialkyldithiophosphate antiwear film formation and removal processes, part II: kinetic model. Tribol Trans 2005;48:567–75. https://doi.org/10.1080/05698190500385187.
[45] Topolovec-Miklozic K, Forbus TR, Spikes HA. Film thickness and roughness of ZDDP antiwear films. Tribol Lett 2007;26:161–71. https://doi.org/10.1007/s11249-006-9189-2.
[46] Johnson KL, Tevaarwerk JL. Shear behaviour of elastohydrodynamic oil films. Proc R Soc London Ser A, Math Phys Sci 1977;356:215–36. https://doi.org/10.1098/rspa.1977.0129.
[47] Fan J, Spikes HA. New test for mild lubricated wear in rolling-sliding contacts. Tribol Trans 2007;50:145–53. https://doi.org/10.1080/10402000701255476.
[48] Lafountain AR, Johnston GJ, Spikes HA. The elastohydrodynamic traction of synthetic base oil blends. Tribol Trans 2001;44:648–56. https://doi.org/10.1080/10402000108982506.
[49] Björling M. Friction in elastohydrodynamic lubrication. Luleå University of Technology; 2014.
[50] Habchi W, Bair S, Vergne P. On friction regimes in quantitative elastohydrodynamics. Tribol Int 2013;58:107–17. https://doi.org/10.1016/J.TRIBOINT.2012.10.005.
[51] Jackson A, Rowe CN. Application of EHL theory to gear lubrication. SAE Tech Pap Ser 1980;1. https://doi.org/10.4271/800670.
[52] Hamrock BJ, Dowson D. Isothermal elastohydrodynamic lubrication of point contacts: Part III—fully flooded results. J Lubr Technol 1977;99:264–75. https://doi.org/10.1115/1.3453074.
[53] Coseausu T, Björling M, Graça B, Campos A, Seabra J, Larsson R. Film thickness in a ball-on-disc contact lubricated with greases, bleed oils and base oils. Tribol Int 2012;53:53–60. https://doi.org/10.1016/J.TRIBOINT.2012.04.018.
[54] Gonçalves D, Cousseau T, Gama A, Campos AV, Seabra JHO. Friction torque in thrust roller bearings lubricated with greases, their base oils and bleed-oils. Tribol Int 2017;107:306–19. https://doi.org/10.1016/J.TRIBOINT.2016.11.041.
[55] Spikes H, Jie Z. History, origins and prediction of elastohydrodynamic friction. Tribol Lett 2014;56:1–25. https://doi.org/10.1007/s11249-014-0396-y.
[56] Höhn B-R, Michaelis K, Kopatsch F. Systematic investigations on the influence of viscosity index improvers on EHL film thickness. Gear Technol 2001;18:30–9.
[57] Dawczyk J, Morgan N, Russo J, Spikes HA. Film thickness and friction of ZDDP tribofilms. Tribol Lett 2019;67:34. https://doi.org/10.1007/s11249-019-1148-9.
[58] Taylor LJ, Spikes HA. Friction-enhancing properties of zddp antiwear additive: Part i—friction and morphology of zddp reaction films. Tribol Trans 2003;46:303–9. https://doi.org/10.1080/10402000308982630.
[59] Taylor LJ, Spikes HA. Friction-enhancing properties of zddp antiwear additive: Part ii—influence of zddp reaction films on ehd lubrication. Tribol Trans 2003;46:310–4. https://doi.org/10.1080/10402000308982631.
[60] Jiang X, Hua DY, Cheng HS, Ai X, Lee SC. A mixed elastohydrodynamic lubrication model with asperity contact. J Tribol 1999;121:481. https://doi.org/10.1115/1.2834093.
[61] Miklozic KT, Forbus TR, Spikes HA. Performance of friction modifiers on ZDDP-generated surfaces. Tribol Trans 2007;50:328–35. https://doi.org/10.1080/10402000701413505.
[62] Spikes HA. Origins of the friction and wear properties of antiwear additives. Lubric Sci 2006;18:223–30. https://doi.org/10.1002/ls.19.

PUBLICATION
II

Friction and temperature mapping of environmentally acceptable gear oils

R. Bayat, A. Lehtovaara

TRIBOLOGIA - Finnish Journal of Tribology, 37 (2020), 4-12
https://orcid.org/0000-0003-2548-3128

TRIBOLOGIA - Finnish Journal of Tribology 3-4 vol 37/2020

SUOMEN TRIBOLOGIAYHDISTYS RY
THE FINNISH SOCIETY FOR TRIBOLOGY
www.tribologysociety.fi

https://doi.org/10.30678/fjt.96048

https://journal.fi/tribologia

Friction and temperature mapping of environmentally acceptable gear oils

Reza Bayat, Arto Lehtovaara

Tribology and Machine Elements, Materials Science and Environmental Engineering, Faculty of Engineering and Natural Sciences, P.O. Box 589, 33014 Tampere University, Tampere, Finland

Corresponding author: Reza Bayat (reza.bayat@tuni.fi)

ABSTRACT

In recent years, environmental issues have raised the demand to protect the environment against the pollution caused by the uncontrolled spillage of lubricating oils. One solution is using Environmentally Acceptable Lubricants (EALs), however, these oils are more expensive than the common mineral oils. The consumers require to test the oil performance using test machines but testing in real machines is costly and time-consuming. Small test machines like ball-on-disc have been previously used for friction mapping and ranking gear oils. In this paper, the friction maps are measured from 0.65 GPa to 1.25 GPa, and temperature maps are devised to experimentally simulate the gear contact along the line of action. Results illustrate that EALs can provide up to 60 % better frictional efficiency that leads to 20 °C cooler oil temperature in high-pressure contacts operating under elastohydrodynamic lubrication (EHL) regime.

Keywords: Elastohydrodynamic lubrication; Environmentally acceptable lubricant; Temperature map; Friction map; Gear oil

1. Introduction

Environmental awareness has grown in recent years, and different industries are changing their values to decrease environmental damages. Lubricant leakage is a source of pollution in the environment that is estimated 40-50% of the 5 million tonnes used lubricant in Europe [1]. Environmentally accepted lubricants (EALs) with low toxicity, and high biodegradability (≥60%) [1], are considerably less harmful to the environment and can be used in environmentally sensitive areas like marine industry and wind turbines. These oils are introduced to the market since the 1970s [2], and still, the oil manufacturers are optimizing their tribological performance.

Ester oils are the most common base oil used for fully formulated EALs. These oils are considerably more expensive than mineral oils. They have lower friction [3–5] and higher thermal conductivity compared to the mineral oil [6]. Their lower friction coefficient signifies less energy loss in the machine components like gears. However, this does not necessarily mean better protection against failure. Understanding oil tribological performance requires further investigations using modeling or testing the oil by different machines. Modeling has been the topic of several studies to investigate the friction [7–11] and temperature variation [12,13] of gears.

For modeling the friction, the most widely used model is the "nonlinear Maxwell" equation proposed by Johnson and Tevaarwerk [14] that is based on Eyring's rheology model. Another model was proposed by Bair that is based on Carreau–Yasuda rheology equation [15]. There have been many debates on the accuracy of these two models [16,17], however, the Eyring model is more commonly implemented thanks to its simplicity and acceptable accuracy [16]. The model proposed by Bair requires more disposable parameters that are difficult to find for industrial oils. With regard to the contact temperature modeling, Archard model [18] has been commonly used, and it is still implemented in the models [3,19]. In this paper, the Eyring model is used for comparing the rheological properties of the oils, and the Archard model is employed for estimating the contact temperature.

The Elastohydrodynamic lubrication (EHL) friction models usually consider a base oil with a known chemical composition, however, fully formulated industrial oils are a mixture of several base oils and additives. Thus, it is more reliable to employ test machines for oils ranking. On the other hand, using real size test machines is costly and time-consuming. Therefore, elaborating less expensive and quicker tests has been the aim of several studies [20–22]. Kleemola and Lehtovaara modeled the gear contact using a twin-disc machine and showed that the shape of the mean friction coefficient curves is similar in both twin-disc machine and gear; however, a difference was observed that

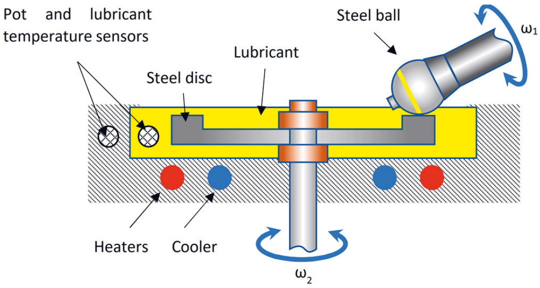

Fig. 1: Schematic of MTM

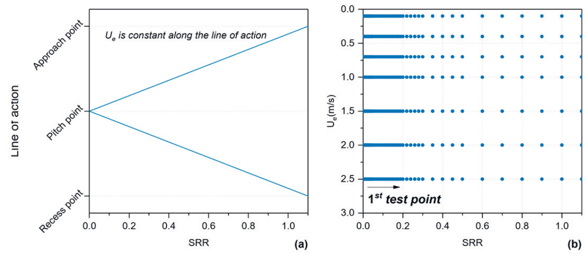

Fig. 2: Estimating friction along the gear line of action: (a) Changes in SRR along the line of action [24]. (b) Test points for measuring the friction and calculating the temperature.

was attributed to the roughness difference between the discs and gear [23]. Björling et. al used a ball-on-disc machine and an FZG machine to rank some oils regarding the friction loss. It was observed that both of the machines give the same ranking [24]. For this ranking, Björling et. al used the friction maps developed earlier in Ref. [25] and estimated the friction at different locations on the line of action of a gear set. This method estimates the variation of friction at different entrainment speeds and sliding-to-rolling ratios (SRRs). The elaborated results can be used for different gear types, and it is not limited to only one specific geometry.

In this paper, the friction mapping method is employed to evaluate the performance of EAL gear oils. In addition, a methodology is devised to plot the temperature maps that show the temperature variation at different working conditions. Firstly, the friction maps are plotted based on the idea of Ref. [24], then using the Archard model, the contact temperature map is plotted by estimating the temperature along the line of action at different entrainment speeds. In order to study the impact of the contact pressures on the EHL friction and temperature, the maps are plotted at four different pressures. This approach graphically represents the interconnection of friction and temperature. Besides, it presents a comparison between frictional and thermal properties of EALs and mineral oils.

2. Experiment detail

The tests were carried out using a mini-traction machine that provided the rolling/sliding contact between a ball and a disc. The tilted ball shaft minimizes the spin, and a load cell attached between the ball shaft and the instrument body measures the friction force. The lubricant and pot temperatures are measured separately and are automatically adjusted by a heater, and a circulating fluid provided by an external heater/cooler equipment. The ball and disc speeds are controlled separately to adjust the oil entrainment speed and sliding-to-rolling ratio (SRR) independently. Entrainment speed and SRR are defined in Eqs. (1)-(3):

$$U_e = \frac{U_d + U_b}{2} \tag{1}$$

$$U_s = U_d - U_b \tag{2}$$

$$SRR = \frac{U_s}{U_e} \tag{3}$$

where U_d and U_b are respectively the disc and ball circumferential velocities in the contact point, U_e is the entrainment velocity and U_s is the sliding velocity.

1.1. Test specimen and lubricants

The ball was manufactured from AISI 52100 steel with a diameter of 19.05 mm, and Rq (Root-Mean-Square roughness) of 50.95 (nm). The disc was from the same material with Rq of 34.08 (nm). Both the ball and disc had the hardness of 750–770 VPN and Young's Modulus of 207 (GPa). For each test, a new ball and disc were cleaned by immersion in toluene and isopropanol in an ultrasonic bath for 10 min.

The tested lubricants include two different EALs with the same viscosity class from different companies and satisfying the US EPA requirements for "Environmentally Acceptable Lubricants". Additionally, two mineral oils were selected for comparison. One mineral gear oil with the same viscosity class, and another mineral engine oil with a similar 40 °C kinematic viscosity that is practically used in ships for gear lubrication. All the oils except M1 that is engine oil, comply with the DIN 51517 part 3 (CLP) standard. The oils specifications can be found in Table 1.

2.1. Friction measurement

Björling et. al explains the correlation between friction at gear contact and a ball on disc machine [24]. In their tested spur gear set with a centre distance of 91.5 mm, gear ratio 1 and normal module 4.5 mm, the SRR varies from 0 to 1.1 at different points along the line of action (Fig. 2 (a)). The SRR represents the position of the point on the line of actions, and the entrainment speed represents the rotational speed of the gear set.

According to the method of Björling et. al [24], the friction was measured in a series of tests at different Ue and SRR. A friction map can be derived by plotting the coefficient of friction (COF) of the measurement points. In this experimental plan, the COF was measured at the data points shown in Fig. 2 (b) covering the whole range of positive SRR.

In order to investigate the effect of pressure, the test was performed at four different maximum Hertzian pressure of 0.65 GPa, 0.95 GPa, 1.10 GPa and 1.25 GPa. The friction map results are shown in Fig. 3-6.

Table 1: Measured lubricants properties

	Kin. Vis. @40 °C (mm²/s)	Kin. Vis. @100 °C (mm²/s)	ρ @15 °C (kg/m³)	VI	Comment
Method	ASTM D445	ASTM D445	EN ISO 12185	ASTM D 2270	
M1	127.60	13.83	908	105	Mineral engine oil
M2	142.50	14.24	888	97	Mineral gear oil
EAL1	147.50	18.84	972	145	Synthetic oil, EAL
EAL2	150.57	18.44	929	137	Synthetic oil, EAL

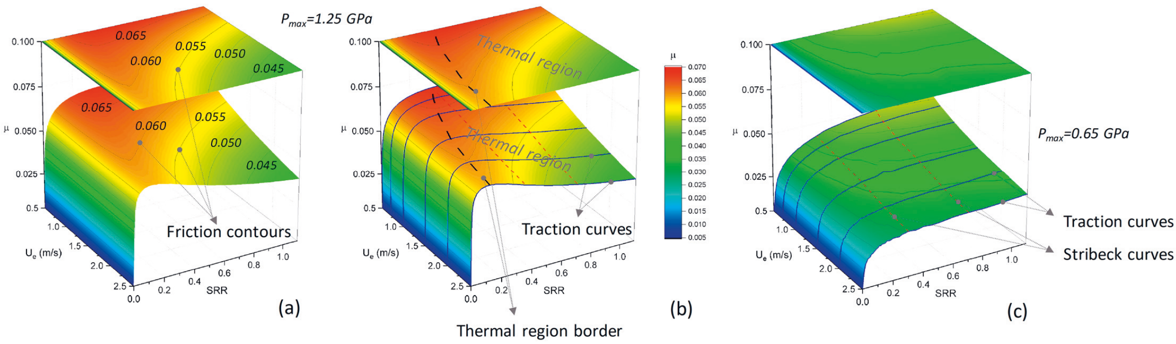

Fig. 3: Extracting 2D friction map from 3D friction map of M1: (a) Friction contours on 2D and 3D friction maps of M1 at P_{max}=1.25, (b) Depiction of the thermal region for M1 at P_{max}=1.25, (c) 2D and 3D friction maps of M1 at P_{max}=0.65, and depiction of traction and stribeck curves

It is noticeable to say that at the entrainment speeds below ~0.5 m/s, the lubrication regime enters to the mixed regime for the used lubricants. Therefore, only the data for the entrainment speeds higher than 0.5 m/s are shown in the friction maps to neglect the effect of asperity contact.

3.1. Temperature calculation

In order to calculate the contact temperature, it is assumed that there is an EHL lubrication regime in the rolling/sliding contact. The heat is generated from shearing and dissipated by conduction in the normal direction, thus there is negligible heat generation by compressive heating or inlet shear heating originated from Poiseuille flow. It is also assumed that the Couette flow is dominant under EHL condition, so the shear strain rate is expressed as:

$$\dot{\gamma} = \frac{U_s}{h_c} \tag{4}$$

By considering the data points that satisfy the specific film thickness values over 3, the contact can be considered as EHL regime that neglects the effect of asperity contact on the friction and heat generation. Considering the aforementioned assumptions, the mean oil film temperature in an EHL increases above the inlet supply temperature by two temperature rise terms: the transient increase in temperature of the contacting surfaces known as the mean flash temperature rise $\Delta\bar{T}_{flash}$, and the second term is the oil film temperature rise above the surfaces denoted by $\Delta\bar{T}_{oil}$. According to Ref. [19], each term can be written as Eqs. 5-7:

$$\bar{T} = T_{supply} + \Delta\bar{T}_{flash} + \Delta\bar{T}_{oil} \tag{5}$$

$$\Delta\bar{T}_{flash} = \frac{1}{(2\pi K\rho c)^{0.5}}\left(\frac{2b}{U_e}\right)^{0.5} q'' \tag{6}$$

$$\Delta\bar{T}_{oil} = \frac{h_c}{8K_{oil}} q'' \tag{7}$$

where K, ρ, and c are respectively the thermal conductivity, density and specific heat of the surfaces (AISI 52100 steel). b is the contact halfwidth and K_{oil} is the oil thermal conductivity. q'' is the rate of heat generation per unit area given by Eq. (8) [19]:

$$q'' = \frac{\mu F U_s}{\pi a^2} = \bar{\tau}\dot{\gamma}h_c \tag{8}$$

where μ is the coefficient of friction (COF), F the normal applied load, $\bar{\tau}$ the mean shear stress calculated by $\bar{\tau} = \mu\frac{F}{\pi a^2}$, $\dot{\gamma}$ the strain rate. h_c is the central film thickness calculated by Hamrock and Dowson's formula [26] and corrected by considering the thermal correction factor presented by Gupta et al. [27]. By using the speed parameter $U = \frac{\eta_0 U_e}{E^* R_x}$, the material parameter $G = \alpha E^*$ and the load parameter $W = \frac{F}{E^* R_x^2}$, the central film thickness can be calculated from Eqs. 9-10:

Table 2: Estimated properties of specimens

	α @40 °C (1/GPa)	Thermal conductivity (W/mK)	Heat capacity (J/kgK)	Density (kg/m³)
Ref.	**[4]**	**[6] for oils, and [19] for ball and disc**	**[19]**	**[19] for ball and disc**
M1	19.95	0.220-0.273	-	Table 1
M2	20.25	0.220-0.273	-	Table 1
EAL1	13.28	0.243-0.295	-	Table 1
EAL2	13.34	0.243-0.295	-	Table 1
Ball and disc AISI 52100 steel	-	21	460	7800

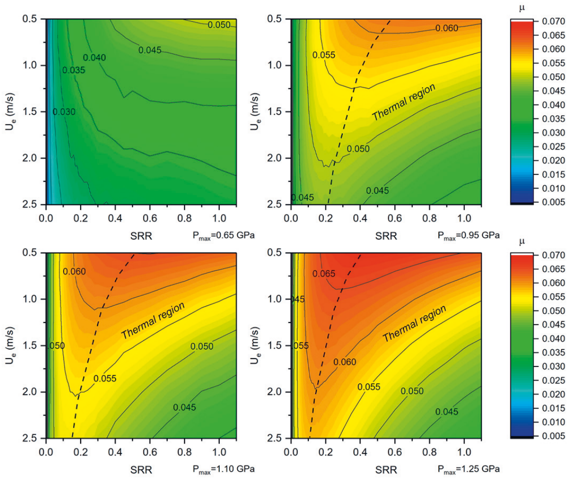

Fig. 4: The COF of M1 at different maximum Hertzian contact pressures

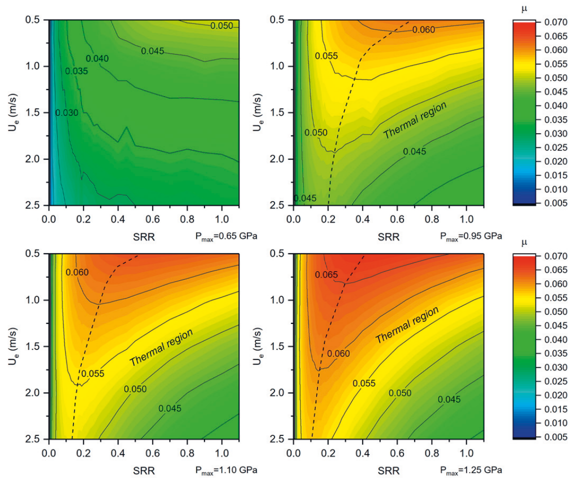

Fig. 5: The COF of M2 at different maximum Hertzian contact pressure

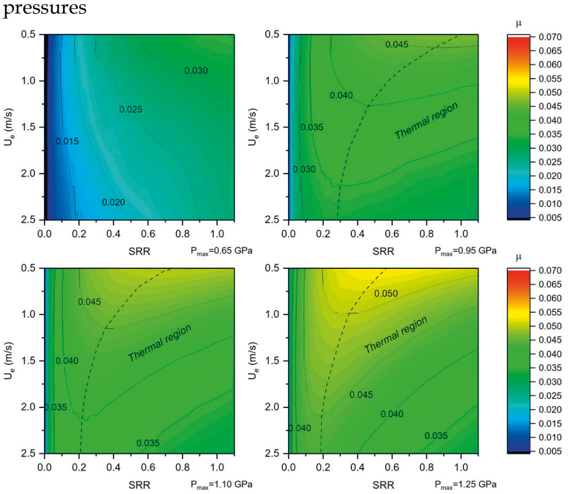

Fig. 6: The COF of EAL1 at different maximum Hertzian contact pressures

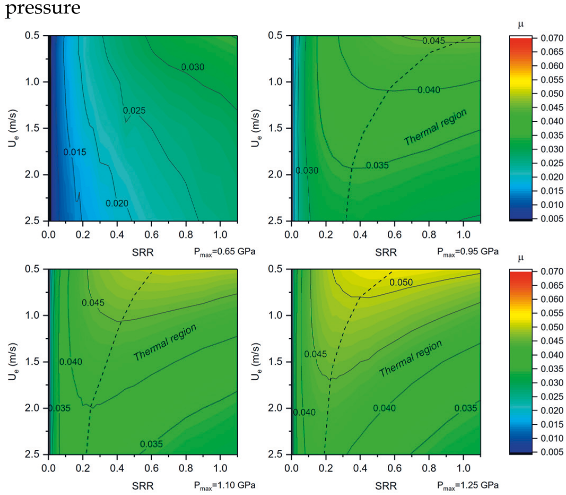

Fig. 7: The COF of EAL2 at different maximum Hertzian contact pressures

$$h_c = h_{c,iso} \cdot \phi_{thermal} \tag{9}$$

$$h_{c,iso} = 2.69 R_x (U^{0.67})(G^{0.53})(W^{-0.068})(1 - 0.61e^{-0.73k}) \tag{10}$$

$$\phi_{thermal} = \frac{1 - 13.2(p_H/E^*)L^{0.42}}{1 + 0.213(1 + 2.23\mathrm{SRR}^{0.83})L^{0.64}} \tag{11}$$

where L is the thermal loading parameter ($L = -\frac{\partial \eta}{\partial T}\frac{U_e^2}{k_{oil}}$), E^* is the reduced Young's Modulus (Pa), R_x the radius of curvature in the x-direction (m), η_0 the dynamic viscosity of the lubricant (Pa s), and $k = 1.03$. The pressure-viscosity coefficient α (Pa^{-1}) was calculated for each pressure using the method presented in Ref. [4].

The film thickness calculation does not consider the shear-thinning effect that leads to overestimation of $\Delta\bar{T}_{oil}$ term. In addition, in this term, the value of 8 in the denominator is based on the assumption that heat is dissipated evenly through the film, and denotes the maximum temperature at the median line of the film [19]. In addition, the thermal conductivity of the oils is estimated based on the data in Ref. [28] by selecting the nearest oil type, and calculating this parameter for each mean contact pressure. The estimated parameters of the samples are shown in Table 2.

For the experimented oils in this study, it is assumed that the contact temperature has a negligible effect on the pressure-viscosity coefficient, thermal conductivity, density and heat capacity.

3. Results and discussion

Figure 3 illustrates the method by which the friction maps are derived. In Fig. 3 (a), a 3D friction map is plotted by evaluating the COF at the data points discussed in section 2.1. Then a 2D friction map is derived by projecting the 3D map to the plane of Ue-SRR while keeping the friction contours and the color variations that illustrate the changes of COF. In Fig. 3 (b), the thermal region and its border are illustrated. According to [14], the thermal region denotes the region in which the shear heating has a dominant effect. Considering a single traction curve in Fig. 3 (b), the thermal region starts from the point at which the COF falls by increasing the SRR. Before the thermal region, there are two other regions: 1) Linear region in which the COF changes linearly with increasing SRR, and 2) non-linear region in which the shear-thinning effect plays its role and leads to a non-linear COF rise [14]. For the case of Fig. 3 (c), no thermal region is observed since the friction does not fall by increasing the SRR. The Hertzian pressure in Fig. 3 (c) is considerably lower than the pressure in Fig. 3 (b), thus it does not lead to a high amount of heat generation.

In addition, the stribeck and traction curves are illustrated in Fig. 3 (c). The traction curves are shown by dark blue solid lines and refer to curves of COF by increasing sliding speed while having a constant entrainment speed. The stribeck curves that are shown by red dash lines, refer to the curves derived from measuring

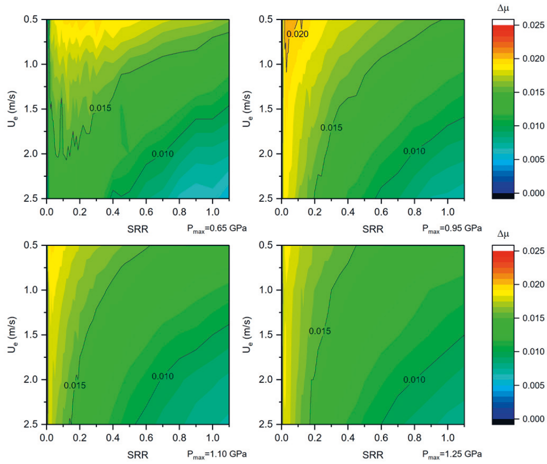

Fig. 8: The difference between COF of M2 and EAL2 at different maximum Hertzian contact pressures

the COF at different entrainment speeds and constant SRR. The traction and stribeck curves of a lubricant can be easily derived for a 2D friction map, at different SRR and entrainment speeds.

The friction maps of the oils are plotted according to the method shown in Fig. 3, then the temperature maps are derived from the friction maps according to the described model. For each oil, the friction and temperature maps are plotted at four different pressures. In these maps, the friction and temperature contours are illustrated, and the thermal regions are shown. It is noticeable that no thermal region was observed in the case of friction maps at the Hertzian pressure of P_{max}=0.65 GPa.

The friction maps of all the oils are shown in Figs. 4-7. For all the cases, by changing the SRR from 0 (pure rolling) to higher values, the friction coefficient first rises and reaches its maximum at the onset of the thermal region. At higher SRRs the heat dissipation becomes effective, and the temperature rises and leads to a reduction of viscosity and lower COF. In conclusion, under the pressures higher than 0.95 GPa, the peak of friction coefficient happens at the regions near the pitch point (low SRR), and the minimum oil viscosity and consequently minimum film thickness is found at the approach or recess points (high SRR).

In Figs. 4-7, in the terms of Stribeck curve at a constant SRR, the increase in entrainment speed leads to lower COF. Since all the friction maps are tested under the EHL regime, the higher entrainment speed at a constant SRR means higher sliding velocity and higher heat generation, thus lowers the oil viscosity and COF.

It can be seen from Figs. 4 and 5 that there is little difference between the COF of two mineral oils. Similarly, this is the case for the EALs (Figs. 6 and 7). Thus, in order to compare the COF of mineral oils with EALs, only one of the mineral oils (M2) was compared with one EAL (EAL2). Figure 8 presents the COF difference between M2 and EAL2 and four different pressures.

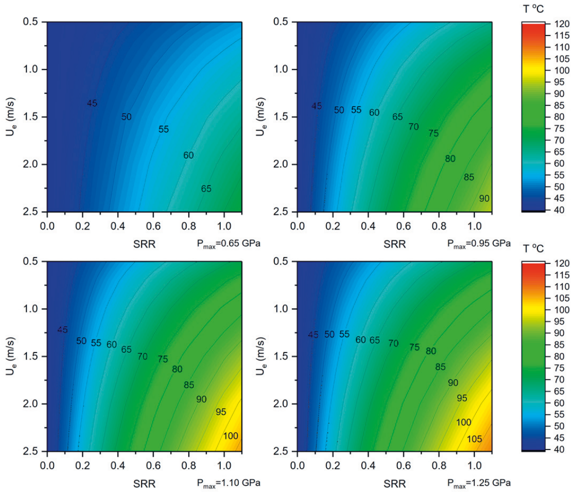

Fig. 9: The Temperature map of M1 at different maximum Hertzian contact pressures

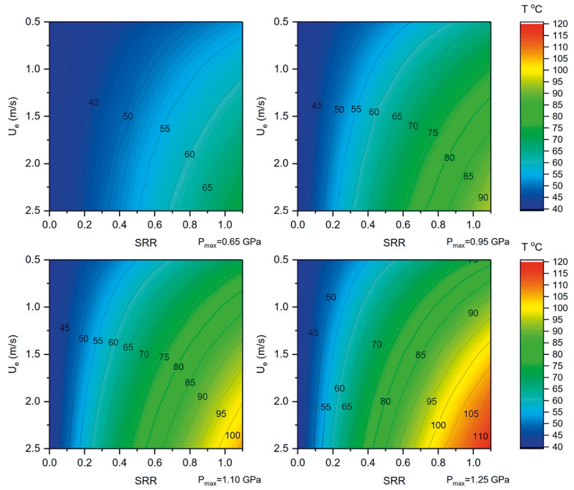

Fig. 10: The Temperature map of M2 at different maximum Hertzian contact pressures

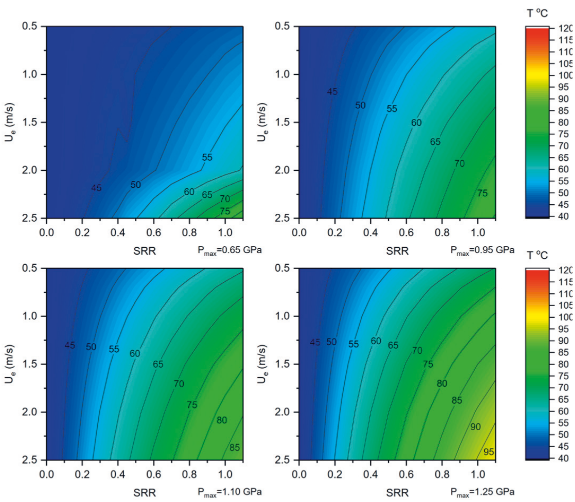

Fig. 11: The Temperature map of EAL1 at different maximum Hertzian contact pressures

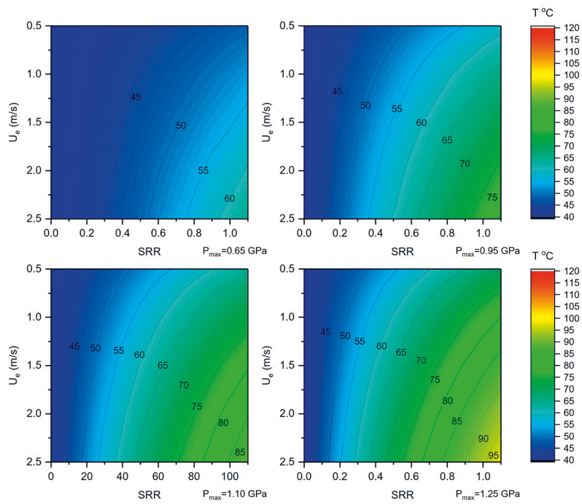

Fig. 12: The Temperature map of EAL2 at different maximum Hertzian contact pressures

Figure 8 shows that the COF decreases by using EALs instead of mineral oils. This reduction is around ~0.02 (60% of mineral oil COF) at low SRR and low Ue, that is the case of roller bearings or regions near the pitch point in gears. However, the COF reduces by ~0.01 (20% of mineral oil COF) at high SRR and high Ue which represents the conditions of the gear tooth tip.

Based on the Eyring stress activation model of isothermal liquid flow, and considering a Barus viscosity-pressure equation, shear stress can be written as Eq. (12) [29]:

$$\tau = \tau_e sinh^{-1}(\frac{\eta_0 e^{\alpha p}\dot{\gamma}}{\tau_e}) \qquad (12)$$

where τ_e is the limiting stress at which shear-thinning becomes significant, η_0 is the viscosity at atmospheric pressure and α is the pressure-viscosity coefficient.

Using Eq (12), τ_e was estimated for the oils M2 and EAL2 by curve fitting on a plot of τ versus $\dot{\gamma}$. The curve fitting was employed for the traction curve at 40 °C, maximum Hertzian pressure of 1.10 GPa, entrainment speed of 0.7 m/s and considering $\tau > \tau_e$ over most of the contact [30]. The results show that τ_e of M2 was approximately 15 % higher than EAL2. On the other hand, from [31] it is observed that the pressure-viscosity coefficient of EALs is smaller. Therefore, the friction reduction by EALs is mainly attributed to two rheological parameters: the lower pressure-viscosity coefficient of EALs, and their lower limiting shear stress at which shear-thinning becomes

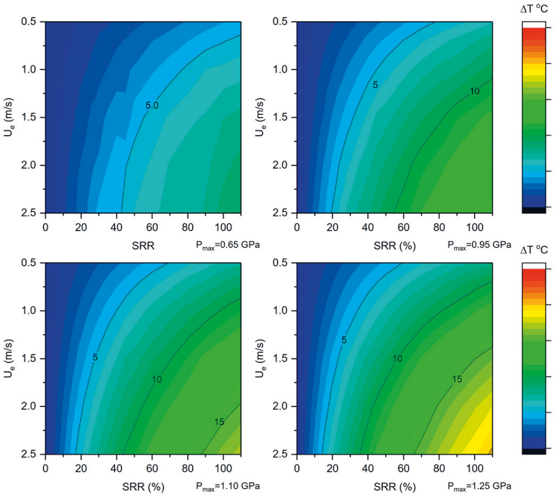

Fig. 13: The difference in temperature of M2 and EAL2 at different maximum Hertzian contact pressures

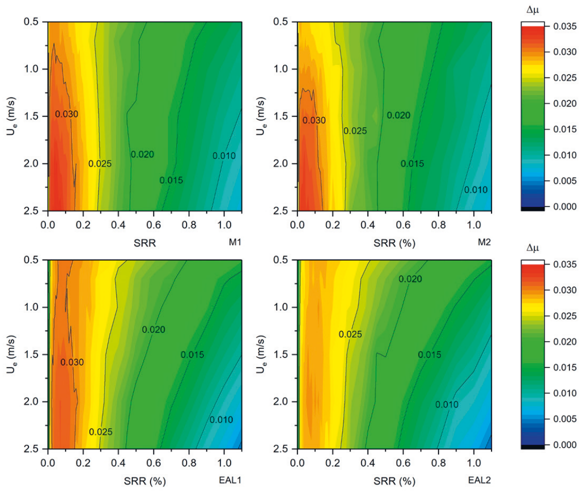

Fig. 14: The difference between COF at P_{max}=0.65 GPa and P_{max}=1.25 GPa for each oil

significant. Regarding the molecular factors contributing to the low COF, Zhang et. al [29] point to the linear chains, flexible groups like C(O)–O–C, and large free volume that reduce the interaction between neighboring molecules.

Figures 9-12 show the temperature maps of the oils at different pressures. Considering the traction curves at a constant entrainment speed, the highest temperature is found at high SRRs, corresponding to the approach or recess points of gear sets. By Increasing the pressure from 0.65 GPa to 1.25 GPa, the maximum temperature of mineral oils increases with the rate of ~77 °C/GPa, while for the case of EALs this rate is ~60 °C/GPa. This lower rate is mainly due to the lower COF and better heat conduction of the oils film in EALs.

In order to compare the temperature of mineral oils with EALs, only one of the mineral oils was compared with one EAL (M2 and EAL2). Figure 13 presents the temperature difference between M2 and EAL2 at four different pressures.

Figure 13 shows that EAL2 has a lower temperature than M2, and their temperature difference ranges from 5 °C at low SRRs, low Ue and low pressure, to 20 °C at high SRR, high Ue and high pressure. According to Eqs. (5)-(7), the lower temperature of EAL2 is a result of its lower COF, and bigger thermal conductivity. By increasing the maximum Hertzian pressure from 0.65 GPa to 1.25 GPa, the temperature difference between these oils grows. This illustrates the higher thermal efficiency of EALs.

In Fig. 13, at low SRRs, the oil temperatures of both oil types show little difference. However, increasing the sliding velocity (high SRR and high Ue) results in a big temperature difference. The high oil film temperature of mineral oils significantly reduces their viscosity which results in decreasing the COF. In Fig. 8, the smaller COF difference at high SRR and high Ue is due to the comparably higher oil film temperature of the mineral oils.

Figure 14 shows that the higher pressure results in COF increase for all the oils that is due to the viscosity increase by pressure. The COF increase is smaller at high SRRs because of the dominance of shear heating. At small SRRs, the COF rise of mineral oils is bigger that can be seen from bigger red areas in mineral oils. This is due to the higher pressure-viscosity coefficient of mineral oils. However, at higher SRRs, the COF rise of mineral oils is smaller that is visible from their larger green and blue area in Fig. 14. This means that the dominance of the temperature rise effect is bigger with the case of mineral oils. In Figs. 4-7, the thermal region shifts to the lower SRR due to increased heat generation by shear stress. It can be seen from Figs. 4-7 that the thermal region starts from lower SRRs for the case of mineral oils signifying the bigger thermal dominance. In conclusion, this variation of COF at different SRRs and Ue suggests that the pressure-viscosity coefficient and limiting shear stress are the effective parameters in the machine elements working at low sliding speeds, while shear heating (or COF) and thermal properties become increasingly effective at high sliding velocities and high pressures.

It should be noted that this study has been primarily concerned with devising a methodology for comparing the industrial EALs with the mineral oils. The friction and temperature values might not be directly transferable to the real machine values. The most important limitation lies in the constant pressure assumed in the current methodology, which is in contradiction with the changing radius and pressure in real gears. Also, in real gear, the surface roughness is higher, which leads to the operation under mixed lubrication regime. In addition, in the temperature model, the mean value is used for different parameters. Also, the effect of the shear-thinning is not considered in calculating the EHL film thickness. Nevertheless, this paper provides a versatile technique for ranking the oils regarding the contact temperature and friction. This methodology provides a comprehensive analysis of several parameters in a few plots. It can be considered as a quick and preliminary test for estimating the oil performance in different gear types. These data elaborated in this experiment are applicable for any gear set in which the SRR and Ue are in the measured range. In case the gear operates in the higher SRR and Ue, a new friction map can be quickly tested to cover the gear working condition.

Conclusion:

The objective of this work was to examine the friction and temperature of the EALs compared to mineral oils. This was achieved by using a ball on disc test equipment to experimentally simulate gear contact. The friction maps were obtained by evaluating the COF at different entrainment speeds and SRRs. Then, a methodology was devised to plot the temperature maps based on the Archard model. Furthermore, the maps were studied at four different contact pressures to study the impact of pressure on friction and oil temperature. In conclusion, the results of this study show that:

- By using an EAL, the COF in the EHL regime reduced from ~60% at low slide-to-roll ratio (SRR) -low entrainment velocity (Ue), to 20% at high SRR-high Ue.
- The friction reduction by EALs was mainly attributed to two rheological parameters: the lower pressure-viscosity coefficient of EALs, and their lower limiting shear stress.
- At higher pressure, friction increased for all the oils. However, this friction growth was smaller in the thermal region where the oil temperature effect becomes dominant. The dominance of the temperature effect was bigger with the case of mineral oils, and it was observed that their thermal region starts at lower SRRs.
- Comparing the oil film temperature, the EALs showed lower oil temperature. The temperature difference between EALs and the mineral oil ranged from 5 ^{o}C at low SRRs, low Ue and low pressure, to 20 ^{o}C at high SRR, high Ue and high pressure. According to the temperature equation, the lower temperature of EALs was the result of their lower friction and bigger thermal conductivity.
- Pressure had a bigger effect on the temperature of mineral oils. The maximum temperature increased with the rate of ~77 ^{o}C/GPa and ~60 ^{o}C/GPa respectively for mineral oils and EALs. The lower was mainly due to the lower COF and better heat conduction of the oils film in EALs.
- This variation of friction at different SRRs and Ue suggest that the pressure-viscosity coefficient and limiting shear stress are the effective parameters in the machine elements working at low sliding speeds, while, friction coefficient and thermal properties become increasingly effective at high sliding velocities and high pressures.

In this study, the estimated temperature and friction are not necessarily the same as what is found in the gear. This method can be further improved by considering the pressure variation along the line of action, measuring the exact thermal properties of the oils, and using a more accurate temperature model by considering the temperature variation at different points in the contact. However, the temperature maps devised in this study, together with the friction maps, present an estimation of the oil energy efficiency, and can be used in further investigations like studying the scuffing protection of the oils. Knowing the working condition of a gear set, the friction and temperature data, or the method can be used to estimate the friction or temperature.

Acknowledgments

We gratefully acknowledge the financial support from Tampere University graduate school.

References

[1] Luther R. Lubricants in the Environment. In: Mang T, Dresel W, editors. Lubr. Lubr. 3rd ed., Weinheim, Germany: Wiley-VCH Verlag GmbH & Co. KGaA; 2017, p. 153–236. https://doi.org/10.1002/9783527610341.ch7.

[2] Norrby T. Environmentally adapted lubricants – where are the opportunities? Ind Lubr Tribol 2003;55:268–74. https://doi.org/10.1108/00368790310496400.

[3] Kim HM, Spikes H. Correlation of Elastohydrodynamic Friction with Molecular Structure of Highly Refined Hydrocarbon Base Oils. Tribol Lett 2020;68:1–14. https://doi.org/10.1007/s11249-020-1265-5.

[4] Brandão JA, Meheux M, Ville F, Seabra JHO, Castro J. Comparative overview of five gear oils in mixed and boundary film lubrication. Tribol Int 2012;47:50–61. https://doi.org/10.1016/j.triboint.2011.10.007.

[5] Martins R, Seabra J, Brito A, Seyfert C, Luther R, Igartua A. Friction coefficient in FZG gears lubricated with industrial gear oils: Biodegradable ester vs. mineral oil. Tribol Int 2006;39:512–21. https://doi.org/10.1016/J.TRIBOINT.2005.03.021.

[6] Larsson R, Andersson O. Lubricant thermal conductivity and heat capacity under high pressure. Proc Inst Mech Eng Part J J Eng Tribol 2000;214:337–42. https://doi.org/10.1243/1350650001543223.

[7] Martin KF. The efficiency of involute spur gears. J Mech Des Trans ASME 1981;103:160–9. https://doi.org/10.1115/1.3254855.

[8] Hua DY, Khonsari MM. Application of transient elastohydrodynamic lubrication analysis for gear transmissions. Tribol Trans 1995;38:905–13. https://doi.org/10.1080/10402009508983487.

[9] Akbarzadeh S, Khonsari MM. Performance of Spur Gears Considering Surface Roughness and Shear Thinning Lubricant. J Tribol 2008;130:021503.

https://doi.org/10.1115/1.2805431.

[10] Larsson R. Transient non-Newtonian elastohydrodynamic lubrication analysis of an involute spur gear. Wear 1997;207:67–73. https://doi.org/10.1016/S0043-1648(96)07484-4.

[11] Björling M, Habchi W, Bair S, Larsson R, Marklund P. Towards the true prediction of EHL friction. Tribol Int 2013;66:19–26. https://doi.org/10.1016/j.triboint.2013.04.008.

[12] Wang KL, Cheng HS. A numerical solution to the dynamic load, film thickness, and surface temperatures in spur gears, part 1 analysis. J Mech Des Trans ASME 1981;103:177–87. https://doi.org/10.1115/1.3254859.

[13] Akbarzadeh S, Khonsari MM. Thermoelastohydrodynamic analysis of spur gears with consideration of surface roughness. Tribol Lett 2008;32:129–41. https://doi.org/10.1007/s11249-008-9370-x.

[14] Johnson KL, Tevaarwerk JL. Shear Behaviour of Elastohydrodynamic Oil Films. Proc R Soc London Ser A, Math Phys Sci 1977;356:215–36. https://doi.org/10.1098/rspa.1977.0129.

[15] Bair S. ”Recent Developments in High-Pressure Rheology of Lubricants”. Tribol Ser 1995;30:169–87. https://doi.org/10.1016/S0167-8922(08)70628-X.

[16] Spikes H, Jie Z. History, Origins and Prediction of Elastohydrodynamic Friction. Tribol Lett 2014;56:1–25. https://doi.org/10.1007/s11249-014-0396-y.

[17] Bair S, Vergne P, Kumar P, Poll G, Krupka I, Hartl M, et al. Comment on “History, Origins and Prediction of Elastohydrodynamic Friction” by Spikes and Jie. Tribol Lett 2015;58:1–8. https://doi.org/10.1007/s11249-015-0481-x.

[18] Archard JF. The temperature of rubbing surfaces. Wear 1959;2:438–55. https://doi.org/10.1016/0043-1648(59)90159-0.

[19] Zhang J, Spikes H. Measurement of EHD Friction at Very High Contact Pressures. Tribol Lett 2020;68:1–12. https://doi.org/10.1007/s11249-020-1281-5.

[20] Johnson KL, Spence DI. Determination of gear tooth friction by disc machine. Tribol Int 1991;24:269–75. https://doi.org/10.1016/0301-679X(91)90029-9.

[21] Höhn B-R, Michaelis K, Doleschel A. Frictional behaviour of synthetic gear lubricants. Tribol Ser 2001;39:759–68. https://doi.org/10.1016/S0167-8922(01)80156-5.

[22] Kleemola J, Lehtovaara A. Development of a high pressure twin disc test device for the simulation of gear contact. Tribologia 2006;25:8–17.

[23] Kleemola J, Lehtovaara A. Experimental simulation of gear contact along the line of action. Tribol Int 2009;42:1453–9. https://doi.org/10.1016/J.TRIBOINT.2009.06.007.

[24] Björling M, Miettinen J, Marklund P, Lehtovaara A, Larsson R. The correlation between gear contact friction and ball on disc friction measurements. Tribol Int 2015;83:114–9. https://doi.org/10.1016/j.triboint.2014.11.007.

[25] Björling M, Larsson R, Marklund P, Kassfeldt E. Elastohydrodynamic lubrication friction mapping – the influence of lubricant, roughness, speed, and slide-to-roll ratio. Proc Inst Mech Eng Part J J Eng Tribol 2011;225:671–81. https://doi.org/10.1177/1350650111403363.

[26] Hamrock BJ, Dowson D. Isothermal Elastohydrodynamic Lubrication of Point Contacts: Part III—Fully Flooded Results. J Lubr Technol 1977;99:264–75. https://doi.org/10.1115/1.3453074.

[27] Gupta PK, Cheng HS, Zhu D, Forster NH, Schrand JB. Viscoelastic effects in MIL-L-7808-type lubricant, part I: Analytical formulation. Tribol Trans 1992;35:269–74. https://doi.org/10.1080/10402009208982117.

[28] Larsson R, Larsson PO, Eriksson E, Sjöberg M, Höglund E. Lubricant properties for input to hydrodynamic and elastohydrodynamic lubrication analyses. Proc Inst Mech Eng Part J J Eng Tribol 2000;214:17–27. https://doi.org/10.1243/1350650001542981.

[29] Zhang J, Tan A, Spikes HA. Effect of Base Oil Structure on Elastohydrodynamic Friction. Tribol Lett 2017;65:1–24. https://doi.org/10.1007/s11249-016-0791-7.

[30] Evans CR, Johnson KL. The Rheological Properties of Elastohydrodynamic Lubricants. Proc Inst Mech Eng Part C J Mech Eng Sci 1986;200:303–12. https://doi.org/10.1243/PIME_PROC_1986_200_134_02.

[31] Bayat R, Lehtovaara A. EHL/mixed transition of fully formulated environmentally acceptable gear oils. Tribol Int 2020:106158. https://doi.org/10.1016/j.triboint.2020.106158.

PUBLICATION
III

Scuffing evaluation of fully formulated environmentally acceptable lubricant using barrel-on-disc technique

R. Bayat, A. Lehtovaara

Tribology International, 160 (2021), 107002
https://doi.org/10.1016/j.triboint.2021.107002

Tribology International 160 (2021) 107002

Contents lists available at ScienceDirect

Tribology International

journal homepage: http://www.elsevier.com/locate/triboint

Scuffing evaluation of fully formulated environmentally acceptable lubricant using barrel-on-disc technique

Reza Bayat [*], Arto Lehtovaara

Tribology and Machine Elements, Materials Science and Environmental Engineering, Faculty of Engineering and Natural Sciences, P.O. Box 589, 33014, Tampere University, Tampere, Finland

ARTICLE INFO

Keywords:
Scuffing
Tribofilm
Environmentally acceptable lubricant
Running-in

ABSTRACT

Scuffing evaluation is challenging due to the catastrophic nature of this failure mode. In this paper, a new scuffing test method was designed for evaluating the scuffing capacity of fully formulated industrial oils. A barrel-on-disc technique was employed in which the specimens are moving in opposite direction under rolling–sliding conditions. The maximum Hertzian pressure could reach up to 3.06 GPa, and the test plan was a combination of increasing-sliding speed and increasing-load steps. Furthermore, the tribofilm evolution was captured using Spacer Layer Interferometry Method (SLIM), and the correlation of tribofilm and micro-scuffing/scuffing was presented. Results revealed the difference between the scuffing capacity of Environmentally Acceptable Lubricants and the Mineral oils which had the same scuffing capacity in their datasheet.

1. Introduction

Environmental considerations force the industries to use Environmentally Acceptable Lubricant (EAL) in locations that there is the risk of environmental pollution. The formulation of these oils is still under development, and it is required to understand their performance difference from conventional mineral oil. One of their differences is their scuffing capacity. Scuffing is a failure recognized by high wear rate and roughened surface, increased temperature and friction, and generated noise and vibration [1]. Compared to other tribological failure types like mild wear and fatigue, scuffing is hard to predict and study because of its catastrophic nature. Savolainen and Lehtovaara showed that even a short overload period can initiate the scuffing [2]. Therefore, choosing the right scuffing test is highly important to prevent misinterpretation of scuffing results.

In order for scuffing to occur, the elasto-hydrodynamic (EHL) film and protective tribofilm must be broken [3], and plastic yielding happens in the sliding surfaces [4]. The collapse of the EHL film is attributed to frictional heat generation [5–8], high lubricant starvation due to accumulated wear products [9], lubricant degradation [10], wettability and roughness of surface [11] and high shear stress [12]. The tribofilm breakdown is related to the desorption of reacted polar molecules generated by EP additive [13]. However, understanding these factors has not resulted in a single accepted theory for the scuffing. The flash temperature hypothesis was amongst the first scuffing theories, suggesting that scuffing occurs when the contact temperature within the central region of the contact reaches a critical value for a given lubricant/surface combination [14]. This theory did not consider the effect of EHL film collapse, thus Dyson proposed a model describing that the critical temperature occurs in the inlet of contact [15]. Cheng and Dyson later added to the theory by considering the effect of asperity heating [16]. More recent theories focus on the evolution of the metallic contact according to the adiabatic shear plastic instability in the near-surface material [17–21]. Ajayi et al. observed a sudden temperature rise in the contact and concluded that it is contrary to the critical temperature theory for scuffing initiation. Ajayi et al. suggested that the sudden temperature rise is the result of scuffing, not its causality [18]. It is noteworthy that examining scuffing theories is not the aim of this paper. These theories were remarked since they are used for explaining the experimental results in the current study.

Scuffing has been studied using different experimental techniques such as Ryder [22], IAE [23], FZG [24,25], Timken [26], four-ball [27] and twin-disc [2,28]. Peng et al. discussed the problems with these methods and divide the causes into two main categories: stationary body, and conventional increasing-load test sequences [29]. The stationary body in four-ball and Timken tests suffers from cumulative wear before scuffing. This wear increases the contact area and reduces the contact pressure. This geometrical transformation can lead to wrong oil ranking in case of testing a low wear capacity oil [29]. One solution for avoiding this problem is using rolling-sliding contact that distributes the wear over the surface and prevents high wear on a single point. Thus, employing tests like Ryder, IAE, FZG are preferred regarding the wear issue. However, in these methods, the increasing-load sequences bring

* Corresponding author.
E-mail address: reza.bayat@tuni.fi (R. Bayat).

https://doi.org/10.1016/j.triboint.2021.107002
Received 11 January 2021; Received in revised form 24 February 2021; Accepted 15 March 2021
Available online 19 March 2021

the unworn fresh asperities in contact at the start of each load step. Thus, the risk of premature scuffing is increased due to the contact of unprotected asperities. In addition, another problem with both conventional rolling-sliding and pure sliding tests is that the sliding speed can not be increased without increasing the rolling speed. Consequently, with increasing the sliding speed the rolling speeds will be higher resulting in the entrainment of more lubricant into the contact and formation of a thick EHL film [29]. To avoid such problems, Ingram et al. employed a ball-on-disc machine to provide a rolling-sliding contact in contra-rotation mode [30]. This technique provided low oil entrainment speed and decoupling of sliding and rolling speeds that allowed performing the scuffing test with increasing-sliding-speed sequences instead of increasing-load sequences. That contra-rotating ball-on-disc method was further improved by Peng et al. aiming for higher repeatability and scuffing prediction [29]. However, the increasing-sliding speed sequences used in these studies fail to differentiate between the performance of various oils with low to high scuffing capacity range.

Real component tests like FZG are critical to examine the performance of a lubricant. Unfortunately, these tests are costly and time-intense. Therefore, laboratory tests can be used for the primary screening and grasping scientifically analyzed results that apply to the real components. Using a fully formulated lubricant is necessary for these prior laboratory tests since the results can be correlated to the real component tests. Considering this fact, these industrial oils have been commonly used in scientific papers as well [31–35]. This paper aims to modify the contra-rotating method for evaluating the scuffing capacity of fully formulated environmentally acceptable lubricant. The modification of the test sequences minimizes the error and captures big or small scuffing capacity differences between the oils. Achieving this goal, the ball specimen is replaced with a barrel specimen to generate high Hertzian pressure. Although using the barrel-on-disc method is not conventional for scuffing test, it has been used for studying micropitting [36], surface/lubricant interactions [37] and white etching cracks [38]. In addition, the spacer layer imaging method (SLIM) is used to capture the tribofilm evolution and illustrate the tribofilm/lubricant interaction during different stages of the scuffing test.

2. Experiment detail

2.1. Experimental rig

The scuffing tests were performed using the barrel-on-disc technique provided by a mini-traction machine (MTM). Fig. 1 shows a schematic view of the test rig and barrel/disc specimens. The barrel and disc are in rolling sliding contact, and the friction force is measured by a load cell mounted between the barrel shaft and the instrument body. The barrel shaft is tilted to minimize the spin, and it is rotating independently from the disc shaft to provide a wide range of rolling and sliding speeds. Rolling speed denotes the lubricant entrainment speed, and sliding speed has a direct relation to the shear stress and heat generation. For this rolling/sliding contact, these speeds are expressed by Eqs. (1) and (2):

$$U_e = \frac{U_d + U_b}{2} \tag{1}$$

$$U_s = U_d - U_b \tag{2}$$

where U_d and U_b are respectively the disc and barrel velocities in the contact point, U_e is the entrainment velocity and U_s is the sliding velocity.

During the tests, the pot and lubricant temperatures were monitored by two separate sensors, one mounted in the pot and another in contact with the lubricant. Adjusting the right temperature, a heater generates the required amount of heat, and the cooler transfers the excessive heat.

Picturing the tribofilm thickness evolution is a key factor in understanding the scuffing mechanism. The stress imposed on the surface and asperities is influenced by the liquid lubricant film, and tribofilm thickness and properties [39]. To achieve this goal, the spacer layer imaging method (SLIM) was used. In this technique, the barrel is uploaded against a spacer layer of transparent silicon dioxide coated with a thin, semireflective layer of chromium. Then, a white light beam is shone into the contact between the specimen and the spacer layer that proves a colored interference image. This image is recorded by the camera shown in Fig. 1 (a). By capturing this image at different intervals, the tribofilm thickness changes can be studied [40].

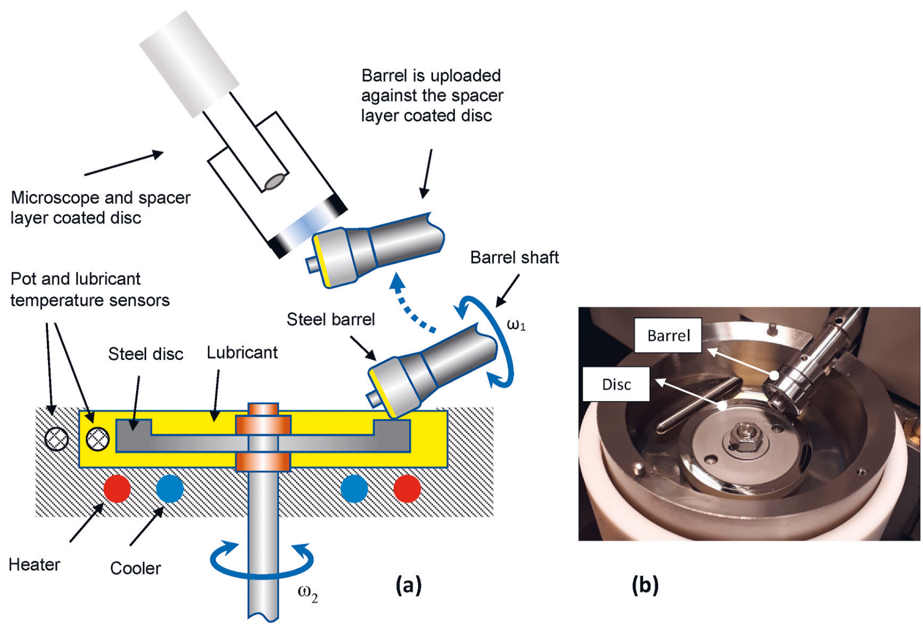

Fig. 1. Barrel on disc test: (a) schematic of MTM with barrel on disc samples (b) an image of the test samples.

2.2. Test specimen

The barrel's diameter was 19.05 mm, and the edge a fillet with 2 mm diameter that was in the contact with a rotating flat disc (Fig. 1). The barrel and disc specimens were both AISI 52100 steel with a hardness of 750–770 H V, elastic modulus of 207 GPa and surface roughness indicated in Table 1, where S_a is the average roughness height of area, and S_q is Root-Mean-Square roughness height of area. For each scuffing test, a fresh barrel and disc were used those were cleaned by immersion in toluene and isopropanol in an ultrasonic bath for 10 min. The roughness parameters and the surface profile were measured by an Alicona InfiniteFocus G5 optical profilometry system. The roughness was measured at three locations with an area of $887 \times 252\ \mu m^2$. The cut-off was 250 μm, and the filter was a Gaussian filter for inclined planar surfaces (ISO 16610–61).

2.3. Tested lubricants

Comparing the scuffing capacity of the environmentally acceptable lubricants, two different EALs with the same viscosity were selected. These two EAL oils meet the US EPA regulations for "Environmentally Acceptable Lubricants", accordingly they demonstrate the VGP requirements for biodegradability, toxicity, and bioaccumulation. For the reference oils, two mineral oils were selected. One of these mineral oils was gear oil from the same viscosity class, and the other one was an engine oil that had a similar 40 °C kinematic viscosity. Except for the case of M1, all the oils have an FZG scuffing capacity of 12+ according to the manufacturer datasheet, and comply with the DIN 51517 part 3 (CLP) standard. The details of oil's properties, and additives elemental composition can be found respectively in Table 2 and Table 3:

2.4. Selecting the test parameters

A scuffing test method for a ball-on-disc test rig has been developed in Refs. [29,30] based on the contra-rotation scuffing test approach. In that contra-rotation scuffing test, the sliding speed increases in scuffing steps while the load and entrainment speed are constant. This criterion is contrary to the conventional scuffing tests in which the increasing-load steps are used. This sliding step criterion [29,30] was designed to avoid the conventional scuffing test problems discussed in section 1. In this paper, the test method is similar to the sliding-step criteria, however, some adjustments are done for testing the high scuffing capacity of fully formulated oils.

The first adjustment is about the running-in stage. It is widely accepted that the surface roughness parameters and distribution of asperity heights are very determinative in the scuffing of machine elements [39]. In addition, running-in not only changes the surface roughness and geometry, it changes the undersurface material properties [17]. One source of high variation in scuffing results is the difference between the micro-topography of every two surfaces. Ingram et al. suggested using the actual test load with very low sliding and entrainment speeds for the running-in stage [30]. Peng et al. observed that a running-in with the actual test load results in considerable damage on the surfaces, and recommended using lower loads to polish the high asperities at the middle of contact [29]. In this paper, a similar low load, low sliding speed running-in test with a duration of 600 s was employed. However, after several experiments with this condition, premature scuffing was observed which means unexpected scuffing at low sliding speeds. To prevent this, an extra short running-in stage was added to the test plan with the same load. These extra running-in periods are performed with the same load as the test, and with lower sliding speed (red points in Fig. 2 denote running-in).

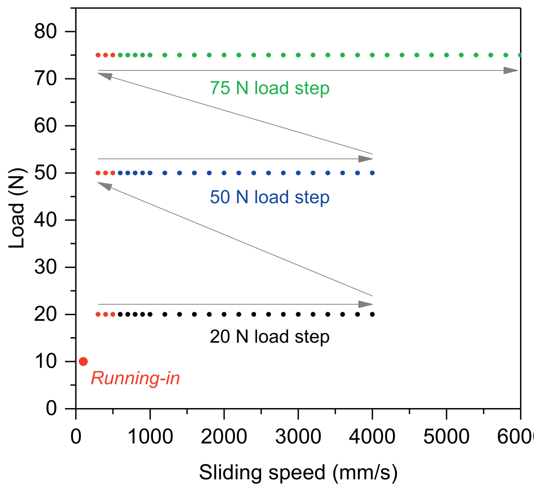

Fig. 2. The variation of the load and sliding speed of the developed scuffing test. The duration for each test point is 30 s, and there is a rest stage of 30 s between each point.

Table 1
Barrel and disc average roughness parameters.

Specimen	Sa (nm)	Sq (nm)
Barrel	90	114
Disc	92	118

Table 2
Measured lubricants properties.

	Kin. Vis. @40 °C (cSt)	Kin. Vis. @100 °C (cSt)	ρ @15 °C (kg/m^3)	VI	Comment
Method	ASTM D445	ASTM D445	EN ISO 12185	ASTM D2270	
M1	127.60	13.83	908	105	Mineral engine oil SAE 40
M2	142.50	14.24	888	97	Mineral gear oil ISO VG 150
EAL1	147.50	18.84	972	145	Synthetic gear oil, Group V, EAL ISO VG 150
EAL2	150.57	18.44	929	137	Synthetic gear oil, Group V, EAL ISO VG 150

Table 3
Elemental analysis of additives in oils according to ASTM D5185.

	Calcium	Magnesium	Boron	Zinc	Phosphorus	Barium	Sulphur
M1	13822	37	1	399	330	0	4704
M2	0	0	36	0	358	0	8391
EAL1	0	0	1	0	864	0	951
EAL2	1	0	0	1	752	0	2080

The second adjustment was about the load in the scuffing test. After tuning the running-in parameters, the first tests were carried out using 20 N load (1.97 GPa) to observe the oils scuffing behavior. With a constant 20 N load, the sliding speed was increased in small steps (Fig. 2 and Table 4). At this load, the mineral oils were showing scuffing, however, no scuffing was observed for the EALs even with sliding velocities of 7000 mm/s. It appeared that the developed sliding speed-step criteria in Refs. [29,30] is not efficient for comparing the oils with a big scuffing capacity difference.

For the case of EALs, after the test with 20 N load, the load was increased by 5 N in several intermediate steps till 75 N that is the limit for the machine (similar to Fig. 2, but with more intermediate load steps). No success was observed with this action and no scuffing was observed for EALs. This is due to a low maximum pressure on the specimen caused by gradual wear on the surfaces which was observed in SLIM images (similar to Fig. 8). This was showing that increasing the load with small steps leads to wear that postpones wear. The same procedure was repeated with 10 N intervals, but it was observed that again the wear persists and prevents scuffing in the machine operational ranges. However, three load-steps of 20 N (Pmax:1.97 GPa), 50 N (Pmax:2.67 GPa), and then 75 N ((Pmax:3.06 GPa) showed promising results. Furthermore, to prevent the excessive wear, the sliding speed was limited to 4000 mm/s for the load step of 20 N and 50 N.

In the final test plan (Fig. 2), a primary running-in is completed, and then the excessive running-in is performed for the load stage of 20 N. After that, the sliding speed increases from 600 mm/s to 4000 mm/s at a load of 20 N (Pmax:1.97 GPa, Pmean:1.31 GPa). If no scuffing appears, the next series of sliding steps are performed with a load of 50 N (Pmax:2.67 GPa, Pmean:1.79 GPa), and then 75 N ((Pmax:3.06 GPa, Pmean:2.05 GPa). It is noteworthy that before each load step, an excessive running-in (red points in Fig. 2) is considered that has the same load as the load-step. This is for preventing the contact between fresh unprotected asperities. In conclusion, the current test method is a combination of the load-step criteria and sliding speed-step contra-rotation method without their disadvantages. The detail of the parameters is given in Fig. 2 and Table 4.

Each test point in Fig. 2 illustrates a test with constant velocity and load in a 30 s long test. The optimum duration of 30 s was also an optimized number. With a 10 and 20 s duration, scuffing can be postponed to one or more sliding steps because there is not enough time for the temperature rise and adhesion between to surfaces, and with longer than 30 s duration the effect of wear plays an adverse role. After each test point, there is a 30 s rest stage to allow the specimens' bulk temperature to return to the oil temperature [29]. At these rest steps, the SLIM image from the barrel surface is captured.

3. Results and discussion

Using the developed test method, the scuffing capacity was assessed for the oils listed in Table 2. This approach compares the scuffing capacity of the oils through a recorded friction-time and PV graph. Three repeats were done for each oil to have an estimation of the test error.

3.1. Ranking the oils scuffing capacity

Fig. 3 shows the recorded friction coefficient of the tested oils during the test stages neglecting the rest stage time. Scuffing was recognized by a rapid and unrecoverable increase in friction coefficient to over 0.2. This friction jump was accompanied by a significant increase in test noise and rig vibrations. In Fig. 3, a clear difference is visible between the oils' scuffing performance. EALs showed better performance compared to the mineral oils, and EAL1 was the best and M1 was ranked the worst oils. Matveevsky suggests that the scuffing risk is related to Friction Power Intensity which is the product of the coefficient of friction before scuffing, mean contact pressure, and sliding speed (FPI = μPUs) [41]. This criterion has been used for predicting the onset of scuffing [16], and it is effective to distinguish between oils with different scuffing performances [29]. Fig. 4 shows FPI at scuffing plotted against mean contact pressure for the tests. A clear difference can be observed between the FPI value of the oils with the mean value of 124 MW/m^2 for oil M1, 307 MW/m^2 for oil M2, 446 MW/m^2 for oil EAL1, and 355 MW/m^2 for oil EAL2.

In Figs. 3 and 4, a good repeatability can be observed for the scuffing capacity and friction results that approved the accuracy of the test. It is noteworthy that the bath oil temperature variation was less than 1 °C

Table 4
Test parameters.

	Running-in	Extra running-in	Test stage	Rest stage
Sliding speed	100 mm/s	300 mm/s-500 mm/s	600 mm/s-4000 mm/s for 20 N and 50 load steps 600 mm/s-6000 mm/s for 70 N	0
Rolling speed	40 mm/s	100 mm/s	100 mm/s	0
Temperature	120 °C	120 °C	120 °C	120 °C
Load	10 N (Pmax: 1.56 GPa)	20 N - Pmax: 1.97 GPa, Pmean: 1.31 GPa 50 N - Pmax: 2.67 GPa, Pmean: 1.79 GPa 75 N - Pmax: 3.06 GPa, Pmean: 2.05 GPa	20 N - Pmax: 1.97 GPa, Pmean: 1.31 GPa 50 N - Pmax: 2.67 GPa, Pmean: 1.79 GPa 75 N - Pmax: 3.06 GPa, Pmean: 2.05 GPa	0
Duration	600 s	30 s per step	30 s per step	30 s

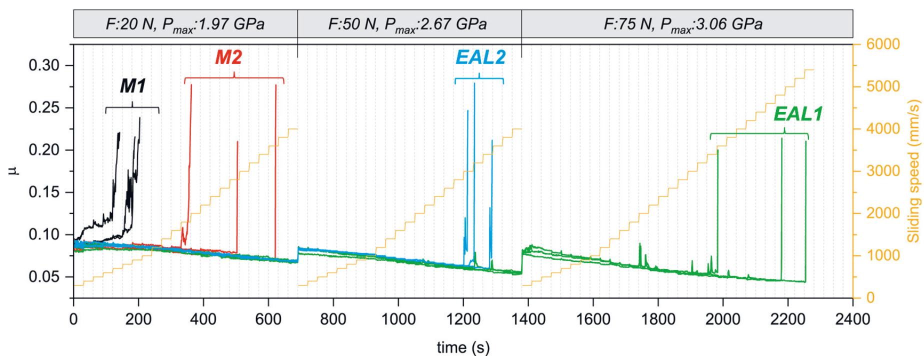

Fig. 3. The friction coefficient, sliding speed and load during the scuffing test of oils.

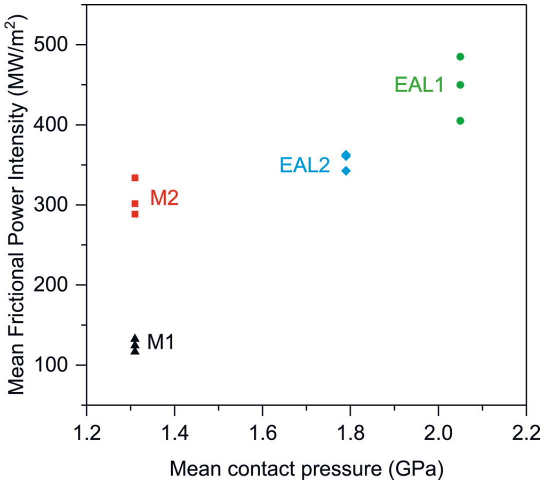

Fig. 4. Mean frictional power intensity at scuffing against mean contact pressure for the tested oils.

Table 5
Estimated dynamic viscosity, pressure-viscosity coefficient and EHL film thickness of the lubricants at the test temperature.

	η @120 °C (mPa s)	α @120 °C (1/GPa)	h_{min} @20 N (nm)	h_{min} @50 N (nm)	h_{min} @75 N (nm)
M1	7.12	12.58	2.35	2.2	2.14
M2	7.065	12.6	2.34	2.19	2.13
EAL1	10.62	8.94	2.61	2.44	2.37
EAL2	9.868	8.88	2.48	2.32	2.25

during the test, and no oil temperature rise was observed before scuffing. This means that the generated heat does not result in the oil temperature increase. On the other hand, the rest steps let the generated heat dissipates and the heating control system keeps the oil temperature constant.

The benefit of low traction (friction) oil on scuffing has been discussed in Ref. [42]. In Fig. 3, the friction is not considerably different for the oils, because they are in a boundary lubrication regime, and in this regime, the oil traction plays a minor role. However, the same oils used in the current study were also used in other studies [43,44], and EAL1 and EAL2 showed considerably lower traction in EHL and mixed regimes.

As EHL film thickness plays a very important role in scuffing, thus the minimum EHL film thickness was calculated using Hamrock and Dowson's formula (Eqs. (4) and (5)) [45].

$$h_{min} = 3.63R_x\left(\frac{U_e\eta_0}{E^*R_x}\right)^{0.68}(\alpha E^*)^{0.49}\left(\frac{F}{E^*R_x^2}\right)^{-0.073}\left(1-e^{-0.68k}\right) \tag{4}$$

$$k = 1.0339\left(\frac{R_y}{R_x}\right)^{0.636} \tag{5}$$

where R_x and R_y are the radius of curvature in the x and y direction (m), U_e is the entrainment speed (m/s), η_0 is the dynamic viscosity of the lubricant (Pa.s) at test temperature, E* is the reduced Young's Modulus (Pa), α is the pressure-viscosity coefficient (Pa^{-1}) at test temperature, F is the applied load (N). Pressure-viscosity coefficient and dynamic viscosity at the test temperature (120 °C) were estimated using a method presented in Ref. [32]. The results are shown in Table 5.

With the film thickness in Table 5 and the surface roughness in Table 1, it is evident that the system is operating under boundary lubrication regime. However, the EALs show higher EHL film thickness in Table 5. Comparing the oils' pressure-viscosity coefficient and dynamic viscosity illustrates that the higher EHL film thickness of EALs is due to their higher dynamic viscosity at the test temperature. The higher viscosity index of EALs helps them to have higher viscosity in high temperature which is beneficial for preventing the failures associated with high temperature. It is noticeable that in Eq. (4), the thermal effect is not considered for calculating the EHL film thickness. Considering the fact that EALs (mainly ester or PAO molecules) have bigger thermal conductivity [46], the difference between the EHL film thickness of EALs and mineral oil can be even higher.

In addition to the EHL film, tribofilm also plays an important role in preventing scuffing failure. Using the SLIM technique, the tribofilm evolution was captured at load stage of F = 20 N, and three sliding speeds of 2200 mm/s, 2800 mm/s and 3400 mm/s. These tribofilm images can be observed in Fig. 5 (the tribofilm for M1 is not shown, because its scuffing happened at much lower speeds). The tribofilm is the dark area along the sliding direction. The exact thickness can be measured using the technique explained in Ref. [43], however, the images are more informative in this case that the tribofilm is not uniformly covering the surface. A darker tribofilm means a higher thickness, and it can be quickly observed that the tribofilm thickness of EALs is higher than that of M2. It was surprising because the mineral oils do not have the restriction of EALs for using environmentally acceptable additives,

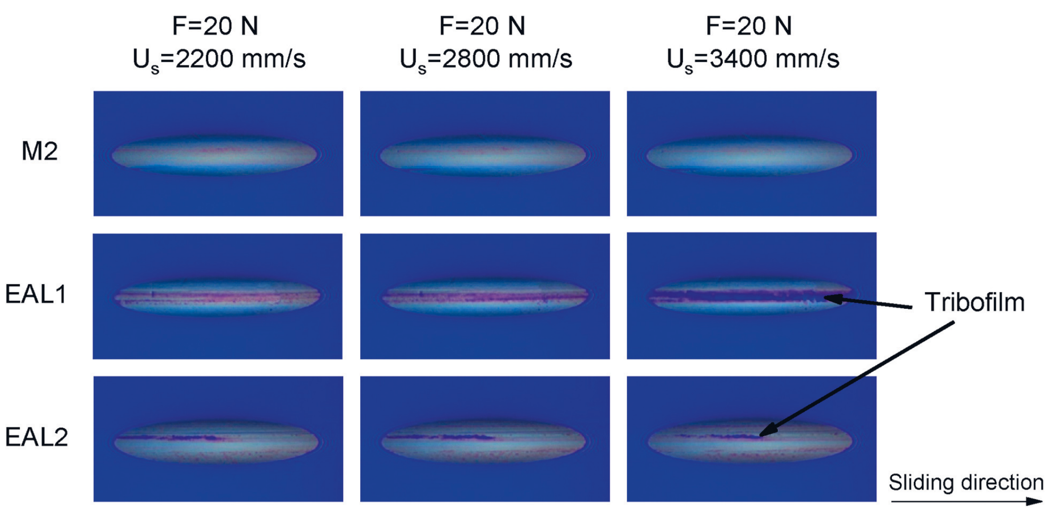

Fig. 5. Tribofilm thickness of oils M2, EAL1 and EAL2 at F = 20 N, and sliding speeds of 2200 mm/s, 2800 mm/s and 3400 mm/s.

thus they usually contain additives with superior performance [32]. From Table 3, it can be seen that M2 contains a considerable amount of sulfuric EP additives. However, these additives do not compensate for the effect of its lower EHL film. With this hypothesis that M2 contains more reactive additives, it can be said that the lower EHL film thickness in this oil results in fast removal of the tribofilm, and prevention of a thick tribofilm formation. This was the case for M1 also, which contained highly reactive additives [43] but could not form a thick tribofilm in this scuffing test due to its low EHL film thickness. In contrast, for the case of EAL1 and EAL2, the higher EHL film thickness enables the tribofilm to be formed. Therefore, these findings imply that a minimum EHL film thickness is always required for tribofilm formation. The EALs showed superior scuffing capacity that is mainly due to their higher viscosity index that allows them to form a thick EHL film. This EHL film not only increases their ability to separate the sliding bodies but also provides the proper condition for a thick tribofilm formation.

It is noticeable to say that except for the case of M1, all the other oil had an FZG scuffing capacity of 12+ according to the manufacturer datasheet. However, using the currently developed technique, the scuffing capacity of the oils is ranked as EAL1>EAL2>M2>M1. Although the test method is similar to what was developed in Refs. [29, 30], the adjustment of parameters and combination of sliding speed-step and load-step enables this test method to evaluate the industrial oil with high scuffing capacity, and distinguish between the scuffing capacity of oils with the same FZG results. However, this does not mean that this test can replace the FZG scuffing test method. FZG test has the advantage of representing real component conditions including impact, pressure and speed variations, as well as bigger curvature, lower wear rate, and higher roughness.

3.2. The relation between tribofilm and scuffing

Figs. 6 and 7 show the SLIM images for the oil EAL1 (rest stage time is not included). In these graphs, only the SLIM images are shown that

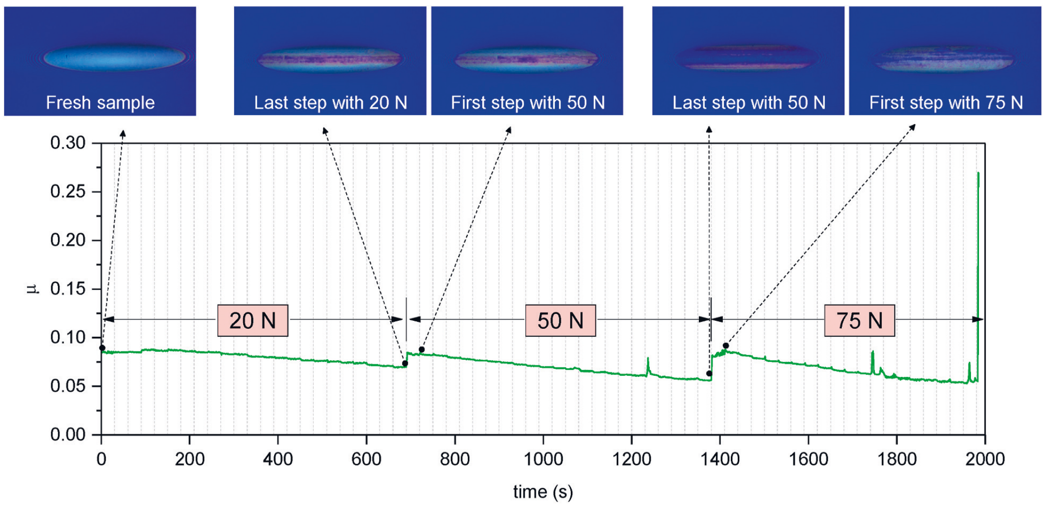

Fig. 6. SLIM images for the scuffing test of EAL1, captured before and after changing the load.

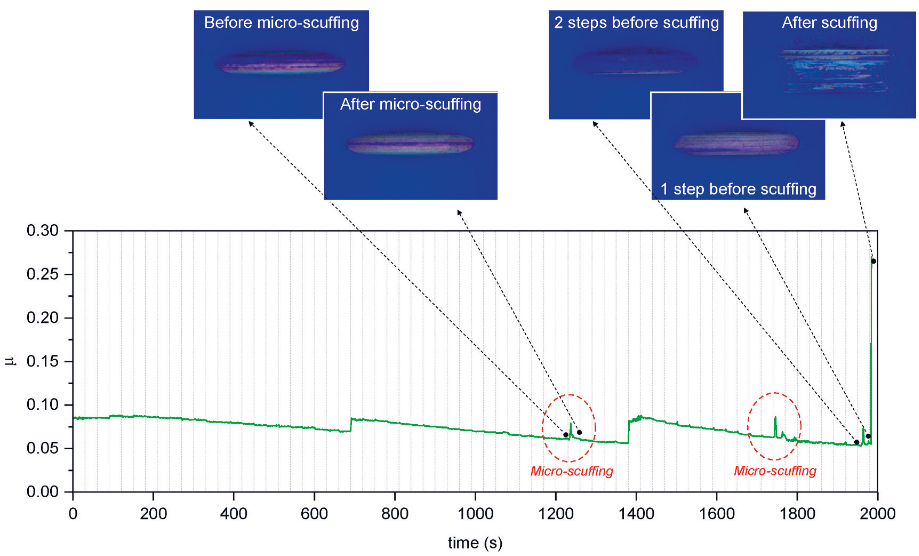

Fig. 7. SLIM images for the scuffing test of EAL1, captured before and after a micro-scuffing and the scuffing.

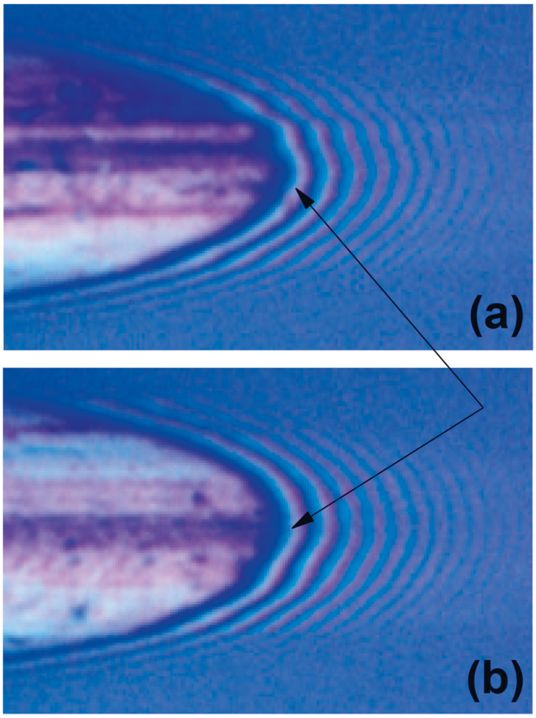

Fig. 8. Geometrical change of the barrel after micro-scuffing: (a) Before micro-scuffing, (b) After micro-scuffing.

contain specific characteristics in this scuffing test. In Fig. 6, the SLIM images are shown just before and after changing the load. It can be seen that after increasing the load, the tribofilm thickness decreased. This is more visible for the case of changing from 50 N to 75 N load. The removal of tribofilm leads to direct contact between the metallic surfaces, but it did not lead to scuffing in this test as the sliding velocity was very low after increasing the load. This is the reason that extra running-in stages were added before each load stage (Fig. 2) to give enough time for the tribofilm to be formed again. This is a very important point that must be carefully inspected in scuffing tests based on step loads (for example FZG scuffing test). In the step-load scuffing tests, by increasing the load, a fresh area of the sample with unworn asperities comes into the contact that is not protected by a tribofilm. In addition, the previously formed tribofilm is also removed. Thus, it can lead to premature scuffing. The current developed test plan prevents this kind of failure by a low sliding speed at the start of the load steps that is a kind of short running-in period. Therefore, it is recommended to have a short running-in with the same load (as the load step) and low sliding speed in a scuffing test. This is an important point to know for the other applications in which overload is critical in scuffing. In such applications, a low-speed running-in with high loads helps the formation of tribofilm over the unprotected contact area of lubricated components. The SLIM images showed that in high load conditions, the tribofilm can cover the contact area in less than 60 s.

In Fig. 7, the SLIM images of oil EAL1 are presented before and after scuffing, and before and after a micro-scuffing. The “micro-scuffing” refers to local scuffing that does not propagate to the whole surfaces, and appears as a sudden rise and quick fall of friction coefficient [4,17,29,39,47–49]. Regarding micro-scuffing, different studies report microstructural change and instantaneous plastic flow accompanied by a temperature rise [17,18,49]. However, the temperature rise and wear of micro-scuffing are not considerable compared to those of the final scuffing [49]. Micro-scuffing appears when the plastic flow of the material does not lead to a total failure, and a “healing” or “quenching” process prevents the scuffing propagation [17,39].

The healing process is attributed to a quick dissipation of heat [19] and reduced normal pressure due to the increased contact area [49]. In the current test, Fig. 7 shows the tribofilm removal after the micro-scuffing. Also, the increasing contact area was detected after the micro-scuffing that is hard to observe in Fig. 7. Thus, the SLIM images were magnified in Fig. 8 to distinguish between the contact area of the barrel before and after the micro-scuffing. In Fig. 8, the widened contact area signifies a small change in the barrel’s edge radius and the removal of a very thin layer from the specimen.

When micro-scuffing happens, a thin layer of material experiences plastic deformation and results in some heat generation. This is the layer in which the rate of thermal softening exceeds the rate of work hardening. After that, a new layer with new mechanical properties comes into contact. If the thermal softening is still so high that can remove that surface, the scuffing propagates [17,18]. In this stage, if the lubricant transfers enough amount of heat, and the tribofilm is recovered quickly, then the healing happens. From Fig. 3, it was observed that the healing process and micro-scuffing of EAL1 happened at the same sliding speeds in which EAL2 experienced scuffing (Fig. 3). This shows that EAL1 had a higher scuffing healing ability. Accordingly, the higher healing ability of EAL1 is attributed to its superior EHL film (Table 5) and tribofilm (Fig. 5). While EAL1 and EAL2 are both from the same oil type, and viscosity class, they show different scuffing capacities. This indicates that minor changes in the lubricant formulation can result in healing of scuffing, and better scuffing capacity of the oil. One probable reason for such a case can be the higher phosphorous content of EAL 1 that leads to a thicker and more reactive tribofilm (Fig. 5) and a better micro-scuffing healing.

Regarding the final scuffing of EAL1 in Fig. 7, a micro-scuffing was also observed just prior to the final friction rise. Before that micro-scuffing, a thick tribofilm was protecting the surface, but after that micro-scuffing, the tribofilm thickness was very thin that provided the condition for the final scuffing. Although after that micro-scuffing the surface was slightly widened, it was not enough to postpone the scuffing. Although the tribofilm-friction graph is shown only for EAL1, the link between the micro-scuffing, scuffing and tribofilm can be generalized for the other tested oils.

3.3. Surface profile before, during and after the scuffing test

To further study the surface modification of the samples, their surface profile was captured by an Alicona InfiniteFocus G5 optical profilometry system. Fig. 9 shows the barrel surface and profile before, during and after the test. Compared to the visible scuffing scar in Fig. 9 (c), no considerable deformation can be observed after the load stage of 50 N (Fig. 9 (b)). However, as it was discussed about SLIM images in section 3.2, micro-scuffing results in small geometrical modifications. This surface modification was hard to measure by Alicona optical profilometer.

The disc was also observed after the 50 N load step, and after scuffing (Fig. 10). Again, no considerable geometrical change was observed after the load stage of 50 N on the disc. This approves the successful implementation of this test method by eliminating the wear adverse effect. In Fig. 10 (b), the wear grooves in the sliding direction show severe cutting happened due to adhesion of the metal surfaces.

4. Conclusion

The objective of this work was to develop a fast contra-rotating method to evaluate the scuffing capacity of fully formulated EALs. The developed test method used a barrel-on-disc specimen setup to reach higher contact pressures up to 3.06 GPa, and employing scuffing steps

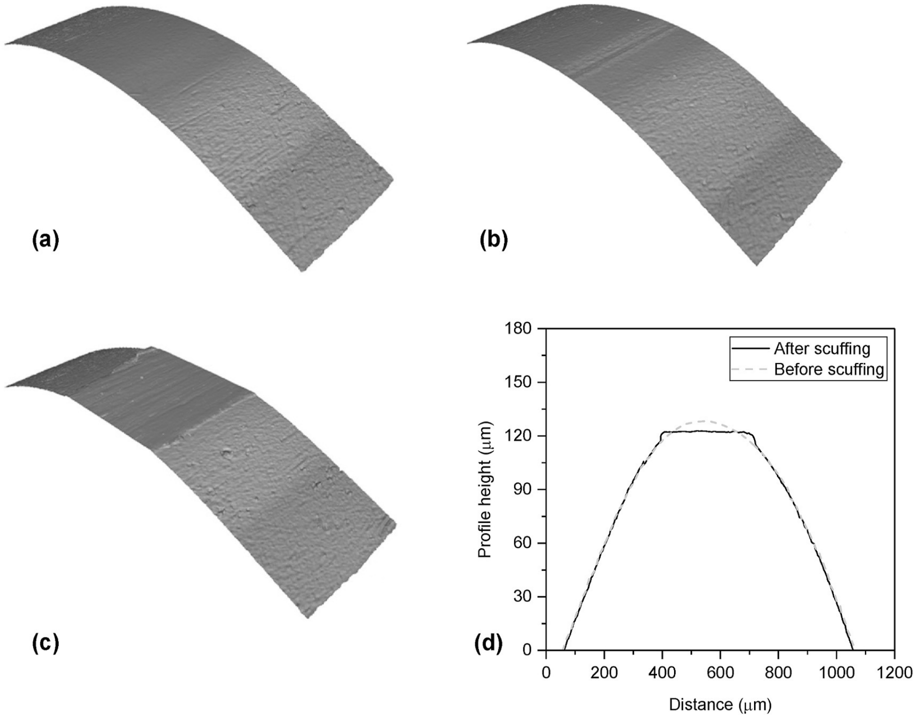

Fig. 9. Example images of the barrel edge for the oils EAL1: (a) new barrel (b) after the load stage 50 N (no scuffing yet) (c) after scuffing (d) barrel profile before and after scuffing.

combining sliding speed steps and load steps. Furthermore, the tribofilm evolution was captured by the SLIM technique to illustrate the interaction between the EHL film and tribofilm. Two industrial EALs formulated for gears and two fully formulated mineral oils were evaluated with this new scuffing test method. The results showed that:

- Careful selection of running-in parameters is very important in achieving reliable scuffing results. In addition to a primary running-in with low load and low speed, a short running-in is recommended before each load step. This short running-in must have the same load as the test to enhance tribofilm coverage on the unprotected areas. Also, this short running-in must have a low sliding speed and short duration to prevent unwanted wear.
- The advantages of the developed test are:
  - o Differentiating between the scuffing capacity of the oils which had similar FZG scuffing capacity in their datasheet.
  - o Providing high sliding speeds while maintaining a low entrainment speed so that high-performance oils can be tested successfully.
  - o Minimizing the wear before scuffing by using rolling–sliding conditions.
- The scuffing is identified by a sudden unrecoverable increase of friction coefficient resulting in a high wear rate and destruction of the surface. Micro-scuffing is identified by a temporary and recoverable friction rise that results in the removal of tribofilm and plastic deformation in several material layers.
- The healing of micro-scuffing happens by small changes in the contact area and accordingly alternation of the normal pressure distribution. In addition, EHL and tribofilm play a significant role in micro-scuffing healing. Small variations in the lubricant formulation have a significant effect on the healing of micro-scuffing.
- After increasing the load in a scuffing test, the thickness of tribofilm decreases that is more evident at high loads. At the high loads, the tribofilm can be recovered if the sliding speed is low. However, at such high loads, if the sliding speed is not low, the increased load brings the fresh unprotected area into the contact and results in unwanted scuffing. Thus, it is recommended that the load increase is accompanied by a low speed to prevent scuffing.
- The tested EALs showed superior scuffing capacity than mineral oils. This was mainly due to their higher viscosity index that allowed them to form a thick EHL film at high temperatures.
- The tested EALs formed a thicker tribofilm in scuffing tests despite having the restriction of using only environmentally acceptable additives. A minimum EHL film thickness is always required for tribofilm formation.

CRediT authorship contribution statement

Reza Bayat: Conceptualization, Methodology, Software, Validation, Formal analysis, Investigation, Resources, Data curation, Writing – original draft, Writing – review & editing, Visualization. **Arto Lehtovaara:** Conceptualization, Writing – review & editing, Supervision, Project administration.

Declaration of competing interest

The authors declare that they have no known competing financial interests or personal relationships that could have appeared to influence the work reported in this paper.

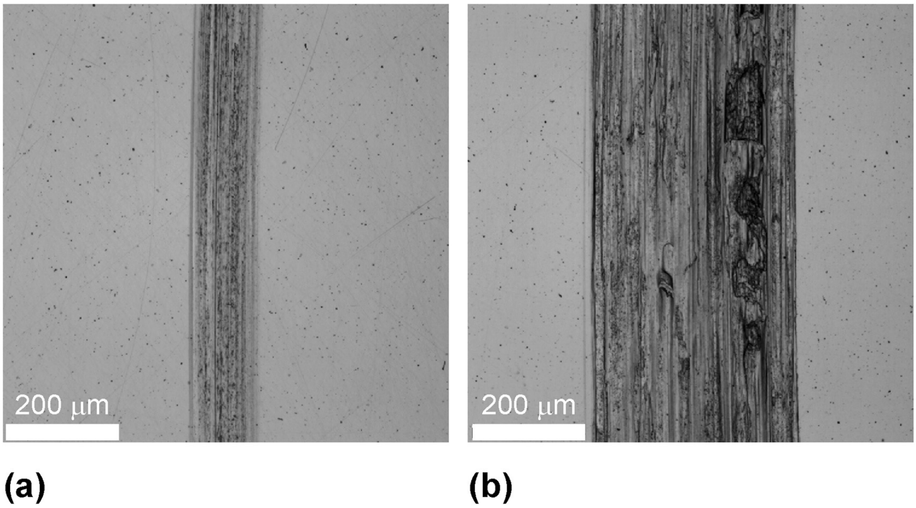

Fig. 10. Example images of the disc for the oils EAL1: (a) after the load stage 50 N (no scuffing yet) (b) after scuffing.

Acknowledgments

We gratefully acknowledge the financial support from Tampere University graduate school.

References

[1] Saeidi F, Shevchik SA, Wasmer K. Automatic detection of scuffing using acoustic emission. Tribol Int 2016;94:112–7. https://doi.org/10.1016/j.triboint.2015.08.021.
[2] Savolainen M, Lehtovaara A. An experimental approach for investigating scuffing initiation due to overload cycles with a twin-disc test device. Tribol Int 2017;109:311–8. https://doi.org/10.1016/J.TRIBOINT.2017.01.005.
[3] Schipper DJ, De Gee AWJ. Lubrication modes and the IRG transition diagram. Lubric Sci 1995;8:27–35. https://doi.org/10.1002/ls.3010080104.
[4] Yagi K, Izumi T, Koyamachi J, Sanda S, Yamaguchi S, Satio K, et al. In situ observation of crystal grain orientation during scuffing process of steel surface using synchrotron X-ray diffraction. Tribol Lett 2020;68:115. https://doi.org/10.1007/s11249-020-01357-y.
[5] Christensen H. Failure by collapse of hydrodynamic oil films. Wear 1972;22:359–66. https://doi.org/10.1016/0043-1648(72)90394-8.
[6] Höhn BR, Michaelis K. Influence of oil temperature on gear failures. Tribol Int 2004;37:103–9. https://doi.org/10.1016/S0301-679X(03)00047-1. Elsevier.
[7] Li S, Kahraman A, Anderson N, Wedeven LD. A model to predict scuffing failures of a ball-on-disk contact. Tribol Int 2013;60:233–45. https://doi.org/10.1016/j.triboint.2012.11.007.
[8] Castro J, Seabra J. Influence of mass temperature on gear scuffing. Tribol Int 2018;119:27–37. https://doi.org/10.1016/j.triboint.2017.10.032.
[9] Yagi K, Ebisu Y, Sugimura J, Kajita S, Ohmori T, Suzuki A. In situ observation of wear process before and during scuffing in sliding contact. Tribol Lett 2011;43:361–8. https://doi.org/10.1007/s11249-011-9817-3.
[10] Batchelor AW, Stachowiak GW. Model of scuffing based on the vulnerability of an elastohydrodynamic oil film to chemical degradation catalyzed by the contacting surfaces. Tribol Lett 1995;1:349–65. https://doi.org/10.1007/BF00174259.
[11] Wojciechowski L, Kubiak KJ, Mathia TG. Roughness and wettability of surfaces in boundary lubricated scuffing wear. Tribol Int 2016;93:593–601. https://doi.org/10.1016/j.triboint.2015.04.013.
[12] Spikes H, Jie Z. History, origins and prediction of elastohydrodynamic friction. Tribol Lett 2014;56:1–25. https://doi.org/10.1007/s11249-014-0396-y.
[13] Spikes HA, Cameron A. Scuffing as a desorption process—an explanation of the borsoff effect. ASLE Trans 1974;17:92–6. https://doi.org/10.1080/05698197408981442.
[14] Blok H. The flash temperature concept. Wear 1963;6:483–94. https://doi.org/10.1016/0043-1648(63)90283-7.
[15] Dyson A. The failure of elastohydrodynamic lubrication of circumferentially ground discs. Proc Inst Mech Eng 1976;190:699–711. https://doi.org/10.1243/pime_proc_1976_190_074_02.
[16] Cheng HS, Dyson A. Elastohydrodynamic lubrication of circumferentially–ground rough disks. ASLE Trans 1978;21:25–40. https://doi.org/10.1080/05698197808982858.
[17] Hershberger J, Ajayi OO, Zhang J, Yoon H, Fenske GR. Evidence of scuffing initiation by adiabatic shear instability. Wear 2005;258:1471–8. https://doi.org/10.1016/j.wear.2004.10.010.
[18] Ajayi OO, Hersberger JG, Zhang J, Yoon H, Fenske GR. Microstructural evolution during scuffing of hardened 4340 steel - implication for scuffing mechanism. Tribol Int 2005;38:277–82. https://doi.org/10.1016/j.triboint.2004.08.011. Elsevier.
[19] Ajayi OO, Lorenzo-Martin C, Erck RA, Fenske GR. Scuffing mechanism of near-surface material during lubricated severe sliding contact. Wear 2011;271:1750–3. https://doi.org/10.1016/j.wear.2010.12.086.
[20] Ajayi OO, Lorenzo-Martin C, Erck RA, Fenske GR. Analytical predictive modeling of scuffing initiation in metallic materials in sliding contact. Wear 2013;301:57–61. https://doi.org/10.1016/j.wear.2012.12.054.
[21] Zhang C, Peng B, Gu L, Wang T, Wang L. A scuffing criterion of steels based on the friction-induced adiabatic shear instability. Tribol Int 2020;148:106340. https://doi.org/10.1016/j.triboint.2020.106340.
[22] American Society for Testing. Materials: ASTM D1947 test method for, load-carrying capacity of petroleum oil and synthetic fluid gear lubricants. 1993.
[23] Energy Institute (formerly Institute of Petroleum, IP): IP 166: 77(R1992) Determination of load-carrying capacity of lubricants—IAE gear machine method.
[24] ISO: ISO 14635 Part 1: gears-FZG test procedures-Part 1: FZG test method A/8,3/90 for scuffing 1736 load-carrying capacity of oils. 2000.
[25] Castro J, Seabra J. Global and local analysis of gear scuffing tests using a mixed film lubrication model. Tribol Int 2008;41:244–55. https://doi.org/10.1016/j.triboint.2007.07.005.
[26] ASTM D2782: Standard test method for measurement of extreme-pressure properties of lubricating grease (Timken Method).
[27] ASTM D2596: Standard test method for measurement of extreme-pressure properties of lubricating grease (Four-Ball Method).
[28] Savolainen M, Lehtovaara A. An experimental investigation of scuffing initiation due to axial displacement in a rolling/sliding contact. Tribol Int 2018;119:688–97. https://doi.org/10.1016/j.triboint.2017.12.007.
[29] Peng B, Spikes H, Kadiric A. The development and application of a scuffing test based on contra-rotation. Tribol Lett 2019;67:37. https://doi.org/10.1007/s11249-019-1149-8.
[30] Ingram M, Hamer C, Spikes HA. A new scuffing test using contra-rotation. Wear 2015;328–329:229–40. https://doi.org/10.1016/j.wear.2015.01.080.
[31] Vrcek A, Hultqvist T, Baubet Y, Björling M, Marklund P, Larsson R. Micro-pitting and wear assessment of engine oils operating under boundary lubrication conditions. Tribol Int 2019;129:338–46. https://doi.org/10.1016/j.triboint.2018.08.032.
[32] Brandão JA, Meheux M, Ville F, Seabra JHO, Castro J. Comparative overview of five gear oils in mixed and boundary film lubrication. Tribol Int 2012;47:50–61. https://doi.org/10.1016/j.triboint.2011.10.007.
[33] Brandão JA, Meheux M, Seabra JHO, Ville F, Castro MJD. Traction curves and rheological parameters of fully formulated gear oils. Proc Inst Mech Eng Part J J Eng Tribol 2011;225:577–93. https://doi.org/10.1177/1350650111405111.
[34] Martins R, Seabra J, Brito A, Seyfert C, Luther R, Igartua A. Friction coefficient in FZG gears lubricated with industrial gear oils: biodegradable ester vs. mineral oil. Tribol Int 2006;39:512–21. https://doi.org/10.1016/J.TRIBOINT.2005.03.021.
[35] Hammami M, Rodrigues N, Fernandes C, Martins R, Seabra J, Abbes MS, et al. Axle gear oils: friction, wear and tribofilm generation under boundary lubrication regime. Tribol Int 2017;114:88–108. https://doi.org/10.1016/J.TRIBOINT.2017.04.018.

[36] Rycerz P, Kadiric A. The influence of slide–roll ratio on the extent of micropitting damage in rolling–sliding contacts pertinent to gear applications. Tribol Lett 2019; 67:1–20. https://doi.org/10.1007/s11249-019-1174-7.
[37] Bergseth E, Zhu Y, Söderberg A. Study of surface roughness on friction in rolling/sliding contacts: ball-on-disc versus twin-disc. Tribol Lett 2020;68:1–15. https://doi.org/10.1007/s11249-020-01310-z.
[38] Gould B, Demas NG, Pollard G, Rydel JJ, Ingram M, Greco AC. The effect of lubricant composition on white etching crack failures. Tribol Lett 2019;67:1–24. https://doi.org/10.1007/s11249-018-1106-y.
[39] Ludema KC. A review of scuffing and running-in of lubricated surfaces, with asperities and oxides in perspective. Wear 1984;100:315–31. https://doi.org/10.1016/0043-1648(84)90019-X.
[40] Fujita H, Spikes HA. Study of zinc dialkyldithiophosphate antiwear film formation and removal processes, part II: kinetic model. Tribol Trans 2005;48:567–75. https://doi.org/10.1080/05698190500385187.
[41] Matveevsky RM. The critical temperature of oil with point and line contact machines. J Basic Eng 1965;87:754–9. https://doi.org/10.1115/1.3650672.
[42] Jackson A, Webster MN, Enthoven JC. The effect of lubricant traction on scuffing. Tribol Trans 1994;37:387–95. https://doi.org/10.1080/10402009408983307.
[43] Bayat R, Lehtovaara A. EHL/mixed transition of fully formulated environmentally acceptable gear oils. Tribol Int 2020;146. https://doi.org/10.1016/j.triboint.2020.106158.
[44] Bayat R, Lehtovaara A. Friction and temperature mapping of environmentally acceptable gear oils. Tribol Fin J Tribol 2020;37:4–12. https://doi.org/10.30678/fjt.96048.
[45] Hamrock BJ, Dowson D. Minimum film thickness in elliptical contacts for different regimes of fluid-film lubrication. 1978. Cleveland, Ohio.
[46] Larsson R, Andersson O. Lubricant thermal conductivity and heat capacity under high pressure. Proc Inst Mech Eng Part J J Eng Tribol 2000;214:337–42. https://doi.org/10.1243/1350650001543223.
[47] Yoon H, Zhang J, Kelley F. Scuffing characteristics of sae 50b38 steel under lubricated conditions. Tribol Trans 2002;45:246–52. https://doi.org/10.1080/10402000208982547.
[48] Matsuzaki Y, Yagi K, Sugimura J. In situ observation of heat generation behaviour on steel surface during scuffing process. Tribol Lett 2018;66:142. https://doi.org/10.1007/s11249-018-1095-x.
[49] Yagi K, Kajita S, Izumi T, Koyamachi J, Tohyama M, Saito K, et al. Simultaneous synchrotron X-ray diffraction, near-infrared, and visible in situ observation of scuffing process of steel in sliding contact. Tribol Lett 2016;61:1–16. https://doi.org/10.1007/s11249-015-0636-9.

PUBLICATION IV

Tribofilm formation of simulated gear contact along the line of action

R. Bayat, A. Lehtovaara

Tribology Letters, 69 (2021), 126
https://doi.org/10.1007/s11249-021-01499-7

Tribology Letters (2021) 69:126
https://doi.org/10.1007/s11249-021-01499-7

ORIGINAL PAPER

Tribofilm Formation of Simulated Gear Contact Along the Line of Action

Reza Bayat[1] · **Arto Lehtovaara**[1]

Received: 2 July 2021 / Accepted: 16 August 2021

Abstract

In this paper, an experimental simulation method was used for evaluating the tribofilm formation in rolling/sliding contact at different points in the line of action. A ball-on-disc test method was employed by which the pressure and slide to roll ratio of gear contact could be simulated. In order to reach a general conclusion, four different oils and two surface roughness were involved in the experiments. The tribofilm evolution was captured using spacer layer interferometry method, and the correlation of tribofilm with the location at the line of action was studied. Results showed that there is a threshold pressure for the tribofilm formation around which the tribofilm growth rate is maximum. Above this threshold pressure, the tribofilm formation is not stable, and the wear is dominant. Below this threshold pressure, the tribofilm growth rate rises by increasing the pressure and the gear contact is safely protected by a stable tribofilm.

Graphic Abstract

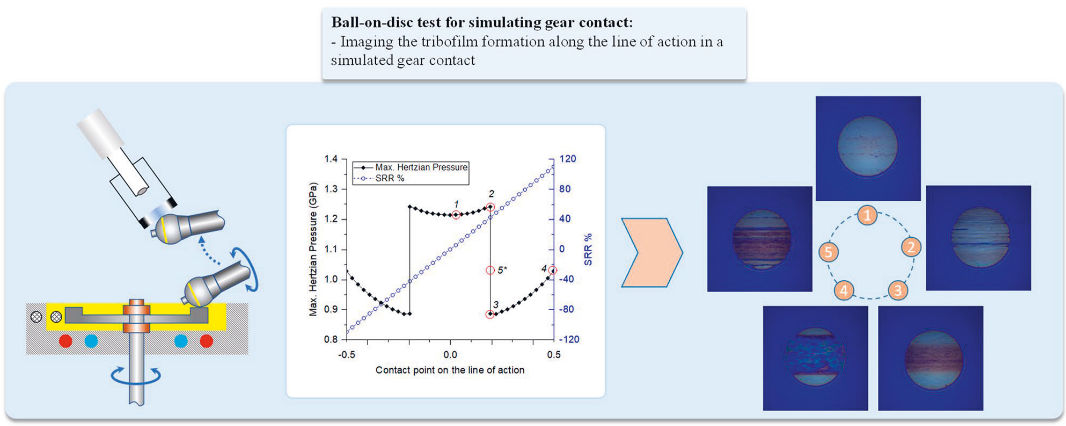

Keywords Tribofilm · Environmentally acceptable lubricant · Gear · Lubrication

1 Introduction

In gears, the teeth are in rolling/sliding contact. When the gear is rotating, the contact condition changes at different locations at the teeth. At the locations near the pitch point, sliding is lower and the pressure is higher. While at the tip of the tooth, the slide to role ratio increases. This variation

✉ Reza Bayat
reza.bayat@tuni.fi

1 Tribology and Machine Elements, Materials Science and Environmental Engineering, Faculty of Engineering and Natural Sciences, Tampere University, P.O. Box 589, 33014 Tampere, Finland

Published online: 27 August 2021

of the contact condition results in different frictional properties, and the appearance of different failure types at the specific points. Pitting is more common at the locations near the pitch point where the pressure is maximum, and the scuffing is found in the tooth tip where the sliding and temperature are the highest. Therefore, for understanding the performance and lifetime of the gears, it is critical to explore the tribological condition of each point on the gear line of action.

FZG test rig is widely used in gear oil testing such as studying frictional behavior of ester and mineral-based oil [1], the effect of base oil type and additives on the pitting in gears [2], and the energy efficiency of mineral base gear oils [3]. Twin disc test is also widely used to study the gears lubrication regarding the effect of surface roughness on film thickness and pressure distribution [4], scuffing initiation caused by the overload [5], pitting [6–8], and wear [9]. Kleemola and Lehtovaara used a twin disc machine to simulate the friction, temperature, and lubrication conditions of gear contact along the line of action [10]. It was indicated that twin-disc measurements can be used for simulating the change of lubrication conditions and the friction behavior trends in real gears [10]. Ball-on-disc test also has been used for simulating the gear contact. It is cheaper, and easy to work with. Björling et al. employed the ball-on-disc test rig for generating the friction maps and used these maps for estimating the friction in a gear set. The results showed that the ball-on-disc test can rank the oils' frictional properties as FZG test did [11]. Regarding the gear application, the ball-on-disc test rig has been widely used also for empirical simulation of the polymer gears [12], friction of the gear oils in different lubrication conditions [13–17], micro pitting [18], and scuffing [19–21]. Tribofilm plays an important role in failure prevention in gear contact, however, to this time, there has not been any paper investigating the tribofilm variation at the gear line of action.

The tribofilm formation has been studied by different techniques. Electrical contact resistance has been used for detecting the formation of anti-wear tribofilm [22], and AFM technique revealed the influence of contact pressure on the tribofilm growth [23]. Other techniques such as XPS and infrared spectroscopy have been also used for this purpose [24], however, spacer layer imaging method (SLIM) is gaining popularity among the other techniques. It is an in situ optical interference method that is quick and enables the accurate estimation of the tribofilm thickness [25]. This technique has been used for studying the influence of slide to roll ratio on the ZDDP tribofilm formation [26], the influence of lubricant on white etching cracking [27], characteristics of the phosphorous and non-phosphorous antiwear films [28], roughness and thickness of ZDDP films [29], and investigating the tribofilm formation during the scuffing test [19, 20]. However, this technique has not been used to specifically study the tribofilm formation mimicking individual contacts during gear meshing.

In this study, a ball-on-disc machine was used to simulate the gear contact along the line of action. The objectives were to investigate the tribofilm thickness evolution and the factors that control the existence of this film in a simulated gear contact. For the simulation of a gear contact, an experimental method was used that tests different points along the line of action with their specific pressure and slide to roll ratio [10]. Picturing the tribofilm at each point, the ball-on-disc test rig was equipped with the SLIM. Four different industrial oils were used to capture the influence of the oil type. In addition, the specimens were manufactured with two different roughness to make sure the results can be generalized to the real components. By investigating the tribofilm evolution in a gear contact, the influence of geometry and surface quality of the gears can be better understood. This can contribute to the gear design, adjusting the working condition and the oil formulation for the gears.

2 Experiment Detail

2.1 Experimental Rig

The tribofilm measurement tests were carried out using a mini-traction machine that provided the rolling/sliding contact between a ball and a disc. Figure 1 shows a

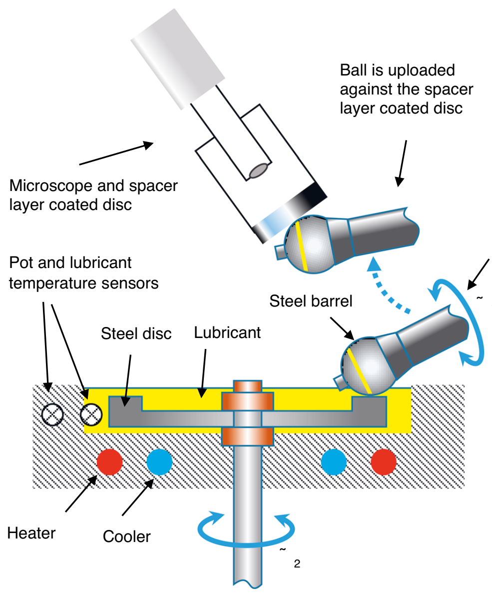

Fig. 1 Schematic of MTM

schematic view of the test rig and ball/disc specimens. The friction force is measured by a load cell mounted between the ball shaft and the instrument body. The ball and disc speeds are controlled independently to achieve a wide range of lubricant entrainment speed and slide to roll ratio. Lubricant entrainment speed, sliding speed, and slide to roll ratio (SRR) are expressed in Eqs. (1), (2), (3):

$$U_e = \frac{U_d + U_b}{2} \tag{1}$$

$$U_s = U_d - U_b \tag{2}$$

$$\mathrm{SRR} = \frac{U_s}{U_e}, \tag{3}$$

where U_d and U_b are respectively the disc and ball circumferential velocities in the contact point, U_e is the entrainment velocity and U_s is the sliding velocity.

During the tests, the pot and lubricant temperatures are monitored by two thermometers placed respectively in the pot wall and lubricant. Adjusting these two temperatures, a heater and a cooling circulating fluid are connected to the pot.

The tribofilm evolution is recorded by a technique called spacer layer imaging (SLIM). At different stages of the tests, the ball is loaded against a spacer layer of transparent silicon dioxide coated with a thin, semireflective layer of chromium. Using a white light source, a colored interference image of the contact is formed and recorded by the camera. The evolution of these interferometry images reveals the tribofilm formation in different stages and conditions [30]. The tribofilm thickness can be calculated according to the technique shown in Ref. [17].

Table 1 Ball and disc average roughness parameters

Specimen		S_a (nm)	S_q (nm)
Ball		8	10
Disc	Smooth	8	10
	Rough	125	173

2.2 Test Specimen

The ball had a diameter of 19.05 mm. The ball and disc specimens were both AISI 52100 steel with a hardness of 750–770 HV and elastic modulus of 207 GPa. All the balls had the same surface roughness, while two different roughness was considered for the disc to investigate the effect of surface roughness (Table 1). In Table 1, S_a is the average roughness height of area, and S_q is the Root-Mean-Square roughness height of area. The roughness values were measured using a Wyko NT1100 optical profilometer. For each test, a new ball and disc were used, and they were cleaned by immersion in toluene and isopropanol in an ultrasonic bath for 10 min.

2.3 Tested Lubricants

Four different oils were tested. Three of them were gear oils that belong to the 150 VG viscosity class. One of these three oils was an environmentally acceptable synthetic oil. Additionally, another mineral engine oil was selected which has a similar 40 °C kinematic viscosity, and it is practically used in ships for gear lubrication. All the oils except oil D that is an engine oil, comply with the DIN 51517 part 3 (CLP) standard. The oils specifications can be found in Table 2.

2.4 Experimental Procedure

Kleemola and Lehrovaara used a twin-disc device for the experimental simulation of gear contact along the line of action [10]. Their spur gear had a center distance of 91.5 mm, gear ratio of 1, normal module 4.5 mm, face width of 20 mm, contact ratio of 1.45, pressure angle of 20°, and profile shift of 0.176. With these specifications, the pressure and SRR of a contact point along the line of action can be estimated as Fig. 2.

In order to study the tribofilm evolution in a gear set, four different points on the line of action are tested (Fig. 2). The tests for each point include running for 120 min under the boundary lubrication, with the specific film thickness of 0.08 for the rough disc, and 0.46 for the smooth disc. The tribofilm images were recorded at different intervals of 15, 30, 45, 60 and 120 min. The tests are performed once with

Table 2 Properties of the used lubricant

	Kin. vis. @40 °C (mm^2/s)	Kin. vis. @100 °C (mm^2/s)	ρ @15 °C (kg/m^3)	VI	Comment
Oil A	148.2	19.1	970	146	Synthetic gear oil, EAL
Oil B	150	15	897	100	Mineral gear oil
Oil C	150	14.7	890	97	Mineral gear oil
Oil D	127.6	13.83	908	105	Mineral engine oil

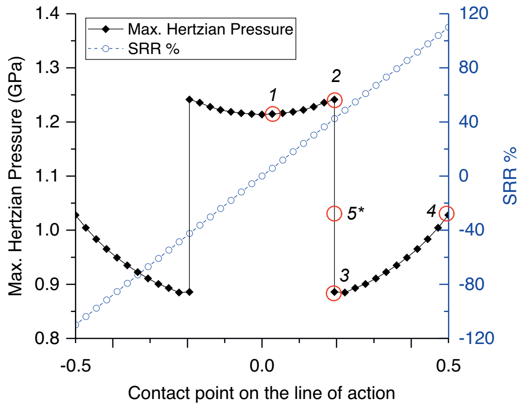

Fig. 2 Maximum Hertzian pressure and SRR along the line of action for a specific gear [10]

the rough disc specimen (S_q 156 nm) and repeated with the smooth disc specimen (S_q 10 nm). The points on the line of action are marked in Fig. 2 as Points 1–4. Also, an additional point is tested which is numbered 5*. This point is not theoretically on the line of action, and it is tested for comparing the effect of pressure and SRR. By comparing this point with Point 4, the effect of SRR can be investigated, and by comparing it with Points 2 and 3, the effect of pressure can be explored. Table 3 shows the parameters of the tested points and the test conditions:

3 Results and Discussion

3.1 Effect of Pressure and SRR

At this stage of experiments, the rough disc specimen was used. For each oil, the tests of 2 h running were performed under the condition specified in Table 3. The tribofilm evolution of the oils A and B is shown in Figs. 3 and 4. In these images, four different points on the line of action are tested (Point 1–4 in Figs. 2 and 3). Also, an additional point is tested which is numbered 5*. This point is not theoretically on the line of action, and it is tested for comparing the effect of pressure and SRR. By comparing this point with Point 4, the effect of SRR can be investigated, and by comparing it with Points 2 and 3, the effect of pressure can be explored.

In Figs. 3 and 4, for the case of Points 1&2, the tribofilm was very thin, and it was hard to be measured due to the wear. However, for Points 3, 4 and 5*, the tribofilm thickness was measured, and the thickness is given in Fig. 5. Points 4 and 5* have the same pressure but different SRR, however, these two points have almost the same tribofilm growth rate in Fig. 5. Thus, it can be said that the SRR has a minor effect on the tribofilm thickness at a constant sliding distance. The same result was found by Shimizu and Spikes for ZDDP additive, and it was concluded that for the same contact pressure, the tribofilm formation does not depend on the SRR [26].

In Figs. 3 and 4, by comparing the Point 5* versus 3 which have the same SRR, the influence of contact pressure can be revealed. By increasing the maximum hertzian pressure from 0.87 Gpa (point 3) to 1.02 GPa (point 5*), the tribofilm thickness grows. This illustrates the effect of contact pressure on the tribofilm growth rate. Zhang and Spikes showed that the shear stress (friction coefficient × contact pressure) controls the rate of tribofilm formation of ZDDP [31], and Spikes claimed that this can be generalized for the other additives according to the Stress-augmented thermal activation theory [32]. Table 4 presents the shear stress and friction force for the case of oils A and B tested with the rough disc. The shear stress of oils C and D were very close to oil B. From Table 4, it is observed that oil A has the highest friction force and shear stress at all the points. Considering its highest tribofilm thickness, this is in agreement with the Stress-augmented thermal activation theory. On the other hand, from Table 4, the shear stress of the Point 5* is higher than that of Point 3 that again approves the Stress-augmented thermal activation theory. However, by comparing the Points 5* versus 2, the tribofilm thickness unexpectedly decreases by increasing the shear stress. Thus, very high shear stress

Table 3 Test conditions

	Point 1	Point 2	Point 3	Point 4	Point 5*
Maximum Hertzian pressure (GPa)	1.21	1.24	0.87	1.02	1.02
SRR %	6.1	42.5	42.5	110	42.5
Entrainment speed (mm/s)	150				
Temperature °C	100				
Duration (min)	120				
Tribofilm measurement intervals (min)	15, 30, 45, 60, 120				
Specimens	Rough disc (S_q 173 nm) and smooth ball (S_q 10 nm)				
	Smooth disc (S_q 10 nm) and smooth ball (S_q 10 nm)				

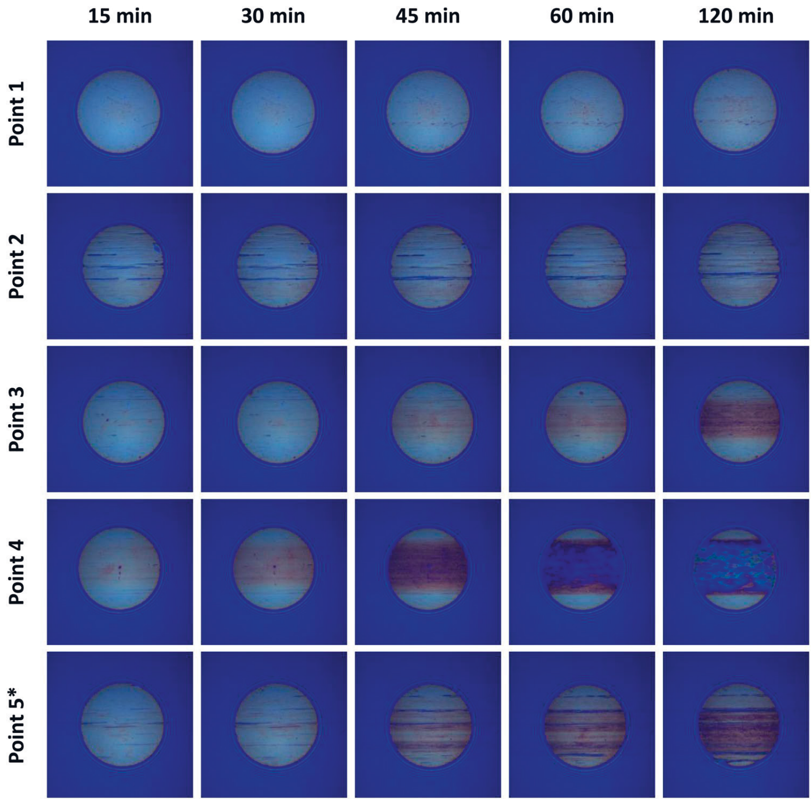

Fig. 3 Tribofilm evolution of the oil A at different points in the line of action

results in the wear on the specimen's surface. It shows that there is an optimum pressure value in which the tribofilm thickness is at maximum. Gosvami et al. observed the same feature, and suggest that at very high pressures, the wear becomes dominant and prevents the tribofilm growth [23]. This high wear can be clearly observed in Figs. 3 and 4, at Point 2. This pressure can be named "tribofilm threshold pressure", above which the wear prevents a stable tribofilm growth, and below which the tribofilm thickness can be estimated by the Stress-augmented thermal activation theory.

For the case of oils C and D (Figs. 6 and 7), the wear was dominant in all the points and no stable tribofilm could be measured. This means that there is a considerable amount of asperity penetration that removes the formed tribofilm. Thus, for these two oils, the pressure is too high, or in the other words, above the tribofilm threshold pressure.

3.2 Effect of Roughness

In order to investigate the influence of roughness, the smooth disc specimen was also used, and the experiments in Table 3 were repeated. For the case of oil A, no considerable tribofilm was formed during 2 h (Fig. 8). The pressure was the same as the tests with the rough discs, and the shear stress of point 2 was around 65 MPa that is near to the amount of shear stress at point 3 in Table 4 for the rough disc. However, no considerable tribofilm or wear was observed. Since there was no wear, it means that the tribofilm removal rate has been very low. Therefore, the low growth rate is due to the small shear stress in the asperity contacts that was not high enough to drive the mechanochemical reaction of the additive molecules. Khaemba et al. used the same specimens and showed that despite the Hertzian pressure being the same, the average asperity pressure in the smooth specimen is around two times lower than in the rough specimens [33]. This emphasizes that the tribofilm threshold pressure is attributed to the pressure at the asperity level. Thus, for oil A, the asperity pressure in the smooth disc was far below the threshold pressure.

For the case of oil D (Figs. 9, 10), a different result was observed. Using the smooth disc (Fig. 9), a thick tribofilm was formed, while no tribofilm has been observed before for the rough disc (Fig. 7). For the case of rough surface test, the wear and tribofilm removal were so high in oil D.

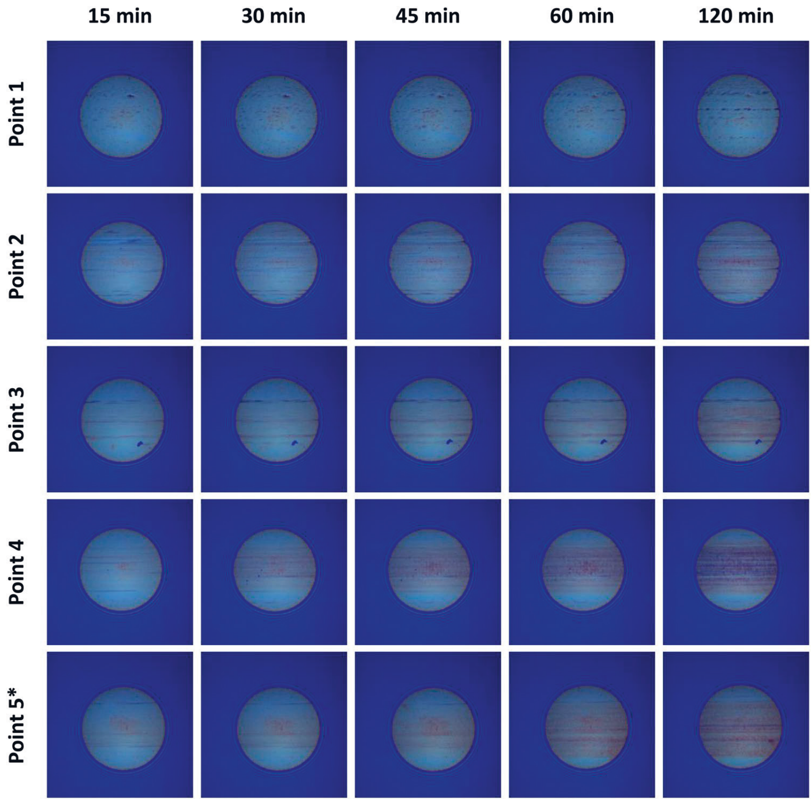

Fig. 4 Tribofilm evolution of the oil B at different points in the line of action

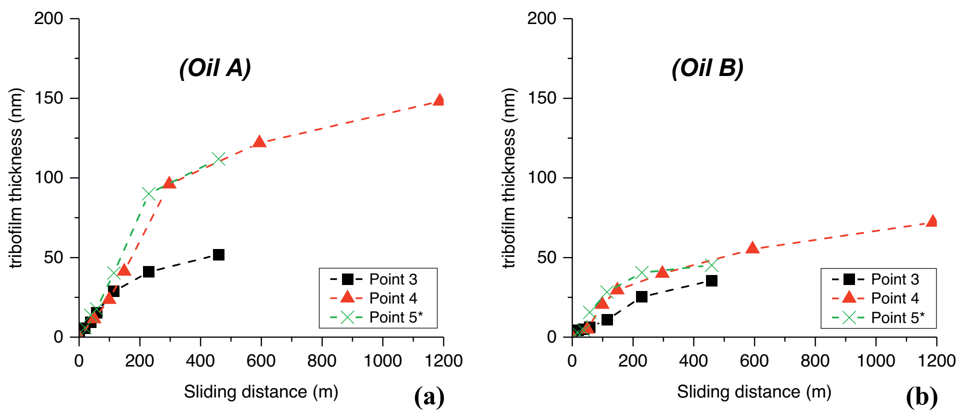

Fig. 5 Tribofilm thickness vs sliding distance for the oils A and B, at different points (rough surface)

Table 4 The shear stress and friction force of the oils A and B at different points

	Shear stress (MPa)/friction force (N)				
	Point 1	Point 2	Point 3	Point 4	Point 5*
Oil A	81.47/6.53	100.64/8.42	68.92/2.89	77.79/4.47	83.60/4.80
Oil B	71.50/5.73	81.32/6.81	59.81/2.51	70.76/4.07	74.00/4.25

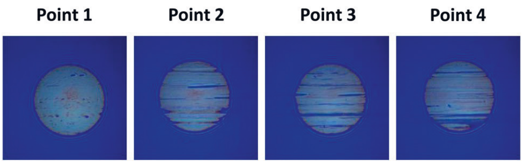

Fig. 6 Ball surface after 120 min test with oil C at different points in the line of action (rough surface)

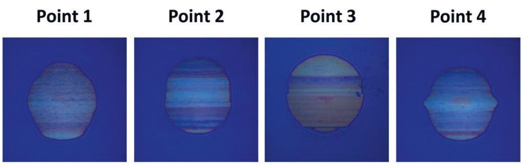

Fig. 7 Ball surface after 120 min test with oil D at different points in the line of action (rough surface)

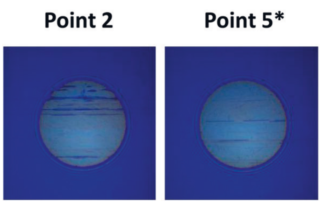

Fig. 8 Ball surface after 120 min test with oil A using a smooth disc

This means that for the oil D, with the rough disc, the asperity pressure was above the threshold pressure, and with the smooth disc, the points were below the threshold pressure, but near to it.

Therefore, the tribofilm threshold pressure is attributed to the pressure in asperity level. Despite having a similar Hertzian pressure and shear stress, the pressure in asperity level can significantly alter the tribofilm formation mechanism.

The specific film thickness for all the oils was calculated according to the method in Ref. [15]. The specific film thickness for all the tested oils was around 0.08 with the rough disc, and 0.45 with the smooth disc. The lubrication regime is in a boundary regime with very low specific film thickness which is not common in the gears and it happens at very low pitch velocity conditions. Such a harsh condition was required for capturing the tribofilm formation within a short time. At higher pitch velocities i.e. higher specific film thicknesses, asperity pressure may decrease hence decreasing the tribofilm growth rate.

3.3 Tribofilm Formation Along the Line of Action

The final tribofilm thickness depends on the equilibrium between the rate of tribofilm growth and removal. Gosvami et al. show that the tribofilm growth rate in a single asperity contact is stress-dependent [23], and it fits a stress-activated Arrhenius model:

$$\Gamma_{\text{growth rate}} = \Gamma_0 \exp\left(-\frac{\Delta G_{\text{act}}}{\kappa_B T}\right), \tag{4}$$

where $\Gamma_{\text{growth rate}}$ is the tribofilm growth rate, and Γ_0 a pre-factor, κ_B Boltzmann constant, T absolute temperature and ΔG_{act} is the free activation energy of the rate-limiting reaction step. ΔG_{act} is assumed to be influenced by the stress according to:

$$\Delta G_{\text{act}} = \Delta U_{\text{act}} - \sigma \Delta V_{\text{act}} \tag{5}$$

Here ΔV_{act} is the activation volume and σ the driving stress. Gosvami et al. assumed this driving stress to be pressure [23], but Spikes believes that it is primarily the shear stress [32]. Based on this model, it can be said that the tribofilm growth rate depends on the pressure (or shear stress) in asperity level (σ), and the additives reactivity (ΔU_{act}).

This stress-activated model for tribofilm growth is widely accepted [31, 32, 34], however, the process of tribofilm removal is not yet well understood and there is no reliable equation that can model it. Jacobs and Carpick used the stress-activated model for modeling the rate of atom loss due to the wear [35], and Felts et al. used a similar model for oxygen removal from graphene [36]. Chen et al. used a linear wear model for the tribofilm removal [37]. In that model, the tribofilm removal rate changes with the height of the tribofilm. Azam et al. used a modified Archard wear model with a variable wear coefficient [38]. This is a logical assumption as the hardness of the tribofilm decreases by its height [39]. However, none of these theories are generally accepted and are not able to model the tribofilm removal under the wear condition. If there was a single accepted theory for the tribofilm removal, the amount of the tribofilm threshold pressure could be calculated by equating the tribofilm growth and removal rate at the moment where there is no tribofilm on the surfaces.

According to the above theories, if the asperity pressure is below the threshold pressure, the tribofilm starts to grow and reaches a specific thickness in which the tribofilm growth

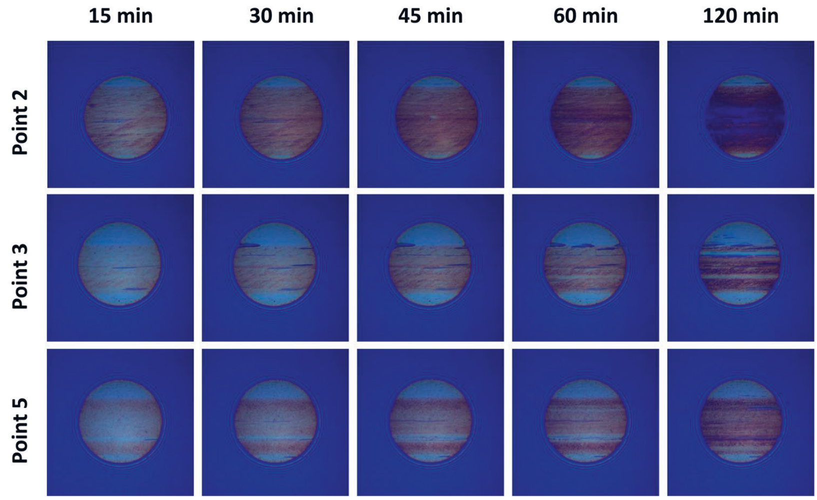

Fig. 9 Ball surface after 120 min test with oil D using a smooth disc

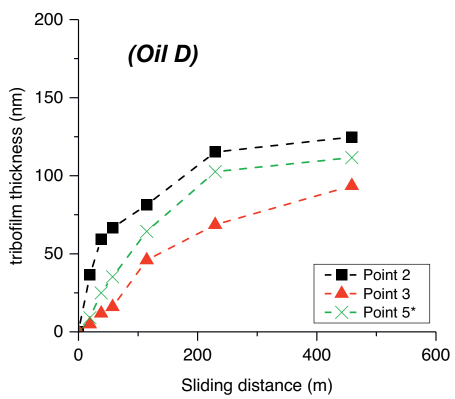

Fig. 10 Tribofilm thickness vs sliding distance for the oils D (smooth surface), at different points

rate is equal to the tribofilm removal rate. Thus, the final tribofilm thickness depends on the equilibrium between the tribofilm growth rate and the tribofilm removal rate [31]. This can be seen in Points 3, 4, and 5* for oils A and B (Figs. 3 and 4). After some time, the tribofilm growth rate and removal rate become equal, and the tribofilm height tends to be constant (Fig. 5). On the other hand, if the asperity pressure is above the threshold pressure, the tribofilm removal rate is bigger than the tribofilm growth rate. Thus, no equilibrium is achieved, and there will be constant wear on the specimens. This is the case that is seen in points 1 & 2 in Figs. 3, 4, and Figs. 6, 7 for the case of oils C and D.

A value for the threshold pressure of oil A can be roughly estimated using the finding of Khaemba et al. [33]. With the same rough disc specimen and smooth ball, Khaemba et al. calculated that the average asperity pressure is 3.9 GPa when the applied pressure is equal to 1 GPa. Such values give the proportion of “real contact area/nominal contact area” equal to 17%. For the case oil A and rough disc, the threshold pressure is between 1.02 and 1.24 GPa. Taking the average of 1.13 GPa for such pressure and considering 17% for the proportion of “real contact area/nominal contact area”, the average asperity pressure is 4.4 GPa. This number is very rough estimated, however, it is comparable to the pressure found by Gosvami et al. [23] for the condition in which wear becomes dominant.

In conclusion, the tribofilm thickness is highly influenced by a specific threshold pressure above which the wear is dominant. Below this threshold pressure, the tribofilm growth rate increases with the pressure. It is very important to note that this pressure is at the asperity level. The tribofilm growth dependence on the pressure, and the threshold pressure can be schematically illustrated as in Fig. 11.

Now, the tribofilm growth rate on this simulated gear contact can be explained. Here the “rate” means nanometer tribofilm per meter sliding distance (Fig. 5). It was discussed that the SRR does not have a considerable influence on tribofilm growth, and it has been verified by another study [26]. Thus, the variation of the tribofilm growth rate along the line of action depends mainly on the pressure.

Considering a specific point on the line of action, the tribofilm growth rate (nm/m) depends on its relative pressure to the tribofilm threshold pressure (Fig. 12). Accordingly, there are three possible scenarios for a gear set:

1. The pressure on the points in the line of action are all below the threshold pressure (case of Fig. 9)

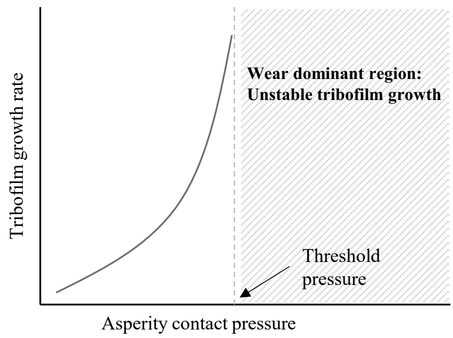

Fig. 11 Schematic of the tribofilm growth rate vs asperity contact pressure

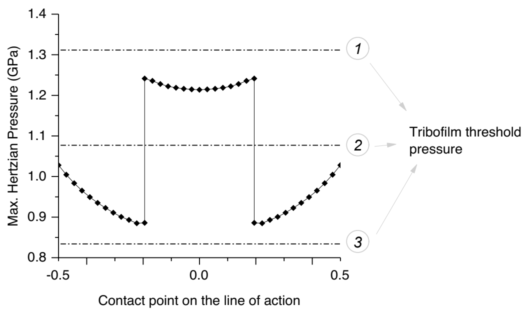

Fig. 12 The tribofilm threshold pressure and the pressure distribution along the line of action for a specific gear

2. The pressure of some points is above, and some points below the threshold pressure (case of Fig. 3)
3. The pressure on the points in the line of action are all above the threshold pressure (case of Fig. 7)

Figure 11 shows these three scenarios. For any one of these cases, the points which are closer to the threshold pressure have the highest tribofilm growth rate (nm/m). Above the threshold pressure, wear is dominant and prevents a stable tribofilm formation. Below the threshold pressure, a stable tribofilm can be formed, but the growth rate depends on how far it is from the threshold pressure. The optimum condition is when all the points are below the tribofilm threshold pressure because the surface can be protected by the formation of a stable tribofilm. According to the discussions, the location of the threshold pressure depends on asperity pressure and the reactivity of the tribofilm, and it can be changed by the roughness, the base oil, or the reactivity of the additives.

In conclusion, it is hard to say that the tribofilm growth rate is higher in the pitch point or the tip of this simulated gear tooth. It is important to pay attention to the unit of tribofilm rate in this context which is nm of tribofilm per meter of sliding distance. This means that in gears, the actual formation time of tribofilm should decrease when moved from pitch point towards tip of the tooth due to linear increase of sliding speed (assuming constant pressure). The higher sliding speeds at the tip zone of gear tooth causes also higher temperature at this zone [10], which was kept within a specific limit in this study and needs further studies. On the other hand, the gear loading may vary largely in different applications, and the Hertzian pressure levels used in this study represent typical values. When the ground gears flanks are new, probably the gear tooth is running above the threshold pressure. However, after the running-in period, the asperity peaks are smoothened, and the conditions are less harsh and more similar to what was tested in this study. Super finished gear surfaces may be near to the roughness levels presented in smooth surfaces in this study. Noticeably to mention that the SLIM technique is hard to be employed for very rough surfaces, and another tribofilm measurement technique should be used to mimic rough (hobbed) surface gear application. However, the results in this paper present insight into the tribofilm formation in gear contact and can be used in future studies.

4 Conclusion

The objective of this work was to investigate the tribofilm film thickness evolution in a simulated gear contact. Besides, it was important to explore the factors that control the existence of tribofilm at different tribological conditions. A ball and disc test equipment provided sliding/rolling contact. Several tests were performed with the specific pressure and slide to roll ratio to mimic the conditions at different points at the line of action. For each test, a separate set of tribofilm images was recorded by the SLIM technique. Four different industrial oils were tested, and the specimens were manufactured in two surface roughness.

The results showed that:

- The tribofilm formation does not depend on the slide to roll ratios in the range of this simulated gear which has low entrainment speed and low temperature rise at different locations along the line of action
- There is a tribofilm threshold pressure around which the tribofilm growth rate is maximum.
- The tribofilm threshold pressure is very sensitive to the surface roughness; thus, it is attributed to the pressure in asperity level. Despite having a similar Hertzian

pressure and shear stress, the pressure in asperity level can significantly alter the tribofilm formation mechanism.
- Above this threshold pressure, the tribofilm formation is not stable, and the wear is dominant. Below this threshold pressure, the tribofilm growth rate rises by increasing the pressure.
- Considering a specific point on the line of action, the tribofilm growth rate mainly depends on its relative pressure compared to the tribofilm threshold pressure. The points which are closer to the threshold pressure have the highest growth rate. The points with higher pressure are prone to damage.

Finding the exact asperity threshold pressure is hard because there is not an accepted theory or model for the tribofilm removal mechanism. However, using this experimental method, the threshold pressure can be found for any combination of gear design, material, and oil.

Acknowledgements We gratefully acknowledge the financial support from Tampere University graduate school.

Author Contributions RB: Conceptualization, Methodology, Software, Validation, Formal analysis, Investigation, Resources, Data Curation, Writing—Original Draft, Writing—Review & Editing, Visualization. AL: Conceptualization, Writing—Review & Editing, Supervision, Project administration.

Funding We gratefully acknowledge the financial support from Tampere University graduate school.

Data Availability The authors confirm that the research in this article is original and that all the data given in the article are real and authentic.

Declarations

Conflict of interest The authors declare no potential conflicts of interest with respect to the research, authorship and/or publication of this article, and we have fully respected the research ethics principles.

Ethical Approval The authors confirm that neither the entire article nor any of its parts have been previously published and is not under consideration elsewhere. Being accepted, this article will not be published elsewhere in the same form, in English or in any other language, without the written consent of the Publisher. Furthermore, the authors declare no potential conflicts of interest with respect to the research, authorship and/or publication of this article, and we have fully respected the research ethics principles.

Consent to Participate All authors (Reza Bayat and Arto Lehtovaara) have contributed to preparing the submitted manuscript entitled "Tribofilm formation of simulated gear contact along the line of action". No other person has significantly contributed to its preparation.

Consent for Publication This article has the full consent of all authors, and all authors have approved the manuscript and its submission and publication on the journal of Tribology Letters.

References

1. Martins, R., Seabra, J., Brito, A., Seyfert, C., Luther, R., Igartua, A.: Friction coefficient in FZG gears lubricated with industrial gear oils: biodegradable ester vs. mineral oil. Tribol. Int. **39**, 512–21 (2006). https://doi.org/10.1016/J.TRIBOINT.2005.03.021
2. Bartz, W.J., Krüger, V.: Influence of lubricants on the pitting fatigue of gears. Wear **35**, 315–329 (1975). https://doi.org/10.1016/0043-1648(75)90079-4
3. Hargreaves, D.J., Planitz, A.: Assessing the energy efficiency of gear oils via the FZG test machine. Tribol. Int. **42**, 918–925 (2009). https://doi.org/10.1016/J.TRIBOINT.2008.12.016
4. Höhn, B.-R., Michaelis, K., Kreil, O.: Influence of surface roughness on pressure distribution and film thickness in EHL-contacts. Tribol. Int. **39**, 1719–1725 (2006). https://doi.org/10.1016/J.TRIBOINT.2006.01.008
5. Savolainen, M., Lehtovaara, A.: An experimental approach for investigating scuffing initiation due to overload cycles with a twin-disc test device. Tribol. Int. **109**, 311–318 (2017). https://doi.org/10.1016/J.TRIBOINT.2017.01.005
6. Oila, A., Bull, S.J.: Assessment of the factors influencing micropitting in rolling/sliding contacts. Wear **258**, 1510–1524 (2005). https://doi.org/10.1016/j.wear.2004.10.012
7. Webster, M.N., Norbart, C.J.J.: An experimental investigation of micropitting using a roller disk machine. Tribol. Trans. **38**, 883–893 (1995). https://doi.org/10.1080/10402009508983485
8. Touret, T., Changenet, C., Ville, F., Cavoret, J., Abousleiman, V.: Experimental investigations on the effect of micropitting on friction—part 1. Tribol. Int. (2019). https://doi.org/10.1016/j.triboint.2019.03.036
9. Bergseth, E., Olofsson, U., Lewis, R., Lewis, S.: Effect of gear surface and lubricant interaction on mild wear. Tribol. Lett. **48**, 183–200 (2012). https://doi.org/10.1007/s11249-012-0004-y
10. Kleemola, J., Lehtovaara, A.: Experimental simulation of gear contact along the line of action. Tribol. Int. **42**, 1453–1459 (2009). https://doi.org/10.1016/J.TRIBOINT.2009.06.007
11. Björling, M., Miettinen, J., Marklund, P., Lehtovaara, A., Larsson, R.: The correlation between gear contact friction and ball on disc friction measurements. Tribol. Int. **83**, 114–119 (2015). https://doi.org/10.1016/j.triboint.2014.11.007
12. Matkovič, S., Kalin, M.: Effects of slide-to-roll ratio and temperature on the tribological behaviour in polymer-steel contacts and a comparison with the performance of real-scale gears. Wear (2021). https://doi.org/10.1016/j.wear.2021.203789
13. Vengudusamy, B., Enekes, C., Spallek, R.: EHD friction properties of ISO VG 320 gear oils with smooth and rough surfaces. Friction **8**, 164–181 (2020). https://doi.org/10.1007/s40544-019-0267-5
14. Hammami, M., Rodrigues, N., Fernandes, C., Martins, R., Seabra, J., Abbes, M.S., et al.: Axle gear oils: friction, wear and tribofilm generation under boundary lubrication regime. Tribol. Int. **114**, 88–108 (2017). https://doi.org/10.1016/J.TRIBOINT.2017.04.018

15. Brandão, J.A., Meheux, M., Ville, F., Seabra, J.H.O., Castro, J.: Comparative overview of five gear oils in mixed and boundary film lubrication. Tribol. Int. **47**, 50–61 (2012). https://doi.org/10.1016/j.triboint.2011.10.007
16. Bayat, R., Lehtovaara, A.: Friction and temperature mapping of environmentally acceptable gear oils. Tribologia (2020). https://doi.org/10.30678/FJT.96048
17. Bayat, R., Lehtovaara, A.: EHL/mixed transition of fully formulated environmentally acceptable gear oils. Tribol. Int. (2020). https://doi.org/10.1016/j.triboint.2020.106158
18. Lainé, E., Olver, A.V., Lekstrom, M.F., Shollock, B.A., Beveridge, T.A., Hua, D.Y.: The effect of a friction modifier additive on micropitting. Tribol. Trans. **52**, 526–533 (2009). https://doi.org/10.1080/10402000902745507
19. Bayat, R., Lehtovaara, A.: Scuffing evaluation of fully formulated environmentally acceptable lubricant using barrel-on-disc technique. Tribol. Int. **160**, 107002 (2021). https://doi.org/10.1016/j.triboint.2021.107002
20. Peng, B., Spikes, H., Kadiric, A.: The development and application of a scuffing test based on contra-rotation. Tribol. Lett. **67**, 37 (2019). https://doi.org/10.1007/s11249-019-1149-8
21. Ingram, M., Hamer, C., Spikes, H.A.: A new scuffing test using contra-rotation. Wear **328–329**, 229–240 (2015). https://doi.org/10.1016/j.wear.2015.01.080
22. Tonck, A., Martin, J.M., Kapsa, P., Georges, J.M.: Boundary lubrication with anti-wear additives: study of interface film formation by electrical contact resistance. Tribol. Int. **12**, 209–213 (1979). https://doi.org/10.1016/0301-679X(79)90190-7
23. Gosvami, N.N., Bares, J.A., Mangolini, F., Konicek, A.R., Yablon, D.G., Carpick, R.W.: Mechanisms of antiwear tribofilm growth revealed in situ by single-asperity sliding contacts. Science **348**, 102–106 (2015). https://doi.org/10.1126/science.1258788
24. Spikes, H.: The history and mechanisms of ZDDP. Tribol. Lett. **17**, 469–489 (2004). https://doi.org/10.1023/B:TRIL.0000044495.26882.b5
25. Cann, P.M., Spikes, H.A., Hutchinson, J.: The development of a spacer layer imaging method (slim) for mapping elastohydrodynamic contacts. Tribol. Trans. **39**, 915–921 (1996). https://doi.org/10.1080/10402009608983612
26. Shimizu, Y., Spikes, H.A.: The influence of slide-roll ratio on ZDDP tribofilm formation. Tribol. Lett. **64**, 1–11 (2016). https://doi.org/10.1007/s11249-016-0738-z
27. Haque, T., Korres, S., Carey, J.T., Jacobs, P.W., Loos, J., Franke, J.: Lubricant effects on white etching cracking failures in thrust bearing rig tests. Tribol. Trans. **61**, 979–990 (2018). https://doi.org/10.1080/10402004.2018.1453571
28. Kapadia, R., Glyde, R., Wu, Y.: In situ observation of phosphorous and non-phosphorous antiwear films using a mini traction machine with spacer layer image mapping. Tribol. Int. **40**, 1667–1679 (2007). https://doi.org/10.1016/J.TRIBOINT.2007.01.021
29. Topolovec-Miklozic, K., Forbus, T.R., Spikes, H.A.: Film thickness and roughness of ZDDP antiwear films. Tribol. Lett. **26**, 161–171 (2007). https://doi.org/10.1007/s11249-006-9189-2
30. Fujita, H., Spikes, H.A.: Study of zinc dialkyldithiophosphate antiwear film formation and removal processes, part II: kinetic model. Tribol. Trans. **48**, 567–575 (2005). https://doi.org/10.1080/05698190500385187
31. Zhang, J., Spikes, H.A.: On the mechanism of ZDDP antiwear film formation. Tribol. Lett. **63**, 1–15 (2016). https://doi.org/10.1007/s11249-016-0706-7
32. Spikes, H.A.: Stress-augmented thermal activation: tribology feels the force. Friction **6**, 1–31 (2018). https://doi.org/10.1007/s40544-018-0201-2
33. Khaemba, D.N., Jarnias, F., Thiebaut, B., Neville, A., Morina, A.: The role of surface roughness and slide-roll ratio on the decomposition of MoDTC in tribological contacts. J. Phys. D Appl. Phys. (2017). https://doi.org/10.1088/1361-6463/aa5905
34. Brizmer, V., Matta, C., Nedelcu, I., Morales-Espejel, G.E.: The influence of tribolayer formation on tribological performance of rolling/sliding contacts. Tribol. Lett. **65**, 1–18 (2017). https://doi.org/10.1007/s11249-017-0839-3
35. Jacobs, T.D.B., Carpick, R.W.: Nanoscale wear as a stress-assisted chemical reaction. Nat. Nanotechnol. **8**, 108–112 (2013). https://doi.org/10.1038/nnano.2012.255
36. Felts, J.R., Oyer, A.J., Hernández, S.C., Whitener, K.E., Robinson, J.T., Walton, S.G., et al.: Direct mechanochemical cleavage of functional groups from graphene. Nat. Commun. (2015). https://doi.org/10.1038/ncomms7467
37. Chen, Z., Gu, C., Tian, T.: Modeling of formation and removal of ZDDP tribofilm on rough surfaces. Tribol. Lett. **69**, 13 (2021). https://doi.org/10.1007/s11249-020-01393-8
38. Azam, A., Dorgham, A., Parsaeian, P., Morina, A., Neville, A., Wilson, M.C.T.: The mutual interaction between tribochemistry and lubrication: interfacial mechanics of tribofilm. Tribol. Int. (2019). https://doi.org/10.1016/j.triboint.2019.01.024
39. Demmou, K., Bec, S., Loubet, J.L., Martin, J.M.: Temperature effects on mechanical properties of zinc dithiophosphate tribofilms. Tribol. Int. **39**, 1558–1563 (2006). https://doi.org/10.1016/j.triboint.2006.01.025